UC Santa Barbara

UC Santa Barbara Electronic Theses and Dissertations

Title

Semidefinite and bootstrap methods in one-dimensional quantum systems

Permalink

https://escholarship.org/uc/item/9c17m919

Author

Hulsey, George

Publication Date

2024

Peer reviewed|Thesis/dissertation

eScholarship.org Powered by the California Digital Library
University of California

University of California
Santa Barbara

Semidefinite and bootstrap methods in one-dimensional quantum systems

A dissertation submitted in partial satisfaction
of the requirements for the degree

Doctor of Philosophy
in
Physics

by

George Hulsey

Committee in charge:

Professor David Berenstein, Chair
Professor Mark Srednicki
Professor Dirk Bouwmeester
Professor Jean Carlson

September 2024

The Dissertation of George Hulsey is approved.

Professor Mark Srednicki

Professor Dirk Bouwmeester

Professor Jean Carlson

Professor David Berenstein, Committee Chair

June 2024

Semidefinite and bootstrap methods in one-dimensional quantum systems

Copyright © 2024

by

George Hulsey

To Millie and Leia, my girls, for everything.

To my family, Mom, Dad, and Teapot, with love.

Acknowledgements

The completion of this thesis has come as the result of many great and kind people supporting me, my work, and my career, for which I could not be more grateful.

First, thanks to my advisor, David Berenstein, for his unmatched intuition, gruff and practical advice, and for guiding me through to the completion of this degree. After joining the group during the pandemic, I am proud of the papers and work we've done under alternative conditions, and I will miss the research process we developed together. Thanks also to my peers in the Berenstein Group: Thomas, for great collaboration in the latter part of my time at UCSB, David Grabovsky, for being unbelievably well-prepared in every regard and being there with me through every high-energy theory class offered by the department; and to Adolfo, Shannon, and the younger generation. Thank you also to my committee members Profs. Mark Srednicki and Dirk Bouwmeester, for joining and supporting this thesis.

And thank you especially to Prof. Jean Carlson. From meeting as a TA to working on the Physics Circus to the glorious proliferation of interdisciplinary work we have collaborated on, I owe the broadening of my horizons to you. Many meetings, slidesets, and email exchanges later, I have learned so much from you about science, quality of execution, complex systems, wildfire, the real world, and more. I have been so lucky to have your guidance and the work we have done together is so unique; I am proud of it. I'm sure there is much more we could have done. Thanks also to Dave Alderson for his advice, practical insight, and patience throughout our investigations of decisions, wildfire, and random walks.

I would be remiss to not thank my undergraduate advisor, Prof. Shamit Kachru. Without your willingness to listen to a headstrong sophomore who marched into your office demanding to learn string theory, I would never have ended up at UCSB let alone

gone to graduate school to study this old lore. Your aphoristic comments brought lofty concepts down to earth and showed me what it means to truly know something. And you were right—now that I am better educated, I know better than to worry about why there are three generations of quarks!

To my graduate friends and colleagues in the program, thanks for great times in San Clemente, for reading groups on topics far beyond my comprehension, and for sharing our excitement for those topics esoteric and exotic. I hope you will keep me apprised of progress in quantum gravity and more as you pursue your glorious futures: Molly Kaplan, Mike Zimet, Sean McBride, Paarth Gulati, Frannie Setti, and others. Thanks also to my many great friends from college, highschool, and beyond who have come to visit Santa Barbara and enjoy with me this beautiful corner of California. And especially to those people that lived with me through the pandemic exploring the trails and mountains of Oregon; Isaac, Conor, Shelley, I am so glad to have your friendship. And to Frits, who probably should have been paid for the amount of consulting he did as I stepped into the machine learning world.

To my family: Mom, Dad, and Teapot, we were so blessed to spend months together in the Ponderosa pines at BBR. I have always counted on you all and that has never let me down. Thanks for indulging practically a quarter century of education and for a lifetime of memories, experiences, and love. To Tutu and Papa, thank you for everything you have given in love and support. Tutu, I could not be happier to have you here to share this moment in my life. If only Papa and Grammy could have been around to see this—their memory is carried on with me, and I hope I would make them proud.

And finally, thanks to my best friend and the love of my life, Millie. I am sure that I am the luckiest man in the world to have you by my side. I am sure that this wouldn't have been possible without you, and I am sure that wherever life leads, I will go there with you and that is all I ever need. I guess little Leia isn't too bad, either.

Curriculum Vitæ

George Hulsey

Education

2024	Ph.D. in Physics (expected), University of California, Santa Barbara.
2022	M.A. in Physics, University of California, Santa Barbara.
2019	B.S. in Physics with Honors, Stanford University.
2019	B.S. in Mathematics, Stanford University.

Publications

GH, D. L. Alderson, J. M. Carlson. "Birth-death-suppression Markov process and wildfires." *Physical Review E* 109 (2024), https://doi.org/10.1103/PhysRevE.109.014110.

GH, D. Berenstein. "One-dimensional reflection in the quantum mechanical bootstrap." *Physical Review D* 109 (2024), https://doi.org/10.1103/PhysRevD.109.025013.

GH, D. Berenstein. "A semidefinite programming algorithm for the quantum mechanical bootstrap." *Physical Review E* 107 (2023), https://doi.org/10.1103/PhysRevE.107.L053301.

GH, D. Berenstein. "Anomalous bootstrap on the half line." *Physical Review D* 106 (2022), https://doi.org/10.1103/PhysRevD.106.045029.

GH, D. Berenstein. "Bootstrapping more QM systems." *Journal of Physics A: Mathematical and Theoretical* 55 (2022), https://www.doi.org/10.1088/1751-8121/ac7118.

GH, D. Berenstein. "Bootstrapping simple QM systems." Preprint, Aug. 2021, (arXiv: 2108.08757 [hep-th]).

GH, S. Kachru, S. Yang, and M. Zimet. "Distributions of extremal black holes in Calabi-Yau compactifications." *Journal of High Energy Physics* 10 042 (2020), https://doi.org/10.1007/JHEP10(2020)042.

Abstract

Semidefinite and bootstrap methods in one-dimensional quantum systems

by

George Hulsey

The bootstrap program in theoretical physics arose out of attempts to determine the structure of conformal field theories in a constraint-oriented, non-Hamiltonian fashion. In recent years, bootstrap methods have seen a strong resurgence in the numerical analysis of quantum mechanical systems without conformal symmetry. In this thesis, we develop the theory of the bootstrap approach to one-dimensional quantum systems. We show how Schrödinger quantum mechanics can be numerically solved by the method and develop the algebraic theory required to adapt the approach to domains with boundary and to scattering problems. We develop and implement efficient semidefinite programming algorithms to rigorously and numerically determine the energy spectra of confining polynomial potentials in one dimension. We also address the problem of spin chains and demonstrate how bootstrap methods can be used to regress conformal data from numerical approximations of the spin correlation functions. Broadly, this work lays a foundation for the theory and application of bootstrap methods to a wide variety of quantum mechanical systems, and also provides a mathematical background of the method and a thorough review of related work in high-energy theory, condensed matter physics, and mathematical optimization. Future directions for research both in wave mechanics and interacting spin systems are proposed.

Contents

Chapter 1

Introduction

The world waited for 30 years from the development of modern quantum mechanics in the early 20th century to the introduction of the first general-purpose programmable computer, and for decades more until the resources of digital computation made themselves available to the scientific public at large. Today, quantum mechanics is a theory with over a century's worth of analytical, theoretical, and now, numerical work. The zoology of quantum mechanical theories has become increasingly diverse and their mechanics increasingly complex. In the present day, massive amounts of computer resources are dedicated to the simulation of interacting quantum systems. Numerical and computational study of quantum mechanics affects our understanding of, among many phenomena, nuclear and hadronic physics, of quantum information and computation, of the chemical properties of novel materials and molecules, and, in a strange loop, of the behavior of the microscopic transistors which constitute the logical primitives of the computers used to study them.

As our understanding of the quantum mechanics has grown, so has the sophistication of the computational methods applied to study it. A large share of computational approaches to quantum problems involve discretization. Oxymoronically, many quan-

tum systems define continuous differential equations that govern the state; for example, the Schrödinger wave mechanics defines a differential eigensystem. Such problems can be solved by discretizing the continuous domain and therefore translating the problem into finite-dimensional linear algebra, which is easily implemented on classical computing hardware. Doing so comes at a cost: the accuracy of the discretized representation increases with the resolution, which in turn increases the computational cost.

For theories in higher dimensions or with more degrees of freedom, the direct discretization approach to determining the dynamical state is doomed by dimensionality. In other theories, we may not even know what the 'state' is! However, in many instances, the state is not the quantity of interest. All that is physically accessible to observers or observational machinery are the measured values of certain observable quantities, like the energy, momentum, or position of a particle. Neglecting philosophical flagellation as to the 'true nature' of quantum measurement, an ensemble of measurements of any observable yields an average, the expected value. In general, expectation values of observables are the only measurable and hence physical manifestations of the quantum dynamics.

In many theories, expectation values are much more tractable objects than states. Indeed, the development of modern quantum field theory relied on the study of correlation functions, expectation values of the similarity of certain observables located at different positions in spacetime. These expectation values can sometimes be written as a path integral. Path integrals integrate a weight, determined by the dynamics, over an infinite-dimensional configuration space of the quantum fields. While no such integral can be explicitly done on a computer, they can be approximated. The Monte Carlo approach to numerical integration involves random sampling of a high-dimensional function in order to approximate its integral. Monte Carlo algorithms see a wide range of applications in numerical dynamics, from quantum mechanics to stochastic processes.

An exemplary outstanding problem in numerical quantum mechanics is an under-

standing of the phenomenon of quark confinement in quantum chromodynamics. By the 1970s, it was understood on purely theoretical grounds that quantum chromodynamics, the theory of the strong nuclear force, was strongly-coupled at low energies, which meant that the traditional tools of e.g. Feynman diagrams in field theory would not work to describe the hadronic phase of the theory. However, an alternative description of the theory was soon put forth by Wilson [1] and later Kogut and Susskind [2]. They imagined the full theory emerged as the continuum limit of a lattice, a discretization of spacetime. In this lattice picture, simple arguments could show that at low energies, the theory developed a confining potential which would lead to the observed formation of color-free quark bound states. To date, the lattice gauge theory remains the most powerful approach to studying the dynamics of strongly interacting theories like QCD. However, it still relies on discretization and on the Monte Carlo approach of estimating integrals of many variables.

However, certain systems are out of reach of Monte Carlo. As its name suggests, the algorithm relies on sampling from the probability distribution created by the path integral measure. Unfortunately, for some systems, especially fermionic systems, the path integral measure may not be positive, and therefore cannot be treated as a probability distribution. This "sign problem" [3] is known to disrupt the ability of Monte Carlo approaches to giving stable numerical results in many theories. This includes lattice QCD at finite baryon number [4], which greatly complicates the study of quark confinement in lattice QCD by Monte Carlo methods.

Around the same time and into the 80s and 90s, bosonic string theory and its supersymmetric cousins emerged as contenders for a theory of quantum gravity. The physics of the string naturally gave rise to conformal quantum theories, field theories invariant under any angle-preserving transformation. While conformal invariance had been known to occur at the critical points of condensed matter systems, the modern formulation of

the theory introduced a new perspective, that of the *bootstrap*.

Conformal invariance is a very strong symmetry. It is so strong that many predictions of the theory—in particular, expectation values of observables—are constrained to take a very specific functional form. There exist more symmetries which relate certain observables to one another, defining precise constraints between expectation values, constraints which must be satisfied regardless of the microscopic origin or the melange of fields present in the theory. The bootstrap approach to conformal field theory did away with the complex descriptions of states, path integrals, action functionals, and regarded the constraints as fundamental. The analytical bootstrap [5] was able to successfully constrain a number of correlation functions using only very general quantum mechanical constraints: symmetries and unitarity. Unitarity is fundamental to any quantum system and is the statement that probability is conserved, or equivalently that information is never lost.

By the turn of the 21st century, the computational resources available to physicists had grown exponentially, and saw wide application to the study of quantum mechanics, including the conformal bootstrap program. In a series of papers [6, 7], computational methods were used to constrain the values of certain parameters of a conformal field theory by the bootstrap approach, relying only on extremely general hierarchies of constraints and conformal symmetry. The success of this approach indicated that the bootstrap program, viewing quantum mechanics through the lens of constraints on expectation values instead of states, could give numerically robust estimates of highly nontrivial aspects of the physics of the theory in question.

It was not long before the bootstrap philosophy graduated from conformal theories to more general quantum mechanical theories. In the last decade, bootstrap approaches have been made to lattice gauge theory, matrix quantum mechanics, electronic systems, Schrödinger quanutm mechanics, and more. They have even been applied to the lattice

QCD problem, though the method is comparatively in its infancy. We will review the recent history of these developments and their context with respect to the present work later in the introduction.

1.1 How to bootstrap

The subject of this thesis is the development of a very general bootstrap approach to one-dimensional quantum mechanical systems. One-dimensional systems are where quantum mechanics was first developed and is therefore a natural place to develop the groundwork for applying a bootstrap approach to more complex systems with many degrees of freedom.

The bootstrap may be generally regarded as a precise hierarchy of 'guess and check'. There are two parts to the process: first, one makes a guess for the value of a certain observable quantity. From this putative value one considers the constraints that exist in the theory and how they may relate the expectation value of other observables to the putative one. Given a set of such values related by the constraints of the theory, one applies a check to verify if the putative values of the observables are consistent with general quantum mechanical requirements. This may be the requirement of invariance under a certain symmetry, but most generally is a requirement related to unitarity.

The dominant view of quantum mechanics is in terms of states $|\psi\rangle$ which are elements of an abstract vector space, the Hilbert space $\mathcal{H}$. Unitarity is the requirement that these states have positive, normalizable inner product with themselves: $\langle\psi|\psi\rangle = 1$. The dynamics of a quantum theory are then represented as functions on the Hilbert space, mapping states to other states. In quantum mechanics, the most common type of dynamics is Hamiltonian dynamics. A system is equipped with a Hamiltonian (energy)

operator $\hat{H}$ which evolves states through time as

$$|\psi(t)\rangle = e^{-i\hat{H}t} |\psi(0)\rangle . \tag{1.1}$$

This evolution is unitary: for a self-adjoint Hamiltonian, the norm of the state does not change over time. Certain states, energy eigenstates, have special properties with respect to the Hamiltonian. They solve the time-independent Schrödinger equation:

$$\hat{H} |\psi\rangle = E |\psi\rangle , \tag{1.2}$$

where E is a number, the energy, and is exactly the expectation value of the Hamiltonian: $E = \langle \hat{H} \rangle_\psi \equiv \langle \psi(t)| \hat{H} |\psi(t)\rangle$. In energy eigenstates, the expectation value of any (Hermitian) operator, an observable, does not change in time. This follows directly from the Schrödinger equation:

$$\frac{d}{dt} \langle \psi(t)| \hat{\mathcal{O}} |\psi(t)\rangle = \frac{d}{dt} \langle \psi(0)| e^{iEt} \hat{\mathcal{O}} e^{-iEt} |\psi(0)\rangle = \frac{d}{dt} \langle \psi(0)| \hat{\mathcal{O}} |\psi(0)\rangle = 0. \tag{1.3}$$

However, one can take a different perspective on quantum mechanics where the operators, not the states, are the primary quantities of interest. Let $\hat{\mathcal{O}}$ be a Hermitian operator on the Hilbert space $\mathcal{H}$. The set of such bounded operators itself forms a normed vector space $\mathcal{B}(\mathcal{H})$ equipped with an involution $\hat{\mathcal{O}} \mapsto \hat{\mathcal{O}}^\dagger$, the Hermitian conjugate or adjoint. Beyond being elements of a vector space, these operators may be multiplied together, giving the space of operators on a Hilbert space the structure of an algebra (a $*$-algebra). Observables are those operators in $\mathcal{B}(\mathcal{H})$ which are fixed points of the involution: $\hat{\mathcal{O}}^\dagger = \hat{\mathcal{O}}$, or self-adjoint operators.

Ehrenfest's theorem relates the evolution of expectation values of observables to the

algebraic relations between operators. In any state ψ, one has the differential equation

$$\frac{d}{dt}\langle\hat{\mathcal{O}}\rangle_\psi = i\langle[\hat{H},\hat{\mathcal{O}}]\rangle_\psi + \left\langle\frac{\partial\hat{\mathcal{O}}}{\partial t}\right\rangle_\psi . \tag{1.4}$$

Consider now operators which have no time dependence, and states ψ which are eigenstates of the Hamiltonian. The Schrödinger equation sets the left hand side to zero and the second term on the right vanishes, leaving only the non-dynamical equation

$$\langle[\hat{H},\hat{\mathcal{O}}]\rangle = 0. \tag{1.5}$$

This is a direct linear constraint on expectation values in energy eigenstates of any Hamiltonian quantum theory, and it will be fundamental to constructing bootstrap algorithms for Schrödinger mechanics. But this constraint is completely general—we have put no specifications on the nature of the eigenstates, the degrees of freedom of the theory, or the physical origin of the quantum mechanics. It is true by virtue of the existence of the Hamiltonian and the operator algebra on $\mathcal{H}$. While it may seem extremely simple in the present context, this type of constraint appears in a wealth of theories. In quantum field theories, the Schwinger-Dyson equations, relating time-ordered n-point functions of quantum fields, are directly analogous to this type of constraint. It can also be viewed as a sort of temporal Ward identity; in quantum field theories, Ward identities relate correlation function which are identified under some symmetry. In this case, the symmetry is time-translation generated by the Hamiltonian.

Having shown the origin of a bootstrapping constraint, we turn to describing the unitarity requirements that constitute the 'check' portion of the basic bootstrap algorithm. Let $\hat{\mathcal{O}} \in \mathcal{B}(\mathcal{H})$ be a bounded operator on a Hilbert space; then, given any state $|\psi\rangle$, the operator $\hat{\mathcal{O}}$ defines a map $\hat{\mathcal{O}} : \mathcal{H} \to \mathcal{H}$ as $\hat{\mathcal{O}}\,|\psi\rangle = |\phi\rangle$. By unitarity, we must have

$\langle\phi|\phi\rangle \geq 0$, which in turn implies that $\langle\psi|\,\hat{\mathcal{O}}^\dagger\hat{\mathcal{O}}\,|\psi\rangle = \langle\hat{\mathcal{O}}^\dagger\hat{\mathcal{O}}\rangle_\psi \geq 0$. Furthermore, this must be true for any state $|\psi\rangle \in \mathcal{H}$.

We can go a step further by considering an operator X which is a complex linear combination of many operators: $X = \sum c_i\hat{\mathcal{O}}_i$. The inequality constraint $\langle X^\dagger X\rangle \geq 0$ must still be true in any physical state by unitarity. Expanding the expectation value, this requires

$$\langle X^\dagger X\rangle = \sum_{i,j} c_i^*\langle\hat{\mathcal{O}}_i^\dagger\hat{\mathcal{O}}_j\rangle c_j = \sum_{i,j} c_i^* M_{ij} c_j \geq 0, \tag{1.6}$$

where we have defined a matrix M of expectation values with elements $M_{ij} = \langle\hat{\mathcal{O}}_i^\dagger\hat{\mathcal{O}}_j\rangle$. Since the above must be true for any choice of the complex constants c_i, unitarity requires that the matrix of expectation values M is positive semidefinite. This is the principal positivity constraint we consider in this work, and as we shall see, it is directly related to a long history of mathematics addressing the classical moment problems.

We have therefore derived, based on completely general quantum mechanical principles of Hamiltonian dynamics and unitarity, linear and semidefinite constraints on expectation values of arbitrary bounded operators. For a system with a infinite number of operators, there are an infinite number of such constraints. The bootstrap program in quantum mechanics is that of identifying optimal ways to leverage these constraints in order to determine bounds on measurable quantities of the quantum system in question.

1.2 Outline of this work

The structure of this thesis is as follows. In the remainder of this section, we review the context of this work in the physics literature and provide an overview of related research preceding the present work and contemporaneous with it.

Chapter 2 concerns the mathematical background of the methods applied to develop

the bootstrap approach. This includes a review of convex optimization, classical moment problems, and hierarchies of semidefinite relaxations. In Chapter 3, we review the basic bootstrap constraints introduced above in the context of Schrödinger quantum mechanics on the real line. We show how they can be used to develop efficient convex optimization algorithms for determining the energy spectrum of Hamiltonians with polynomial potentials. In Chapter 4, we generalize this approach to domains with boundary. Since the perspective taken by the bootstrap is fundamentally algebraic, boundary conditions are integrated in a rather unfamiliar way. We furthermore show how these methods can be extended to address scattering problems. In Chapter 5, we address the problem of bootstrapping spin chains and show how conformal data may be determined from numerical semidefinite methods.

1.3 Literature review and this work in context

The research and results of this thesis are part of a recent resurgence in work on bootstrap methods applied to a wide variety of quantum systems. However, many underlying techniques, ideas, and motivations come from less recent developments in high energy theory, mathematical optimization, and condensed matter theory. We attempt to give a thorough overview of these different threads of research.

The conformal bootstrap

The inception of the conformal bootstrap program goes back to the pioneering work of Polyakov in developing non-Hamiltonian formulations of conformal field theories in the mid-1970s [8]. Much subsequent work was done in developing the modern understanding of CFTs [9, 10, 11], with a motivation at the time being the understanding of the world-sheet superstring theory. It took 30 years of development of CFT before the ideas of the

bootstrap began to be applied numerically; indeed, the optimization algorithms required were not developed until the late 1990s.

Around the late 2000s and into the present day, various works began leveraging the tools of conformal symmetry coupled with modern optimization algorithms to numerically constrain the space of conformal theories and the associated conformal data [12, 13]. In particular, the 3D Ising model was 'solved' by these numerical techniques [14, 15, 16] and the modern conformal bootstrap was born. By 'solved', we mean that the conformal weights of primaries and operator-product expansion coefficients of the theory were numerically determined to a high degree of precision. Soon, a dedicated semidefinite algorithm was developed, using a multiple-precision optimization solver, to bootstrap arbitrary CFTs to any desired level of accuracy, provided one has any desired level of computational power [6]. These techniques were applied to variety of CFTs of multiple physical origins, including fermionic theories and vector $O(N)$ models [17, 18]. By the late 2010s, the theory and application of these methods was well-developed [19, 20, 21]. These works laid the foundation for the expansion of bootstrap methods outside the regime of conformally constrained theories. The white papers [22, 23] give a thorough review of the history of this program as well as new and future developments.

Semidefinite methods in condensed matter systems

Semidefinite methods were introduced to the conformal bootstrap in 2015, but their relevance to the ground-state problem in condensed matter physics had been recognized and applied years earlier. Initial investigations along these lines considered reduced density matrices, submatrices of the full mixed state of an interacting many-body quantum system [24]. By leveraging the unitarity constraints on these submatrices, which implies their positive-semidefiniteness, ground state properties can be estimated without any description of the ground-state wavefunction [25]. While these approaches were not re-

ferred to as bootstrapping, their thesis and methods were, in a general sense, completely analogous to the bootstrap program as laid out in this work. As advances were made in large-scale semidefinite optimization [26], these methods were revisited and applied with success to a variety of many-electron and condensed-matter systems [27, 28, 29, 30, 31]. Subsequent work linked the reduced density matrix theory and semidefinite methods in electronic systems to approximations of hard (in the complexity theory sense) problems [32, 33, 34], comparing the semidefinite approach to the hard ground state problem to 'industry standard' variational methods like density functional theory [35]. The semidefinite approach to ground state problems was simultaneously formalized outside of its introduction in the context of the reduced density matrix theory [36, 37].

In the last four years, these semidefinite methods have seen a strong resurgence [38, 39, 40, 41, 42, 43], likely related to novel developments in the theory of non-commutative optimization [44, 45, 46, 47]. New work describes how semidefinite methods can address observables beyond the ground state energy [48, 49, 50, 51]. Semidefinite methods in condensed matter systems remain an active area of research, and have been coupled with the more traditional variational approaches to yield huge improvements in numerical analysis of condensed matter systems [52, 53].

The bootstrap program in high-energy theory

The bootstrap program, with its roots in conformal field theory, has always been associated with high-energy theory. In 2020, Lin [54] published work showing how bootstrap methods could be used to address matrix models, using the loop equations and various positivity conditions to constrain the physics of the theory. Soon after, Han et al. [55] extended the work of Lin and demonstrated simple applications to one-dimensional quantum mechanics and to the matrix quantum mechanics, obtaining basic bounds on energies and other observables. These works kickstarted a large body of related research applying

bootstrap methods to a wide array of systems both familiar and unfamiliar to numerical quantum mechanics. Classic textbook systems, fermionic models, multi-matrix integrals, quantum field theories, and a variety of other quantum systems were analyzed by bootstrap methods within a few years of the paper of Lin [56, 57, 58, 59, 60, 61, 62, 63, 64]. The techniques even found applications in string theory [65, 66, 67]. In particular, Lin extended his early work to an analysis of the BFSS matrix theory. This theory contain fermionic degrees of freedom, introducing a sign problem. It describes M-theory, a conjectured high-energy limit of all string theories and hence of all physics. That the bootstrap can approach this (M)onster is testament to its generality and power.

With this activity came a better understanding of the methods, the relevant families of constraints, and ways to improve the computational efficiency of the method by leveraging symmetries of the problem [68]. Kazakov et al. developed the method for application to lattice Yang-Mills theory, a theory where semidefinite methods had previously been completely absent in favor of the traditional means of lattice computation [69]. Some work began to address spin systems [70, 71] from the perspective of high-energy theory, though strong connections were not made with the existing condensed matter literature on reduced density matrix theory and the associated semidefinite methods.

The work in this thesis was published in a series of papers [72, 73, 74, 75, 76] contemporaneous with the developments outlined above. To date, the renaissance of bootstrap methods in high-energy theory continues [77, 78, 79, 80, 81, 82, 83], with some recent reviews summarizing the progress and noting the relation of these methods to the mathematical study of moment problems and positive measures [84, 85].

The great promise of bootstrap methods lies in their generality. While their development originated in the extremely constrained world of conformal field theory, modern work has shown that these methods can be applied to essentially any system with algebraic quantum structure. The details of the system in question greatly inform the

implementation of the methods, and much work remains to be done for these methods to gain the maturity of more well-established numerical approaches. It is a principal goal of this thesis to develop fully the theory of bootstrap analysis for simple, well-understood quantum systems, and to thereby pave the way for its future. The computational resources available for these methods have never been greater, and will surely only increase in the foreseeable future.

Chapter 2

Convex optimzation, moment problems, and semidefinite relaxations

The bootstrap program lies at the intersection of classical mathematics, modern numerical optimization algorithms, and physics. At its core is the fundamental physical constraint of unitarity. Unitarity takes many guises but may be construed generally as the preservation of probability: both the conservation of probability and its positivity.

Beyond unitarity, the dynamics of physical systems are almost universally understood in terms of optimization: the principle of least action extremizes a functional over a space of configurations, leading to the Euler-Lagrange equations and the physical dynamics of the theory in question.

Semidefinite methods, and semidefinite programs, combine the positivity constraints of unitarity with the optimization objectives so commonly seen in physics. While the history of semidefinite methods in mathematics stretches back a century or more, only since the turn of the millenium have we had computer resources and algorithms capable

of efficiently solving semidefinite-constrained optimization problems. In this chapter, we will develop the necessary background in semidefinite programming, the theory of moment problems, and the combination of the two which constitutes the mathematical backdrop of the bootstrap program.

2.1 Convex optimization and semidefinite programs

Convex optimization concerns the minimization (resp. maximization) of a convex function over a convex set. In such problems, local optima are global optima and such optima are guaranteed to exist. While many optimization problems of interest may not be naturally convex, they may often be translated into a convex form by the introduction of new variables or by some other reformulation. In this section we review the basic ideas of convex optimization and use these to introduce semidefinite programs, a wide class of convex optimization problems that include many questions of interest for the quantum mechanical bootstrap.

Recall that an optimization problem is defined by an objective function to be extremized, a domain of optimization, and a set of inequality constraints:

$$\begin{aligned} &\text{minimize} && f(x); \quad x \in \mathbb{R}^n, \\ &\text{subject to} && g_i(x) \leq b_i; \quad i = 1, \ldots, m. \end{aligned} \tag{2.1}$$

The *feasible domain* $D \subset \mathbb{R}^n$ is defined as the subset of the domain of x where all constraints are satisfied. Note that any equality constraint may be formally rewritten as a pair of inequality constraints: $\{g(x) = a\} \cong \{g(x) \leq a, g(x) \geq a\}$.

The goal of any optimization problem is therefore to extremize the objective over the feasible domain. A convex optimzation problem is one in which the objective function is convex and the feasible domain D is convex. Many functions of interest in physics are

convex, including any linear function, exponentials, power functions, entropy, and more. Perhaps the simplest type of convex optimzation problem is the linear program:

$$\begin{aligned} \text{minimize} \quad & f(x) = c^T x + d, \\ \text{subject to} \quad & Gx \preceq h, \\ & Ax = b. \end{aligned} \tag{2.2}$$

Here, the matrices G, A are numerical and the inequality $\preceq$ applies element-wise to the vectors Gx, h. The set of vectors with non-negative entries forms a cone, which is always a convex space. A natural generalization is to consider a quadratic form as the objective function, leading to a quadratic program:

$$\begin{aligned} \text{minimize} \quad & f(x) = (1/2)x^T P x + q^T x + r, \\ \text{subject to} \quad & Gx \preceq h, \\ & Ax = b. \end{aligned} \tag{2.3}$$

Here, the matrix P must be symmetric (i.e. a quadratic form). Quadratic programs encompass many familiar problems: least-squares regression, damped harmonic oscillation, classical statistical mechanics, and many others. They may be solved efficiently and robustly despite the objective function being non-linear. Of course, linear programs are a subset of quadratic programs with $P = 0$.

Just as quadratic programs generalize linear programs, introducing non-linearity while preserving convexity, semidefinite programs generalize quadratic programs to an even wider class of problems, potentially with extreme non-linearity within the objective function and constraints. Consider the set defined by $\{x \geq 0,\ z \geq 0,\ xz \geq y^2 \mid (x, y, z) \in \mathbb{R}^3\}$. This set is not obviously convex. However, the same set may be written in terms of a 2×2 matrix in the positive-semidefinite (PSD) cone in $\mathbf{S}^2$, the space of 2×2 symmetric

matrices:

$$X = \begin{bmatrix} x & y \\ y & z \end{bmatrix} \in \mathbf{S}^2_+ \quad \Longleftrightarrow \quad x \geq 0, \quad z \geq 0, \quad xz \geq y^2.$$

Being a cone, the set of PSD symmetric matrices is convex, and the conditions on x, y, z may be compactly rewritten as $X \succeq 0$. For completeness, we note that a matrix X is PSD iff all of its eigenvalues are positive, or equivalently if $v^T X v \geq 0$ for all vectors v of suitable shape.

Semidefinite programs (SDPs) are convex optimization problems over the cone $\mathbf{S}^n_+$ of $n \times n$ PSD matrices.[1] The primal form of the SDP has a symmetric/Hermitian matrix variable X subject to convex constraints generalizing those seen in the quadratic and linear programs:

$$\begin{aligned} \text{minimize} \quad & \operatorname{tr}(CX), \\ \text{subject to} \quad & \operatorname{tr}(A_i X) \geq b_i, \quad i = 1, \ldots, p; \\ & X \succeq 0, \ X \in \mathbf{S}^n_+. \end{aligned} \tag{2.4}$$

As a set, semidefinite programs contain both quadratic and linear programs. Roughly, linear programs correspond to semidefinite programs on diagonal matrices X.

An SDP may also be written in the linear matrix inequality (LMI) form:

$$\begin{aligned} \text{minimize} \quad & c^T x, \\ \text{subject to} \quad & x_1 A_1 + \cdots + x_p A_p \preceq B. \end{aligned} \tag{2.5}$$

This formulation is useful when one wishes to enforce equality constraints between certain optimization variables x_i, as these can be explicitly integrated into the problem construction. In the primal formulation, such equalities must enter as trace constraints. These formulations are equivalent and related to one another by convex duality, a generalization of the familiar Legendre transform in classical mechanics [86].

[1] Unlike the extrema of the objective function, the acronyms in this field are not optimal.

Formulating nonlinear problems as semidefinite programs

Many non-linear optimization problems may be recast as SDPs and hence identified as convex. As a basic example, consider the very nonlinear objective function

$$\begin{array}{ll} \text{minimize} & \frac{(c^T x)^2}{d^T x}, \\ \text{subject to} & Ax + b \geq 0, \text{ elementwise} \end{array} \tag{2.6}$$

minimized over x in the feasible domain defined by $d^T x \geq 0$. This problem can be written in an explicitly convex way as an SDP. First one introduces a "slack" variable t as

$$\begin{array}{ll} \text{minimize} & t, \\ \text{subject to} & Ax + b \geq 0, \ \frac{\left(c^T x\right)^2}{d^T x} \leq t. \end{array} \tag{2.7}$$

The first constraint $Ax + b \geq 0$ can be written in SDP form as

$$\text{diag}(Ax + b) \succeq 0,$$

where we construct a diagonal matrix from the vector entries. The second constraint is $t(d^T x) - \left(c^T x\right)^2 \geq 0$ for positive $d^T x$. This is equivalent to

$$D = \begin{bmatrix} t & c^T x \\ c^T x & d^T x \end{bmatrix}; \quad D \succeq 0. \tag{2.8}$$

Therefore, the problem (2.6) equivalent to the SDP

$$\begin{array}{ll} \text{minimize} & t, \\ \text{subject to} & \begin{bmatrix} \text{diag}(Ax + b) & 0 \\ 0 & D \end{bmatrix} \succeq 0. \end{array} \tag{2.9}$$

The reformulation into a manifestly convex form came at the cost of introducing a new variable t to the optimization.

A non-linear problem of interest of us is that of eigenvalue extremization: given a PSD matrix M, we would like to maximize the minimal eigenvalue. If we parametrize the matrix elements as $M = M_0 + \sum_i x_i M_i$, we have the optimization problem

$$\begin{aligned} \text{maximize} \quad & \lambda_{\min}(M(x_i)), \\ \text{subject to} \quad & M \succeq 0. \end{aligned} \tag{2.10}$$

The eigenvalues of M are horribly non-linear functions of the variables x_i. However, by introducing a slack variable t we can write

$$\begin{aligned} \text{maximize} \quad & t, \\ \text{subject to} \quad & \lambda_{\min}(M(x_i) - tI) \geq 0. \end{aligned} \tag{2.11}$$

which is equivalent to the linear matrix inequality SDP

$$\begin{aligned} \text{minimize} \quad & -t, \\ \text{subject to} \quad & M - tI \succeq 0. \end{aligned} \tag{2.12}$$

In Section 3.3 we will use the semidefinite formulation of eigenvalue extremization to define an efficient semidefinite algorithm for finding Schrödinger bound states.

2.2 The classical moment problems

Having introduced semidefinite programs, we shift gears and consider some classical mathematical problems in measure theory. The bootstrap method is intimately related to the classical moment problems, polynomial optimization, and questions of positivity over

semialgebraic sets. In this section, we begin by discussing the relationship of moments of measures and positive polynomials which naturally leads into a discussion of the classical moment problems. These classical results will appear later when we apply these ideas to quantum mechanical systems.

2.2.1 Positive and sum-of-squares polynomials

It is a fundamental fact in the theory of rings and real algebraic geometry that a real, positive polynomial of one variable can be decomposed as a sum of squares (s.o.s.) of polynomials:

$$p(x) \geq 0, \ \forall x \in \mathbb{R} \quad \Leftrightarrow \quad p(x) = \sum_i h_i(x)^2. \tag{2.13}$$

However, the same cannot be said for polynomials in multiple variables [87]. Hilbert's 17th question posed the weaker claim that all non-negative polynomials (in any dimension) can be written as sums of squares of rational functions, a claim later proved in the affirmative by Artin [88].

At the heart of the question is the gap between non-negativity and having a s.o.s. decomposition. First, let us formally characterize what it means for a multivariate polynomial to be a sum of squares. In any dimension, let $v_d(\mathbf{x})$ be a vector of the canonical basis of monomials of degree at most d, i.e. in $\mathbb{R}$, $v_3(x) = [1, x, x^2, x^3]^T$, in $\mathbb{R}^2$, $v_2(\mathbf{x}) = [1, x, y, x^2, xy, y^2]^T$, and so on. A polynomial $p(\mathbf{x})$ of degree $2d$ is s.o.s. if and only if there exists a real symmetric, positive semidefinite matrix Q such that $p(\mathbf{x}) = v_d(\mathbf{x})^T Q v_d(\mathbf{x})$ [87].

In fact, this form naturally defines a semidefinite program to check whether a polynomial is s.o.s.. The vectors of monomials $v_d(\mathbf{x})$ naturally define a set of symmetric

matrices B_α as

$$v_d(\mathbf{x})v_d(\mathbf{x})^T = \sum_\alpha B_\alpha \mathbf{x}^\alpha, \tag{2.14}$$

where one should regard $\alpha \in \mathbb{N}^n$ as a set of indices representing the powers of each component of $\mathbf{x}$ in a given monomial. Then, $p(\mathbf{x}) = \sum p_\alpha \mathbf{x}^\alpha$ has a sum-of-squares representation if the following semidefinite program has a non-empty feasible domain:

$$\begin{aligned} \text{minimize} \quad & \text{(any function of } Q\text{)}, \\ \text{subject to} \quad & Q \succeq 0, \quad \operatorname{tr}(QB_\alpha) = p_\alpha. \end{aligned} \tag{2.15}$$

This is the first of many intersections of semidefinite programming and the present questions of positivity. Since semidefinite programs may be solved efficiently using e.g. interior-point algorithms, identifying whether a given polynomial is a sum of squares can therefore be efficiently (polynomially) checked.

In general the sets of non-negative polynomials and s.o.s polynomials are certainly not equivalent, and we can make a relatively precise measurement of their difference. Let $P[\mathbf{x}]_d$ be the set of positive polynomials in n variables of degree d and let $\Sigma[\mathbf{x}]_d$ be the analogous set of s.o.s. polynomials. We have $P[x]_d \cong \Sigma[x]_d$ when $n = 1$, but $\Sigma[\mathbf{x}]_d \subseteq P[\mathbf{x}]_d$ in higher dimensions[2]. If we identically restrict these sets to subsets of finite volume $\tilde{P}[\mathbf{x}]_d$, $\tilde{\Sigma}[\mathbf{x}]_d$[3], one can show that the ratio of their volumes is bounded below as [87]

$$n^{(d/2-1)/2} \lesssim \left(\frac{\operatorname{vol}(\tilde{P}[\mathbf{x}]_d)}{\operatorname{vol}(\tilde{\Sigma}[\mathbf{x}]_d)} \right). \tag{2.16}$$

Ignoring the necessary restrictions, this result says that as we increase the degree of the polynomial, the set of positive polynomials begins to exponentially outweigh the set of

[2]There are only three cases, found by Hilbert, in which the sets reach an equality. In n dimensions and with polynomials of degree d, the sets are equal for $(n, d) = (1, d)$, $(n, 2)$, or $(2, 4)$ [89].

[3]In particular, we restrict $P[\mathbf{x}]_d, \Sigma[\mathbf{x}]_d$ to their elements homogenous under scaling and with integral 1 over the unit sphere S^{n-1}.

s.o.s. polynomials. It may therefore seem unlikely that 'most' positive polynomials admit a s.o.s. decomposition.

However, while finding an exact s.o.s representation of any non-negative polynomial may be an exponentially doomed task, one can always find a close approximation. In particular, any non-negative polynomial may be perturbed to an arbitrarily small degree to yield a sum-of-squares. Formally, $\Sigma[\mathbf{x}]_d$ is dense in $P[\mathbf{x}]_d$ with respect to the ℓ_1 norm of the coefficients. This is a deep result which forms the backbone of the semidefinite methods we develop in this thesis. As we will see, the bootstrap makes heavy use of sums of squares and their ability to approximate arbitrary positive quantities.

We now turn to a generalization of the sum-of-squares/positivity question by considering positivity over restricted domains in $\mathbb{R}^n$. Define a general semialgebraic set $\mathbb{K}$ as the positive locus of a set of polynomials $g_j(\mathbf{x})$:

$$\mathbb{K} = \{g_j(\mathbf{x}) \geq 0 \mid j = 1, \ldots, m,\ \mathbf{x} \in \mathbb{R}^n\}. \tag{2.17}$$

One can ask whether a polynomial $p(\mathbf{x})$, positive on $\mathbb{K}$, has an s.o.s. decomposition. Under certain mild assumptions on $\mathbb{K}$[4], Putinar's Positivstellensatz ('theorem of positive location') states that if $p(\mathbf{x})$ is positive on $\mathbb{K}$, then it admits a decomposition as

$$p(\mathbf{x}) = q_0(\mathbf{x}) + \sum_{j=1}^{m} q_j(\mathbf{x}) g_j(\mathbf{x}), \tag{2.18}$$

where the q_j are s.o.s.. The existence of this decomposition is crucial in proving the solutions to the classical moment problems in the next section.

[4]One should assume either that the g_i are affine or that some restriction of the g_i, e.g. $i = 1, \ldots m-k$, define a compact subset of $\mathbb{K}$ (see Thm. 2.14 in [87]).

2.2.2 The moment problems

The results of the previous section are intimately related to the study of measures μ and their moments.[5] The general moment problem asks, given a sequence $(y_\alpha)_{\alpha\in\mathbb{N}^n}$, whether there exists a 'representing' measure μ on some set S such that

$$y_\alpha = \int_S \mathbf{x}^\alpha d\mu. \tag{2.19}$$

The sequence (y_α) may be infinite, defining the full moment problem, or finite, defining the truncated moment problem.

To connect the moment problem to the theory of positive polynomials, one first defines a linear operator $L_\mathbf{y}(\cdot)$ which substitutes a variable $\mathbf{x}^\alpha$ with the putative moment y_α of equal degree. Let us now state a result of great importance: the Riesz-Haviland theorem [87]. Let $(y_\alpha) \subset \mathbb{R}$ be a sequence (where generically $\alpha \in \mathbb{N}^n$) and let $\mathbb{K} \subset \mathbb{R}^n$ be a closed semialgebraic set. Then there exists a representing measure μ, with

$$\int_\mathbb{K} \mathbf{x}^\alpha d\mu = y_\alpha; \quad \forall \alpha \in \mathbb{N}^n, \tag{2.20}$$

if and only if $L_\mathbf{y}(f) \geq 0$ for all polynomials f non-negative on $\mathbb{K}$.

This theorem links the existence of a representing measure μ, and hence a solution of the moment problem on $\mathbb{K}$, to the positivity of a functional on the set of non-negative polynomials over the semialgebraic domain. This theorem can be informally restated in the language of quantum mechanics. A quantum state $|\psi(\mathbf{x})\rangle$ furnishes a measure $|\langle\mathbf{x}|\psi(\mathbf{x})\rangle|^2 d\mathbf{x}$. A sequence of values y_α are the moments of this measure if and only if the linear functional $L_\mathbf{y}(\cdot) = \langle\psi(\mathbf{x})|\,(\cdot)\,|\psi(\mathbf{x})\rangle$—the expectation value—is positive on all positive operators. Positivity of the expectation is a direct consequence of unitarity and

[5] We are only interested in increasing measures μ, such that $d\mu$ is positive.

can be proven by passing to an eigenbasis of the operator in question, where it is PSD diagonal by assumption.

Using the Riesz-Haviland theorem we can now introduce and prove the solutions of the three classical moment problems for one-dimensional, real domains. In all the following, let $(y_j)_{j\in\mathbb{N}}$ be a putative sequence of moments. We will address the question of existence of a representing measure on $\mathbb{R}, \mathbb{R}_+$, and the interval $[a, b]$.

The Hamburger moment problem

The most basic of the classical problems is the Hamburger moment problem, which seeks a representing measure on $\mathbb{K} = \mathbb{R}$. First, assume a representing measure exists. Then by Riesz-Haviland we must have $L_y(f) \geq 0$ on all non-negative polynomials f and in particular for those where $f(x) = g(x)^2$. This implies

$$L_y(f) = L_y(g^2) = \sum_{i,j} g_i L_y(x^{i+j}) g_j = \sum_{i,j} g_i (y_{i+j}) g_j \geq 0, \tag{2.21}$$

where g_j are the coefficients of $g(x)$ in the canonical basis. Define the infinite Hankel matrix $H(y)$ by its elements $H(y)_{ij} = y_{i+j}$. The positivity condition above, which must be valid for any choice of the g_i, can be restated as positive semidefiniteness $H_n(y) \succeq 0$ for all $n \times n$ principal submatrices $H_n(y)$ of $H(y)$.

To go the other way, assume that $H_n(y) \succeq 0$, defined as above, for $\forall n$. Let $f(x)$ of degree $2n$ be non-negative on $\mathbb{R}$; then $f(x)$ is a sum-of-squares and we can write $f(x) = \sum_j q_j(x)^2$. Let $\mathbf{q}_j$ be the vector of coefficients of the polynomial $q_j(x)$. In order for a representing measure to exist we must have $L_y(f) \geq 0$, or equivalently

$$L_y(f) = \sum_k f_k y_k = L_y\left(\sum_j q_j(x)^2\right) = \sum_j \mathbf{q}_j^T H_n(y) \mathbf{q}_j \geq 0, \tag{2.22}$$

where the last inequality follows from the assumption that $H(y) \succeq 0$.

Therefore, the Hamburger moment problem solution is that a sequence (y_j) has a representing measure μ on $\mathbb{R}$ if and only if the Hankel matrix with elements $H(y)_{ij} = y_{i+j}$ is positive semidefinite. This matrix is called a moment matrix (with respect to 1). The proof given here relies on the theorem of Riesz-Haviland to prove the equivalency, but often, one only needs the necessity of the semidefinite condition for polynomials which are already sums of squares.

The Stieltjes moment problem

Consider now the moment problem on $\mathbb{K} = \mathbb{R}_+$. This set can be defined as a semialgebraic subset of $\mathbb{R}$ as $\mathbb{R}_+ = \{x \geq 0 \mid x \in \mathbb{R}\}$. Assuming that a representing measure for a sequence (y_j) exists, we can repeat the first direction of the proof of the Hamburger problem. Let $L_y(f) \geq 0$ for all $f(x)$ positive on $\mathbb{R}_+$; requiring this for $f(x) = g(x)^2$ leads to the identical condition $H(y) \succeq 0$ as before. However, on $\mathbb{R}_+$, the condition must also be true for $f(x) = xg(x)^2$, since $x \geq 0$. This gives an additional positivity condition on an infinite Hankel matrix $S(y)$ with elements $S(y)_{ij} = y_{1+i+j}$. Therefore, the existence of a representing measure for (y_j) on $\mathbb{R}_+$ implies $H(y) \succeq 0,\ S(y) \succeq 0$. One may be tempted to additionally consider a positive polynomial of the form $f(x) = x^n g(x)^2$. However, for any $n \neq 0, 1$, the resulting conditions are already encapsulated by the positivity of $H(y),\ S(y)$. Note that $S(y)$ is the moment matrix with respect to x, sometimes referred to as a localizing matrix.

To prove the other direction we apply Putinar's Positivstellensatz. Assume $H(y), S(y) \succeq 0$. Let $f(x)$ be non-negative on $\mathbb{R}_+$, then by (2.18) we have a decomposition $f(x) = g(x) + xh(x)$ where g, h are sums of squares. The action of the functional L_y on f is

therefore

$$L_y(f) = L_y(g) + L_y(xh) = \sum_j \mathbf{g}_j^T H_n(y)\mathbf{g}_j + \sum_j \mathbf{h}_j^T S_n(y)\mathbf{h}_j \geq 0, \tag{2.23}$$

which is positive by our assumptions, and hence by Riesz-Haviland implies the existence of a representing measure. The Stieltjes problem of representing measures on $\mathbb{R}_+$ thus generalizes the Hamburger problem by requiring a new positivity condition on $S(y)_{ij} = y_{1+i+j}$ in addition to $H(y) \succeq 0$.

Other moment problems

With the basic structure of the proof laid out, we simply state the solution of the final real moment problem without proof. The Hausdorff problem asks for representing measures on the closed interval $[a, b]$ for some sequence (y_j). By the same logic as before, this requires $H(y) \succeq 0$. The closed interval may be semialgebraically defined as $[a, b] = \{(b - x)(x - a) \geq 0 \mid x \in \mathbb{R}\}$, leading to a positivity condition $C(y) \succeq 0$ where

$$C(y)_{ij} = (a + b)y_{1+i+j} - aby_{i+j} - y_{2+i+j}. \tag{2.24}$$

The positivity conditions of the moment problems derived above apply to formally infinite matrices. In practice, one generically only has access to a finite sequence of putative moments $(y_j)_{j=1}^{2n}$. The truncated moment problem asks whether these moments have a representing measure. Specializing to the case of measures on $\mathbb{R}$, it is clear that one still must have $H_n(y) \succeq 0$. However, while necessary if a measure exists, this positivity condition is insufficient to guarantee the existence of a measure. This is simply because the condition $H_n(y) \succeq 0$ is only a small sub-constraint of the full positivity constraint.

Curto and Fialkow [90, 91] study the truncated moment problem and ask what con-

ditions must be met on the finite matrices $H_n(y)$ in order that existence of the measure can be guaranteed. They determine that if the rank of $H_n(y)$ saturates at some value n—that is, that $\text{rank}(H_{n+k}(y)) = \text{rank}(H_n(y))$ for $k \geq 0$—then the sequence y has an atomic (discrete) representing measure. While we repeat this result for completeness, bound energy eigenstates in quantum systems are never associated to atomic measures (or their momentum wavefunctions would not be normalizable). Therefore any finite truncation of the moment matrix will never guarantee precisely the existence of a representing measure, but will always be a necessary condition for its existence.

2.3 Semidefinite relaxations

A relaxation of a system of constraints is a weakening of the system by enforcing only some subset of the relevant constraints. That is, a relaxation is an approximation of a set of exact constraints. In a general sense, this is a path often taken in physics, both numerically and analytically. Presently, we introduce the notion of a semidefinite relaxation, where a (possibly infinite) set of constraints is relaxed to yield a semidefinite constraint on a finite matrix. We review how these relaxations may form hierarchies and demonstrate their use in the context of the moment problem and additionally in the context of polynomial optimization. Bootstrap methods are in general a means of constructing a physically-informed semidefinite relaxation of an infinite set of physical constraints. Making such a relaxation allows one to circumvent or approximate the exponential complexity of a wide class of optimization problems.

Let us consider a general class of optimization/moment problems where the domain of optimization is the set of positive measures on a semialgebraic set $\mathbb{K}$. Let $f(\mathbf{x})$ be a polynomial and let

$$\mathbb{K} = \{g_j(\mathbf{x}) \geq 0 \mid \mathbf{x} \in \mathbb{R}^n,\ j = 1, \ldots, m\} \tag{2.25}$$

as before. Consider the optimization problem over measures $\mu(\mathbb{K})$ given by

$$\begin{array}{ll} \text{maximize} & \int_{\mathbb{K}} f(\mathbf{x}) d\mu, \\ \text{subject to} & \int_{\mathbb{K}} h_j(\mathbf{x}) d\mu \leq \gamma_j, \end{array} \tag{2.26}$$

for some constants γ_j. We can rewrite the problem in terms of the moments $y_\alpha = \int_{\mathbb{K}} \mathbf{x}^\alpha d\mu$ and associated linear functional $L_{\mathbf{y}}(\cdot)$ as

$$\begin{array}{ll} \text{maximize} & L_{\mathbf{y}}(f), \\ \text{subject to} & L_{\mathbf{y}}(h_j) \leq \gamma_j; \quad y_\alpha = \int_{\mathbb{K}} \mathbf{x}^\alpha d\mu. \end{array} \tag{2.27}$$

To construct the relaxation, we define the moment matrix $M(\mathbf{y})(a,b) \equiv L_{\mathbf{y}}(\mathbf{x}^a \mathbf{x}^b)$. Lassere [87] gives the *primal relaxation* of the problem (2.26) as

$$\begin{array}{ll} \text{maximize} & L_{\mathbf{y}}(f), \\ \text{subject to} & L_{\mathbf{y}}(h_j) \leq \gamma_j; \quad M_K(\mathbf{y}) \succeq 0,\ M_{K-d_j}(g_j \mathbf{y}) \succeq 0, \end{array} \tag{2.28}$$

where $2d_j$ is the degree of $g_j(\mathbf{x})$ and K is some integer large than twice the degree of the highest degree polynomial in $\{g_j, h_j\}$.[6] All that has happened is that we have relaxed the condition that $\mathbf{y}$ is derived exactly from a representing measure to the positivity conditions on the (finite) $K \times K$ moment matrices with respect to 1 and the polynomials $g_j(\mathbf{x})$. In the limit $K \to \infty$, these positivity conditions become equivalent to the existence of the representing measure, a direct consequence of Putinar's Positivstellensatz and the Riesz-Haviland theorem.

We refer to the relaxation (2.28) as the Lasserre relaxation of depth K. Note that at successive depths $K+1, K+2, \ldots$, the feasible domain of the optimization can never

[6] Strictly speaking, we are brushing some issues of odd degree/parity under the rug; see [87] for the exact statement of this theorem.

increase, as the constraint set at each depth strictly contains the constraints at all lower depths. These successive relaxations, each less 'relaxed' than the previous, form a hierarchy, the infinite limit of which is the exact measure optimization problem of (2.26). The relaxed problem (2.28) is, of course, a semidefinite program.

Therefore, this hierarchy of relaxations—the Lasserre hierarchy—provides a means to estimate the solution of (2.26) to arbitrary accuracy as $K \to \infty$ and at each depth is solvable to arbitrary precision in polynomial time. Specifically, interior-point algorithms for SDPs involving $n \times n$ matrices and m constraints have time complexity $\mathcal{O}(m^{3/2}n^3)$ and memory complexity $\mathcal{O}(mn^2)$.

2.4 Non-commutative polynomial optimization

The discussion of the last sections completes the theory of moment problems that is relevant for the development of the bootstrap approach to Schrödinger quantum mechanics. However, when we address quantum spin chains, the flavor of the problem will be slightly different, and, notably, the variables involved are non-commutative. To build some background for the spin chain bootstrap, we introduce a very general class of polynomial optimization problems: let $p(\mathbf{x}), q_j(\mathbf{x})$ be polynomials, and consider the optimization problem

$$\begin{aligned} \text{minimize} \quad & p(\mathbf{x}), \\ \text{subject to} \quad & q_j(\mathbf{x}) \geq 0. \end{aligned} \tag{2.29}$$

For general p, q_j, this problem falls into the NP complexity class. The general form has as special cases many familiar (and difficult) optimization problems, such as binary linear programming and the max-cut problem [89]. While exponentially difficult to solve exactly, the problem (2.29) may be approximated by polynomially efficient methods using the Lasserre hierarchy.

The constraints define a semialgebraic set $\mathbb{K} = \{q_j(\mathbf{x}) \geq 0\}$ while the objective function may be restated as

$$\text{minimize}_{\mathbb{K}} \quad p(\mathbf{x}) \quad \Leftrightarrow \quad \text{maximize}_{\mathbb{R}} \quad \rho \quad \text{s.t. } p - \rho \geq 0 \text{ on } \mathbb{K}. \tag{2.30}$$

From Putinar's Positivstellensatz we know a s.o.s. decomposition of polynomials positive on $\mathbb{K}$, which in this case are $p(\mathbf{x}) - \rho$ in addition to the $q_j(\mathbf{x})$, and we may therefore use the relaxation (2.28) to successively approximate the solution of the general polynomial problem (2.29). This is known as the sum-of-squares relaxation of the polynomial optimization problem [89].

The natural quantum-mechanical generalization of polynomial optimization is to promote the variables $\mathbf{x}$ to be non-commuting operators. While the commuting optimization problem (2.29) is NP-hard, the non-commuting problem can in general be "Quantum-Merlin-Arthur" (QMA) hard [92]. The QMA class is the quantum generalization of NP: problems in NP are exponentially difficult to solve but may be polynomially checked by a classical algorithm, while QMA problems may be polynomially checked by a quantum algorithm. There are problems in NP which are 'easier' than QMA-complete tasks. The complexity of this non-commutative optimization problem is directly related to the known complexity of finding the ground state of an interacting spin chain, a class of problems which has been extensively addressed in the physics literature [93, 94].

The theory of non-commutative optimization is rather new [44, 46], though its results have already been applied in numerous physical contexts, especially in condensed matter and quantum information theory. The authors in [44] define the general non-commutative polynomial optimization problem in the following fashion. Let $X = (\hat{\mathcal{O}}_1, \hat{\mathcal{O}}_2, \ldots)$ be a set of operators on a Hilbert space $\mathcal{H}$, and let $p(\mathbf{x}), q_j(\mathbf{x})$ be polynomials as above. The operators X should belong to the Banach space of bounded operators on $\mathcal{H}$, i.e.

$X \subset \mathcal{B}(\mathcal{H})$, which we assume is endowed with the involution †; the conjugate-transpose. The optimization occurs over the space of triples $(\mathcal{H}, X, \psi)$ where ψ is a normalized vector in the Hilbert space, defining the problem

$$\begin{aligned} \text{minimize} \quad & \langle\psi|p(X)|\psi\rangle, \\ \text{subject to} \quad & q_i(X) \succeq 0. \end{aligned} \tag{2.31}$$

The inequality constraints become (operator) positive semidefiniteness constraints, which depend on the polynomials $q_j(\mathbf{x})$, the operators X, and the Hilbert space $\mathcal{H}$. Recall that by definition an operator is positive semidefinite if $\langle\psi|\hat{\mathcal{O}}|\psi\rangle \geq 0$ for all $|\psi\rangle \in \mathcal{H}$.

A natural first step would be to ask if there exists a non-commutative generalization of Putinar's theorem, and, indeed, such a generalization was given by Helton and McCullough [95]. However, their theorem applies to the dual formulation of the problem (2.31), which we will neglect to include at present.

To define the non-commutative analog of the Lasserre hierarchy, we must first put some conditions on the feasible domain. Roughly, one requires that the feasible domain is bounded: if $X_1, \ldots, X_n$ satisfy $q_i(X) \succeq 0$, then we can choose a constant C such that $C^2 - (X_1^\dagger X_1 + \cdots X_n^\dagger X_n) \succeq 0$. [7] In the context of spin systems, where all operators are strings of Pauli operators and linear combinations thereof, this condition is always met [44].

Let $(y_w)_{|w|\leq 2K}$ be a sequence indexed by 'words' w; strings of (non-identity) operators of some maximum length $2K$. In the commutative case, words can be identified by their degree $\alpha \in \mathbb{N}^n$, but with non-commutative variables a more complex indexing is required. Non-commutative moment matrices are defined as $M_K(y)_{vw} = y_{v^\dagger w}$ where we carry out the non-commutative multiplication $v^\dagger w$ to find the index of the sequence element at position (v, w) in the moment matrix. The sequence admits a moment representation,

[7] The exact statement is that the quadratic module generated by the q_i is *Archimedean*, see e.g. [96]

analogous to a representing measure, if there exists a normalized state $|\psi\rangle$ such that $y_w = \langle\psi| w(X) |\psi\rangle$. This implies that $M_K(y) \succeq 0$, a necessary condition for the sequence (y_w) to be derived from a physical state.

Having made the analogies, we can now state the non-commutative analog of Lasserre's relaxation. The problem (2.31) admits a hierarchy of relaxations of depth K, where $2K \geq \{\deg p,\ \deg q_i\}$, defined as

$$\begin{aligned} &\text{minimize} && \textstyle\sum_w p_w y_w, \\ &\text{subject to} && y_1 = 1; \quad M_K(y) \succeq 0; \quad M_{K-\deg q_i}(q_i y) \succeq 0. \end{aligned} \tag{2.32}$$

Clearly, the optimum p_K lower bound the exact optima $p_K \leq p^\star$ of the problem (2.31). In fact, in [44], the authors show that with the boundedness condition stated earlier, one has the convergence property $\lim_{K\to\infty} p_K = p^\star$. In a system with a finite Hilbert space, this global optimum is reached at a finite value of K at which K is the total number of unique operators in the algebra $\mathcal{B}(\mathcal{H})$.

While we repeat these results for completeness, it is clear that morally, the ideas behind the Lasserre relaxation generalize quite naturally to the non-commutative setting. Furthermore, the physical systems to which we apply these tools generally satisfy all the auxiliary properties required for proofs of existence and convergence to hold.

This concludes the mathematical background we need to use the bootstrap approach in a wide range of physical systems. As we apply these ideas to Schrödinger mechanics, scattering problems, and spin chains, we will add some conditions and modify others in order to enforce or constrain particular physical behaviors of interest. The key takeaway of this chapter is the notion of hierarchies of relaxations: that one can constructively generate successively accurate approximations of a exact, highly non-linear optimization problem, and that these relaxations generate rigorous bounds on the exact optimum of

interest.

Chapter 3

Bootstrap methods on the real line

With the mathematical setting established, we turn to the physics and develop the bootstrap approach to Schrödinger problems on the real line. We consider the time-independent Schrödinger equation with a confining potential $V(x)$. Normally, one views the problem as a differential eigensystem. The Hamiltonian defines a second-order linear ordinary differential equation for the wavefunction $\psi(x)$:

$$\hat{H}\psi(x) = -\frac{1}{2M}\frac{d^2}{dx^2}\psi(x) + V(x)\psi(x) = E\psi(x). \tag{3.1}$$

Self-adjoint Hamiltonians define a set of energy eigenstates and eigenvalues $(\psi_n(x), E_n)$ which are the objects of interest. The difficulty is that one must determine both these data given only the potential $V(x)$.

The traditional algorithmic approach to such a problem is to discretize the domain and in turn generate a matrix representation of the differential operator $\hat{H}$. This transforms the Schrödinger equation into a finite-dimensional eigenvalue equation which may be diagonalized and solved by any number of numerical routines. This is always an approximation, one which grows in fidelity as the resolution of the discretization increases.

However, the memory and computational cost of numerical matrix diagonalization grows quickly as the matrix size increases.

While exact diagonalization gives approximations both of the eigenstates $\psi_n(x)$ and their eigen-energies E_n, there are very few instances in which one actually needs access to the exact wavefunction of a system. The only measurable quantities in quantum mechanics are the expectation values of operators: $\langle\hat{\mathcal{O}}\rangle \equiv \langle\psi|\hat{\mathcal{O}}|\psi\rangle$ (in this section and throughout, we will use the compact notation $\langle\hat{\mathcal{O}}\rangle$ to refer to the expectation of an operator $\hat{\mathcal{O}}$ in some unknown energy eigenstate). Observables in Schrödinger mechanics include the energy, positional moments $\langle x^n\rangle$, moments of momentum, or mixed moments thereof.

The bootstrap provides a way of detecting or approximating these data without determining the state itself. One may view this as solving the problem for the observables directly, and ignoring the mostly redundant information contained in the exact form of the wavefunction, information which will never enter into an experimental measurement. In this chapter, we develop the bootstrap approach in Schrödinger mechanics from first principles and observe how it may be used to determine the spectrum of one-dimensional Hamiltonians.

3.1 Basics of the bootstrap

Generally speaking, the bootstrap method works as follows: initial guesses are made for some parameters (data) of the model, and from these guesses a list of predictions based on the dynamics is made. We apply consistency checks to these predictions recursively and reject initial guesses which fail the checks at a given step. Construction of these recursive consistency checks relies on two basic identities. First, on an eigenstate of the

Hamiltonian it is true that certain expectation values vanish identically:

$$\langle [\hat{H}, \hat{\mathcal{O}}] \rangle = 0, \tag{3.2}$$

where $\hat{\mathcal{O}}$ is some operator in the theory. This identity states that the expectation value of any observable in an energy eigenstate is constant in time. It is also true, by virtue of the eigenvalue equation, that in states of energy E we have

$$\langle \hat{H}\hat{\mathcal{O}} \rangle = E\langle \hat{\mathcal{O}} \rangle. \tag{3.3}$$

Secondly, one always has generic positivity constraints of the form

$$\langle \hat{\mathcal{O}}^\dagger \hat{\mathcal{O}} \rangle \geq 0, \tag{3.4}$$

which hold for any operator $\hat{\mathcal{O}}$. This can be viewed as positivity of the norm of the state $\hat{\mathcal{O}}|\psi\rangle$, a requirement of unitarity. In one-dimensional systems equipped with standard kinetic terms in the Hamiltonian, these constraints create closed recursion relations which can be initialized by guessing the energy E and perhaps a few positional moments of the putative state.

One hopes that the solutions (i.e. values of E and other initialization data) that pass all the tests will eventually converge to actual solutions of the theory, and from this we can learn nontrivial facts about the theory in question. In practice, with finitely many constraints, one hopes that the allowed region becomes small enough that one can learn a lot about the theory. This is not guaranteed. In the examples we will see this convergence in most cases, but when it happens is not clear *a priori*. We also see that in principle, with enough computational resources, we can recover all the (bound state) energy levels of these systems with arbitrarily high precision, though with increasing computational

resources as we move up the spectrum.

In the interest of testing the method's performance, we will address a number of classic Schrödinger systems, beginning with the harmonic oscillator and culminating with the solution of an arbitrary polynomial potential on any subdomain of the real line. Some of these models also admit analytical solutions which allows us to test the efficacy and accuracy of the method. We will characterize the accuracy, precision, and convergence of the bootstrap method for these one-dimensional quantum mechanical problems; i.e. finding eigenvalues for the time-independent Schrödinger equation.

For our focus on one-dimensional quantum mechanics, we consider Hamiltonians of the form

$$\hat{H} = \frac{p^2}{2M} + V(x), \tag{3.5}$$

where $[x, p] = i$ as usual. To each energy eigenstate of $\hat{H}$ is associated an energy E and a sequence of moments $\{\langle x^n \rangle\}_0^\infty$. Knowing the energy and all the moments is equivalent to knowing the probability distribution function associated to the wavefunction of some given eigenstate. The goal of the quantum mechanical bootstrap is to approximately identify the energies and moments $\langle x^n \rangle$ corresponding to the eigenstates of $\hat{H}$.

3.1.1 Moment recursion

We start by applying the method of [55] to obtain a recursion relation for the positional moments. Starting from the identities

$$\langle [\hat{H}, \hat{\mathcal{O}}] \rangle = 0; \qquad \langle \hat{H}\hat{\mathcal{O}} \rangle = E \langle \hat{\mathcal{O}} \rangle, \tag{3.6}$$

we can relate different moments of x, p. For example, take $\hat{\mathcal{O}} = x^s$ and let $\hat{H}$ be the generic Hamiltonian (3.5) with $M = 1$. Using the first identity above gives a relation

$$\langle[\hat{H}, x^s]\rangle = 0 \quad \Longrightarrow \quad s\left\langle x^{s-1}p\right\rangle = \frac{i}{2}s(s-1)\left\langle x^{s-2}\right\rangle.$$

This does not depend on the potential $V(x)$. If we similarly take $\hat{\mathcal{O}} = x^m p$, we get such dependence:

$$0 = m\langle x^{m-1}p^2\rangle + \frac{1}{4}m(m-1)(m-2)\langle x^{m-3}\rangle - \langle x^m V'(x)\rangle. \tag{3.7}$$

Finally we can involve the energy E by considering the second identity above and taking $\hat{\mathcal{O}} = x^{m-1}$:

$$E\langle x^{m-1}\rangle = \frac{1}{2}\langle x^{m-1}p^2\rangle + \langle x^{m-1}V(x)\rangle. \tag{3.8}$$

By combining these relations we can eliminate the expectations values of mixed operators $\langle x^n p^m\rangle$. The result is a recursion relation for the moments $\langle x^n\rangle$ which depends on the energy E of some eigenstate. This recursion relation captures the dynamics of the Hamiltonian:

$$0 = 2mE\langle x^{m-1}\rangle + \frac{1}{4}m(m-1)(m-2)\langle x^{m-3}\rangle - \langle x^m V'(x)\rangle - 2m\langle x^{m-1}V(x)\rangle. \tag{3.9}$$

We note that the $m = 1$ case of this relation is nothing but the virial theorem:

$$E = \frac{1}{2}\langle xV'(x)\rangle + \langle V(x)\rangle. \tag{3.10}$$

To use any recursion relation, we need a minimal set $S = \{E, \langle x\rangle, \ldots\}$ which can initialize the recursion. We call such a set the 'search space'. It will contain the energy and a few moments $\langle x^n\rangle$. The dimension $s_* \equiv \dim(S)$ will depend on the potential. For

polynomial potentials, the expectation should be that $s_* \sim \deg V(x)/|G|$ where G is any discrete symmetry group of the Hamiltonian (generically $\mathbb{Z}_2$). Some examples are given below:

- $V(x) = \frac{1}{2}\omega^2 x^2; \quad S = \{E\}$
- $V(x) = gx^3; \quad S = \{E, \langle x\rangle, \langle x^2\rangle\}$
- $V(x) = gx^2 + hx^4; \quad S = \{E, \langle x^2\rangle\}$

One can show that $s_* = 1$ only for the Coulomb and harmonic oscillator potentials[1]. We always normalize states by demanding that $\langle x^0\rangle = 1$.

3.1.2 Positivity constraints and moment problems

Given a Hamiltonian $\hat{H}$, we can generate a recursion relation and identify the minimal search space S. Then, choosing a point $s \in S$, we can construct a moment sequence from the recursion relation (3.9). We now need some way of physically accepting or rejecting such a (finite) moment sequence $\{\langle x^n\rangle\}_0^N$. We first motivate a physical condition as in [55, 58], relying on the positivity of the norm. Let $\hat{\mathcal{O}} = \sum_n c_n x^n$. Then, for any $c_n \in \mathbb{C}$, we have

$$0 \leq \langle \hat{\mathcal{O}}^\dagger \hat{\mathcal{O}}\rangle = \sum_{ij} c_i^* \langle x^{i+j}\rangle c_j \equiv \sum_{ij} c_i^* M_{ij} c_j, \tag{3.11}$$

since the quantity is a norm of some state in the Hilbert space. In the above we have defined $M_{ij} = \langle x^{i+j}\rangle$. Considering these as matrix elements of some symmetric matrix M, the above constraint can be rephrased as $M \succeq 0$; i.e. M is positive semi-definite. M is, of course, exactly equivalent to the positivity matrix $H(y)$ constructed in the solution

[1] A necessary condition is that the virial theorem relates $E = \alpha\langle x^n\rangle$ for some n, so that determining E determines a moment directly. Secondly, this must be enough data to generate all the other moments. This only occurs for these two potentials, possibly with an angular momentum barrier if the variable x is properly restricted.

of the Hamburger moment problem. The state ψ, which enters implicitly through the expectation value, defines the representing measure $d\mu = |\langle x|\psi\rangle|^2 dx$, the existence of which necessitates (and implies) the positivity condition $M \succeq 0$.

3.2 Systems on the real line

In this section we study how the moment recursion may be used to identify valid regions of the search space. To begin, we use a naive grid search algorithm. This shows how the regions allowed by the positivity checks appear and allows visualizations of the convergence of the method. In the following section, we will develop and implement a much more efficient semidefinite programming algorithm to obtain the same results with much less computational cost.

3.2.1 The harmonic oscillator

No study of Schrödinger quantum mechanics would be complete without addressing the simple harmonic oscillator system: $\hat{H} = p^2/2 + x^2/2$. The moment recursion relation for the harmonic oscillator is given by

$$s\langle x^s\rangle = 2E(s-1)\langle x^{s-2}\rangle + \frac{1}{4}(s-1)(s-2)(s-3)\langle x^{s-4}\rangle. \tag{3.12}$$

We use $\langle x^0\rangle = 1$ and $\langle x^2\rangle = E$ to set up the recursion, and we use $\langle x^{2m-1}\rangle = 0$ for all odd values, from the even properties of the potential. With the recursion, all moments can be explicitly determined by the energy E.

At first, it might seem that the odd moments of the distribution are superfluous; that turns out not to be the case. The Hankel matrix with the odd moments leads to additional constraints. The simplest such constraint is that all even moments are

positive. For example, consider the 4×4 Hankel matrix obtained from the harmonic oscillator recursion:

$$M_{4\times4} = \begin{pmatrix} 1.000 & 0 & E & 0 \\ 0 & E & 0 & 1.500E^2 + 0.3750 \\ E & 0 & 1.500E^2 + 0.3750 & 0 \\ 0 & 1.500E^2 + 0.3750 & 0 & 2.500E^3 + 3.125E \end{pmatrix} \tag{3.13}$$

We see that there are two independent matrices, one made from the intersection of the even columns and rows, and another from the intersection of the odd columns and odd rows. The first constraint, from the odd-odd 1×1 matrix M_{11} is that $E \geq 0$. There is no additional constraint from the 2×2 even matrix made of $M_{00}, M_{0,2}, M_{2,2}$. The results of the constraints are shown in Fig. 3.1.

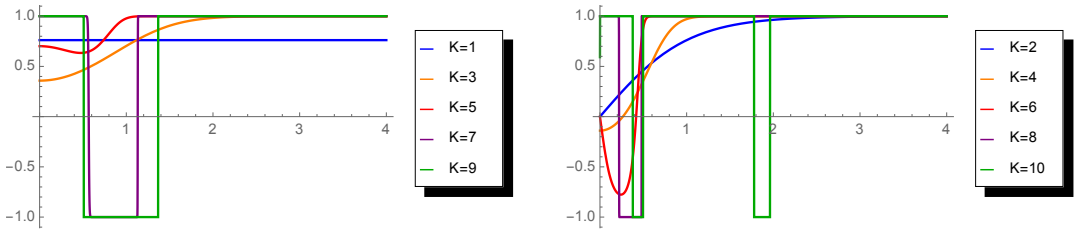

Figure 3.1: Constraint regions for $K \times K$ matrices, split between even columns on the left and odd columns on the right. The horizontal axis is the guess for the energy. We plot $\tanh(\det(M))$ for the different size matrices for added visibility. Only the region where all curves are positive is valid. We see that the $K = 4, 6$ odd matrices are crucial for removing the lower values of E and that negative windows start opening up for larger K that start separating the different eigenvalues.

In the figures, we see that the allowed region for energies starts fragmenting as we increase K. The determinant functions are determinants of polynomials, so there is a finite number of zeros. It necessarily follows that to see more energies individually, we need to go to higher order in K. At a much larger value of $K = 55$, Fig. 3.2 shows the appearance and fragmentation of multiple energy levels. We note that doing this

procedure naively requires high numerical precision, as the harmonic moments $\langle x^n \rangle$ grow super-exponentially in n.

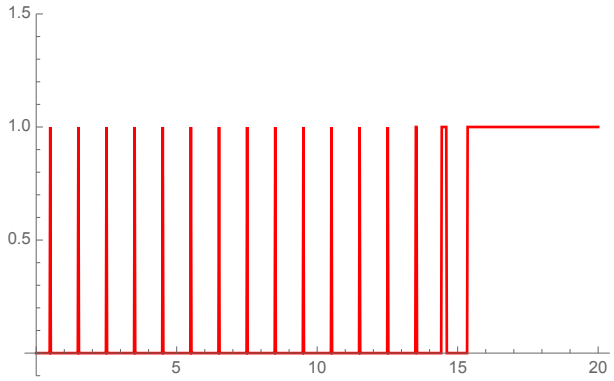

Figure 3.2: Allowed Harmonic oscillator energies at level $K = 55$. The peaks are small windows at the half integers. The horizontal axis is the energy, and the vertical axis is an indicator function if a point is allowed or not. Fifteen energy levels are resolved.

3.2.2 The Double Well

With the basics of the method demonstrated for the harmonic system, we turn to a more complex model: the double well. We take the following Hamiltonian:

$$\hat{H} = p^2 + gx^2 + x^4.$$

Note that we use $M = 1/2$ which matches the conventions of [55]. We will consider $g < 0$ which is the regime in which we expect non-perturbative contributions due to instantons. In these conventions, states with $E < 0$ live in the double well and states with $E > 0$ live above it. Our goal is to identify the performance of the bootstrap method in systems which exhibit non-perturbatively suppressed behavior. The bootstrap approach to this system also was studied in [57], released contemporaneously with the present work. Our analysis confirms and expands on their results.

Moment recursion and classical limit

The double-well bootstrap has a 2-dimensional search space in the sense that the values $\{E, \langle x^2 \rangle\}$ determine all higher moments $\langle x^n \rangle$ via the following recursion relation valid for $n \geq 4$:

$$\langle x^n \rangle = \frac{(n-3)}{(n-1)} E \langle x^{n-4} \rangle - \frac{(n-2)}{(n-1)} g \langle x^{n-2} \rangle + \frac{(n-3)(n-4)(n-5)}{4(n-1)} \langle x^{n-6} \rangle. \tag{3.14}$$

As usual this recursion reproduces the virial theorem; in the above it occurs at $n = 4$:

$$E = 2g\langle x^2 \rangle + 3\langle x^4 \rangle. \tag{3.15}$$

There are various aspects of the dynamics that we expect the bootstrap to reproduce. Let us start by considering the system classically. The potential is bounded below by $\min V = -g^2/4$. For any $E > -g^2/4$ the turning points x_1, x_2 are defined by $E = V(x_i)$ (care must be taken to choose the correct branches when $E < 0$). The period is defined as an integral over an orbit of the motion:

$$T = \oint dt = \int_{x_1}^{x_2} \frac{1}{\sqrt{E - gx^2 - x^4}} dx.$$

Note that with $M = 1/2$ one must be extra careful with prefactors in these equations. The classical analogue of $\langle x^2 \rangle$ is simply the average of $x(t)^2$ over a period of the motion, which in the integral form is

$$\langle x^2 \rangle_{\text{cl}} = \frac{1}{T} \int_{x_1}^{x_2} \frac{x^2}{\sqrt{E - gx^2 - x^4}} dx. \tag{3.16}$$

This defines a curve in the $E, \langle x^2 \rangle$ plane. We expect that quantum states of the system live relatively close to this curve, and that they approach the curve increasingly in the

semiclassical limit. This allows a smart initialization of the search space—instead of searching random points, we can look in a neighborhood of the curve defined by (3.16).

Quantum mechanically, we can make a few predictions about the dependence of various quantities on the coupling g. The first of these is the ground state energy. In the limit of deep wells (which is $g \to -\infty$) each well behaves approximately as a harmonic oscillator, and the ground state energy is twofold degenerate. Perturbation theory determines [97]

$$E_0(g) = -\frac{g^2}{4} + \sqrt{2|g|} - \frac{1}{|g|} - \frac{9}{8\sqrt{2}|g|^{5/2}} + \hat{\mathcal{O}}(1/|g|^4). \tag{3.17}$$

The second term gives the harmonic contribution and the latter offer corrections. However, it is well-known that instanton effects break the ground-state degeneracy. Performing a one-loop path integral over fluctuations around the instanton solution (see e.g. [98]) we expect to see a ground-state energy splitting

$$\Delta E_0^{(1)} = \frac{8|g|^{5/4}}{2^{-1/4}} \frac{1}{\sqrt{\pi}} \exp\left[-\frac{\sqrt{2}}{3}|g|^{3/2}\right]. \tag{3.18}$$

This contribution is exponentially suppressed in the deep well limit, which is the same regime in which we expect the formula to become increasingly accurate. In fact, we can go a step further and include fluctuation interactions—this is a two-loop calculation in the Feynman jargon. Doing so gives a more refined estimate

$$\Delta E_0^{(2)} = \frac{8|g|^{5/4}}{2^{-1/4}} \frac{1}{\sqrt{\pi}} \exp\left[-\frac{\sqrt{2}}{3}|g|^{3/2} - \frac{71\sqrt{2}}{48|g|^{3/2}}\right]. \tag{3.19}$$

In the following sections we present results from bootstrapping this system for a range of couplings g. We will see that all the (highly non-trivial) predictions above are supported by the bootstrap data.

Naive algorithm implementation

The basic algorithmic structure is the same as that described for the harmonic oscillator system, with a few technical modifications since the search space is two-dimensional. From a set of points corresponding to candidate values of $E, \langle x^2 \rangle$, we use the recursion (3.14) to generate higher moments up to $\langle x^{2K-2} \rangle$ for some K. Then we construct the $K \times K$ Hankel matrix $M_{ij} = \langle x^{i+j} \rangle,\ 0 \leq i, j \leq K-1$ and check that it is positive-definite.

We implemented the naive bootstrap algorithm in `Python`. For a given value of g a cursory search was made in a wide envelope surrounding the classical curve (3.16) at some low constraint depth K_0. From there the algorithm continued to higher depth, generating new grids of finer resolution around sets of allowed values at each iteration. We were able to obtain data for values of the coupling $g \in [-8.75, -3]$, and for energies $E \in [-g^2/4, 5]$ at each value of g. We searched depths $K_0 = 5 \leq K \leq 20$ which was more than sufficient to uncover the non-perturbative behavior. Because of the relatively modest size of the matrices involved, the `float64` datatype used was sufficiently precise to avoid egregious numerical errors.

Bootstrap results

Here we present some example data from the double well bootstrap as well as spectral predictions extracted from the bootstrap data. Fig. 3.3 gives an example of the data from the bootstrap, with the classical curve (3.16) superimposed.

The spectral data was obtained by choosing the highest value of K with well-conditioned data for a given coupling. The disparate islands of allowed parameter values were clustered and their energies extracted from the centroids of the clusters. Fig. 3.4 shows the spectrum, as a function of g, extracted in this way. With these data we can test the path integral predictions for the splitting. First, we can isolate the ground state energy as a

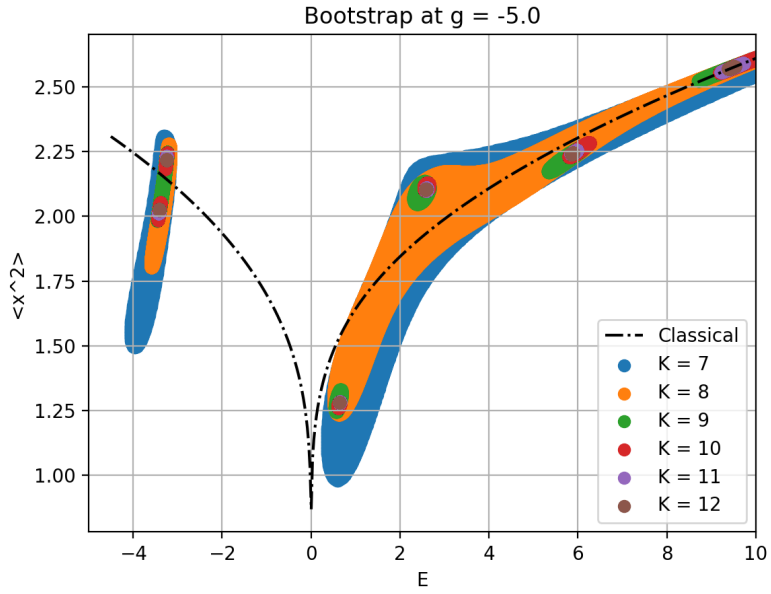

Figure 3.3: Example bootstrap data for $g = -5$. The ground state splitting is clearly visible as is adherence to the classical curve in the semiclassical regime. Islands form and separate as K increases.

function of g. By combining the predictions (3.17) and (3.19) we can get a ground state energy estimate which incorporates the splitting. This is included on the left in Fig. 3.5. We can also test the splitting prediction (3.19) alone, on the right. Agreement is best in the asymptotic regime where this analysis is valid, for large negative g.

3.2.3 The microcanonical bootstrap

Nakayama [62] explored the idea of bootstrapping the microcanoncial ensemble (MCE) of a given system. This is exactly the $\hbar \to 0$ limit of a quantum system: normalizabilty and probabilistic interpretations remain but the dynamics are altered. Here, expectation values are understood to be taken in a probability measure over states given a fixed energy. Specifically, one term of the moment recursion (that proportional to $\hbar$) vanishes.

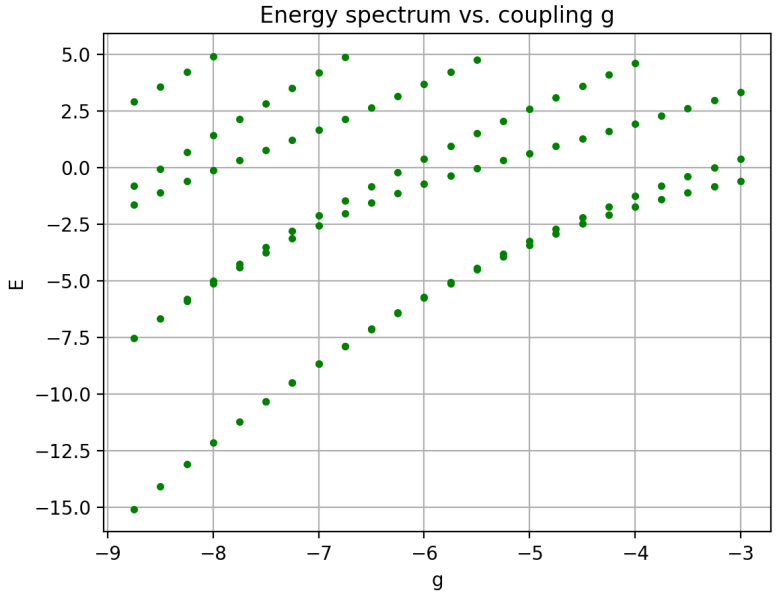

Figure 3.4: Spectrum versus coupling g. The splitting is visible for some values of g; for sufficiently low values depths $K > 20$ would be required to resolve the difference. Error bars are included but too small to see.

The quantum mechanical recursion for moments of measures on $\mathbb{R}$ was

$$0 = 2mE\langle x^{m-1}\rangle + \frac{1}{2}m(m-1)(m-2)\langle n-3\rangle - \langle x^m V'(x)\rangle - 2m\langle x^{m-1}V(x)\rangle. \quad (3.20)$$

The MCE moment recursion for a general potential on $\mathbb{R}$ is

$$0 = 2mE\langle x^{m-1}\rangle - \langle x^m V'(x)\rangle - 2m\langle x^{m-1}V(x)\rangle. \quad (3.21)$$

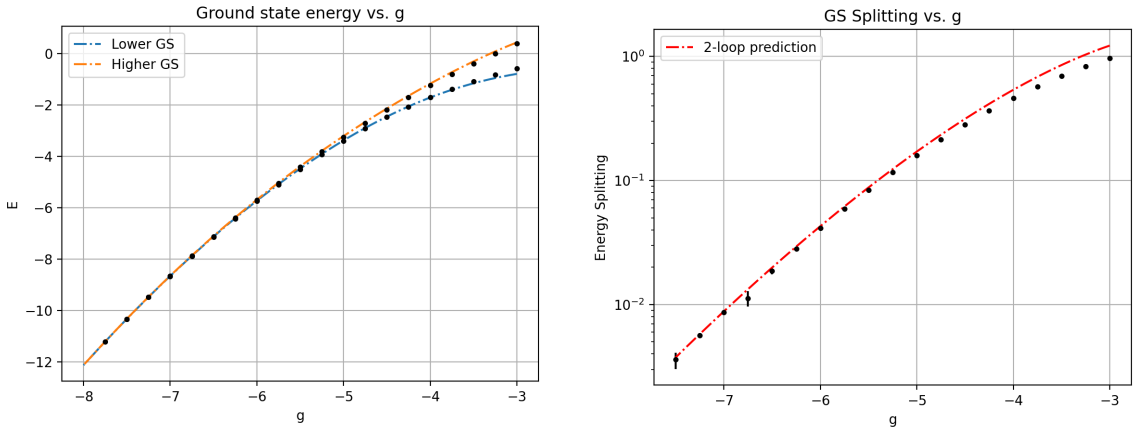

Figure 3.5: Comparison of non-perturbative formulae to bootstrap data in the double well: left, dependence of (split) ground state on g; right, dependence of ground state splitting ΔE_0 on g. Bootstrap data are black points, predictions are dotted lines. Note the second plot is on a logarithmic scale.

Nakayama considers this for the double-well potential $V(x) = -x^2 + x^4$. They performed a numerical bootstrap checking positivity of the Hamburger matrix, which takes the form

$$M^{(K)} = \begin{bmatrix} 1 & 0 & \langle x^2 \rangle & \cdots & \langle x^{K-1} \rangle \\ 0 & \langle x^2 \rangle & & & \vdots \\ \langle x^2 \rangle & & \ddots & & \vdots \\ \vdots & & & \ddots & 0 \\ \langle x^{K-1} \rangle & \cdots & \cdots & 0 & \langle x^{2K-2} \rangle \end{bmatrix}.$$

The result of checking positivity of this matrix in the $\{E, \langle x^2 \rangle\}$ plane is shown in Fig. 3.6. The result is that for energies $E > 0$, which live above the double well, checking positivity of the Hamburger matrix works well to constrain the search space. At successive depths K the allowed region of parameter space shrinks to a small envelope around the classical $E, \langle x^2 \rangle$ curve. This was the result of Nakayama, who noted that the large 'peninsula' for $E < 0$ persists at higher depths of the Hamburger matrix. They conjectured that the peninsula was a feature of the MCE bootstrap, not a bug.

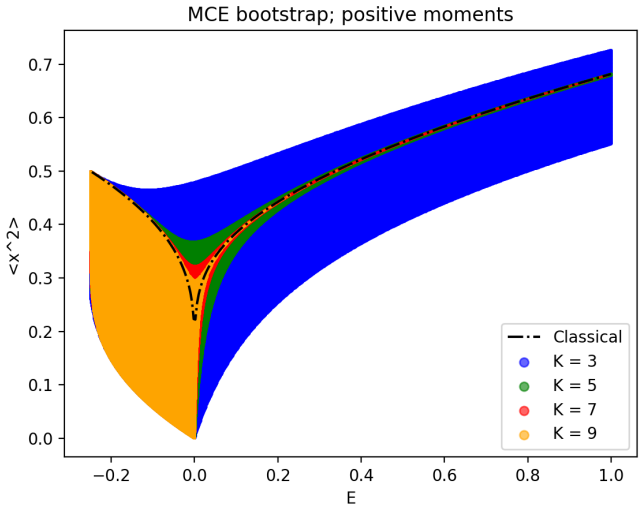

Figure 3.6: Allowed parameter values for various depths K of the Hamburger matrix and classical relation pictured. For $E < 0$ a large 'peninsula' appears.

This would be surprising: the expectation should be that the exact allowed region ($K \to \infty$) in the MCE bootstrap is exactly the classical curve relating $E, \langle x^2 \rangle$—since every member of the ensemble is just the classical system. This is apparently not the result obtained using just the Hamburger matrix.

However, there is a large family of constraints that are missing. For any energy $E < 0$, the classical particle spends no time at the origin. In other words, given an energy $E < 0$, the associated classical motion has zero support as $x \to 0$ in phase space. As a result, all (classical) inverse moments of x are finite. This is to say that when $E < 0$, the following integral over the classical motion converges for $\forall n \in \mathbb{Z}$:

$$\langle x^n \rangle_{\text{cl}} = \frac{1}{T} \oint \frac{x^n}{\sqrt{E + x^2 - x^4}} \, dx,$$

where the integral here is over an orbit of the classical motion defined by the turning points $x_i : -x_i^2 + x_i^4 = E$. Since all the inverse moments are well-defined, we may consider operators $\hat{\mathcal{O}}_I = \sum_{n=-K}^{K} c_n x^n$ acting on states. This will descend to a positivity constraint on a new Hankel matrix M_I which contains inverse as well as positive moments. The

$K \times K$ matrix M_I will take the form

$$M_I^{(K)} = \begin{bmatrix} \langle x^{-(K-1)} \rangle & \langle x^{-(K-2)} \rangle & \cdots & \langle x^{-1} \rangle & 1 \\ \langle x^{-(K-2)} \rangle & \langle x^{-(K-3)} \rangle & & & \langle x \rangle \\ \vdots & & \ddots & & \vdots \\ \langle x^{-1} \rangle & & & \ddots & \langle x^{K-2} \rangle \\ 1 & \langle x \rangle & \cdots & \langle x^{K-2} \rangle & \langle x^{K-1} \rangle \end{bmatrix}.$$

Norm positivity $\langle \hat{\mathcal{O}}_I^\dagger \hat{\mathcal{O}}_I \rangle \geq 0$ implies that $M_I^{(K)} \succeq 0$ for all depths K. This becomes an additional positivity constraint which is well-defined for $E < 0$.

To integrate this into the bootstrap, we simply use the recursion (3.21) to generate negative moments, using the parameters $E, \langle x^2 \rangle$ to initialize as in the previous subsection. Then we can carry out a bootstrap checking only the Hamburger positivity constraint for energies $E > 0$ as before, but checking positivity of both the Hamburger matrix and the new matrix M_I for energies $E < 0$. The result, shown in Fig. 3.7, conforms to expectations: the bootstrap converges everywhere to a small envelope surrounding the classical curve. This simply shows that to get the bootstrap to work properly, one needs to consider all physically allowable constraints. By including these inverse moments one can cut down on the peninsula of allowed parameter space. In our study of bootstrapping half-line problems, we will see the same type of behavior, where extra positivity constraints can assist in removing large regions of the search space which are physically inaccessible due to the boundary conditions.

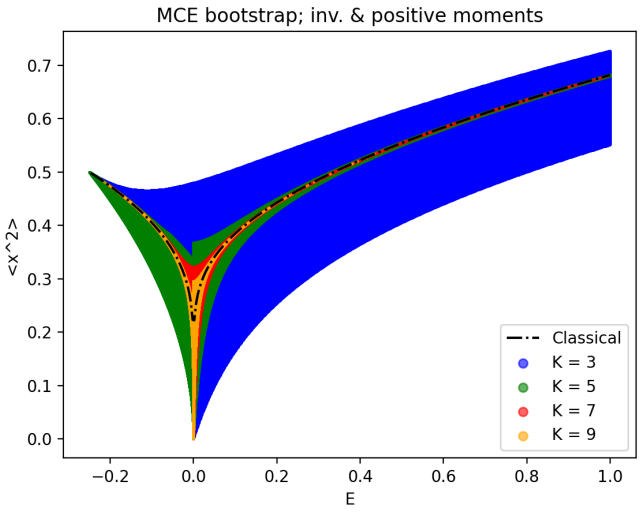

Figure 3.7: 'Fixed' MCE bootstrap for various depths K. Including the new positivity constraint removes the 'peninsula' and the bootstrap converges everywhere to the classical curve.

3.3 A semidefinite programming algorithm for the bootstrap

The bootstrap for one-dimensional Schrödinger problems relies on generating a recursion for the positional moments $\langle x^n \rangle$ from the two constraints

$$\langle [\hat{H}, \hat{\mathcal{O}}] \rangle = 0; \quad \langle \hat{H}\hat{\mathcal{O}} \rangle = \langle \hat{H} \rangle \langle \hat{\mathcal{O}} \rangle = E \langle \hat{\mathcal{O}} \rangle, \tag{3.22}$$

which assume that the state is an eigenstate of energy E. The goal is to either reject or accept a putative value for E as physically allowable at a given depth K of the recursion using the positivity/unitarity constraints on the moment matrix.

Previously, we had taken a grid search approach where the search space consisted of the energy E and various other positional moments. By brute-force checking values, we could generate moment sequences at any point in the state space and check to see if the positivity constraint on M was satisfied. This approach was mildly assisted by using the

classical physics to test a specific region of the search space.

However, this naive approach scales terribly with the dimension of the search space. For high degree potentials, where many positional moments are needed to initialize the recursion, a grid-search algorithm is dimensionally doomed. We therefore need some other way to formulate the problem in order to handle the general polynomial potential on $\mathbb{R}$.

Since the fundamental test of points in the search space is positive semidefiniteness of a matrix, it is tempting to view the problem through the lens of semidefinite programming. However, if E is a variable determined from the other ones (i.e. other moments $\langle x\rangle, \langle x^2\rangle$, etc), the latter constraints in (3.22) are nonlinear in the moments $x_n \equiv \langle x^n\rangle$ and hence non-convex. One may choose to omit the nonlinear constraints and be left with a linear problem; this is the route in [37, 70], where one minimizes the value of the energy given some positivity constraints. The tradeoff is that one is only able to solve for the ground state in the absence of the nonlinear constraints. This will be the problem of interest for us when we consider the physics of spin chains in the final chapter.

An alternative approach to linearization to the one we take here is to apply a convex relaxation of the non-linear constraints in (3.22). In this context, the relaxation is done by turning the equality into an inequality: instead of enforcing $\langle \hat{H}\hat{\mathcal{O}}\rangle = \langle \hat{H}\rangle\langle \hat{\mathcal{O}}\rangle$, one only requires $\langle \hat{H}\hat{\mathcal{O}}\rangle - \langle \hat{H}\rangle\langle \hat{\mathcal{O}}\rangle \geq 0$, which is a semidefinite constraint on a diagonal matrix. This method has been applied in the study of the large N bootstrap [99, 69] to relax non-linearities in the Yang-Mills (or matrix model) loop equations that arise from large-N factorization. We comment that the large N factorization of expectation values is essentially analogous to the eigenstate constraint we use here; both large-N physics and quantum eigenstates essentially behave 'classically' compared to other states in the theories in question.

We take a different approach. A simple way to linearize the problem is to fix the

value of energy E and test if E is an allowed value. At each fixed value of the energy the recursion is linear in the x_n. Consider an arbitrary potential of even degree d:

$$V(x) = \sum_{n=1}^{d} a_n x^n. \tag{3.23}$$

The recursion relates moments x_n with $n \geq d$ to lower moments. For $m \geq 0$ it may be written

$$x_{d+m} = \frac{1}{2a_d(d+2m+2)} \Big[4(m+1)Ex_m + m(m^2-1)x_{m-2} - 2\sum_{n=1}^{d-1}(n+2m+2)a_n x_{n+m} \Big]. \tag{3.24}$$

Generically, initializing the recursion requires the energy as well as the first $d-1$ moments, with $x_0 = 1$.

From the moments we construct the $K \times K$ Hankel matrix with elements $M^{(K)}_{ij} = x_{i+j}$, where $0 \leq i, j \leq K-1$. The unitarity constraint is that $M \succeq 0$. Before applying the recursion, we may write $M^{(K)}$ as a linear function of the first $2K-2$ moments:

$$M^{(K)} = \sum_{m=0}^{2K-2} x_m \mathcal{B}_m \succeq 0, \tag{3.25}$$

where the matrices $\mathcal{B}_m$ define the Hankel structure:

$$\mathcal{B}_m = \begin{cases} 1 \text{ if } i+j = m,\ 0 \leq i, j \leq K-1, \\ 0 \text{ otherwise.} \end{cases} \tag{3.26}$$

The recursion (3.24) relates the x_m with $m \geq d$ to those with $m < d$; it thus defines

another set of symmetric $K \times K$ matrices $F_n(E)$ by the equality

$$\sum_{m=0}^{2K-2} x_m \mathcal{B}_m = M^{(K)} = \sum_{n=0}^{d-1} x_n F_n(E), \tag{3.27}$$

where the x_n for $1 \leq n \leq d-1$ will function as variables for the semidefinite optimization problem. Without proof, we believe that this method depends crucially on the fact that as one increases K, the number of optimization variables stays constant while the matrix elements of the $F_n(E)$ become increasingly complicated rational functions of the energy.

As $K \to \infty$, the Hankel matrix $M^{(K)}$ defined above will be positive definite only for E in the spectrum of $\hat{H}$: we have seen this in the previous examples and it is expected to be true generally, though no rigorous proof of this claim exists. Finite K is a truncation of an infinite set of constraints. We expect the Hankel matrix to be positive definite in some disjoint set $S_K \subset \mathbb{R}$ which strictly contains the spectrum of $\hat{H}$. Moreover, the x_n are uniquely determined by E. Numerical experiments, in [70] and our own work, have shown that the convergence to the eigenvalues (and the moments) is exponentially fast in the size of the truncation. Furthermore, $S_{K+1} \subset S_K$, etc. This weak convergence property allows efficient search strategies in a bootstrapping algorithm.

The main problem for the naive bootstrap algorithm of previous sections is that a search is done both in E and in the moments. Our present goal is to find an optimal value of the moments for fixed energy E rather than doing a blind search. Moreover, if the problem fails to find a solution of the constraints, we want a numerical measure of how far we are from satisfying the constraints. This semidefinite algorithm addresses these issues so that in the end one is left only with a scan over energies E.

The bootstrap as an optimization problem

How do we test if a symmetric matrix $M^{(K)}$ is positive? If the matrix is Hermitian, then the condition of being positive (definite) is equivalent to the minimal eigenvalue of $M^{(K)}$ being positive. We test positive definiteness by considering the minimal eigenvalue of $M^{(K)}$ as a function of the primal variables x_i. Define an optimization problem

$$\text{maximize } \lambda_{\min}\left(M^{(K)}(x_i, E)\right). \tag{3.28}$$

If the optimal value is negative, the energy value E can be safely excluded from the set S_K. The goal is to solve this optimization problem for a range of energies and to thereby determine the set S_K. The algorithm proceeds by searching this set at depth $K+1$, and iteratively converges to the spectrum (or a subset thereof).

The problem (3.28) defines an objective function which is highly nonlinear in the variables x_i. However, we know the problem of eigenvalue extremization to have an equivalent formulation as a SDP with linear objective [86]. We can write down a problem equivalent to (3.28) in SDP form, using the decomposition (3.27):

$$\begin{aligned} &\text{maximize} && t, \\ &\text{subject to} && \textstyle\sum_{n=0}^{d-1} x_n F_n(E) - tI \succeq 0, \end{aligned} \tag{3.29}$$

where the slack variable t has been introduced to linearize the objective. This is an SDP in linear matrix inequality (LMI) form with d optimization variables $\mathbf{x} = (t, x_1, ..., x_{d-1})$. [2] Allowed energies correspond to optima of this program where t is positive.

Notice that even if the energy is not physically allowed, the optimization problem will find a solution: a sufficiently large negative t will always make it possible to satisfy

[2] In some SDP solvers, the algorithm must be written as a minimization problem. This is done by minimizing $-t$ instead.

the positive matrix constraint. We thus obtain for the K we are testing a value t that is positive or negative and an optimal value of the moment variables. The maximum t, which we label $t^\star$, is a measure of how close to success we are. As we scan over E (at fixed K), $t^\star$ will depend continuously on E and it is possible to estimate when it will become positive by using e.g. the Newton method. It thus serves not only as a diagnostic of failure, but it also gives a way to scan intelligently in E.

For problems in higher dimensions $d \geq 2 + 1$, the constraints (3.22) are not enough to determine recursively all the moments from a finite search space. Conceptually, there is no obstacle to proceed in these higher dimensional setups. The main issue would be understanding the optimal way to eliminate variables and how different truncation schemes might perform. We will encounter these exact issues when studying $1 + 1d$ quantum spin chains.

The SDP algorithm

With the SDP formulation, the bootstrap algorithm proceeds as follows. Given a potential V, take an initial set of energy values $S_0 = \{E_i\} \subset \mathbb{R}$. For each fixed value of the energy, solve the SDP (3.29) at some initial depth K_0. Energies E_i for which the optimum $t^\star$ is positive form the set S_{K_0}, which serves as the search set at depth $K' > K_0$. Iterating this procedure will result in a set of intervals within S_0. These intervals define sharp bounds on the exact spectrum of $\hat{H}$, in the sense that the bounds are rigorous and can only shrink as K increases.

A persistent issue with the bootstrap is the rapid growth of the matrix elements. The magnitude of the largest matrix entries scales super-exponentially with K. For example, in the harmonic oscillator, $\langle x^n \rangle \sim \Gamma(n/2)$ in eigenstates. As a result, using single or double precision floats results in serious numerical error after $K \sim 10$. Similar issues were encountered in the conformal bootstrap program, which necessitated the use of an

arbitrary-precision SDP solver [6]. We found the same to be necessary in order to obtain comparably high precision to finite-element methods.

To numerically solve the problem, we used SDPA-GMP [100], a primal-dual interior point SDP solver built on the GMP (GNU multiple precision) arithmetic library. The SDP was set up in `Python`, where the recursion was computed and used to generate the $F_n(E)$ for an array of energy values. This program wrote input and output files for SDPA-GMP, which solved the optimization problem (3.29) for each considered value of E. These results were read back into `Python`, generically resulting in intervals of energy where positivity was satisfied. These intervals were used to generate new, finer resolution arrays which were fed back into the algorithm just described. We worked with ~ 60 digit (200 significant bits) precision. The code implementing this algorithm is publicly available on GitHub.

The main benefit of the SDP approach is that we can search a very high dimensional space very efficiently. With the naive algorithm, we were constrained to potentials of degree ≤ 4 due to the brute-force nature of the algorithm. Now, potentials of essentially arbitrary degree can be solved in comparable time.

3.3.1 Example: a high-degree potential

To show that this SDP method is able to obtain high-precision results for excited states in a search space of large dimension, we considered as a simple example the degree 8 potential

$$V(x) = \frac{1}{2}x^2 - x^4 + \frac{1}{8}x^8. \tag{3.30}$$

This has 8 primal variables (including t); although since the potential is even, the number effectively reduces to 4 primal variables. We search over the energy range $[0, 15]$ which we know to contain the first five excited states. We started the search at matrices of size

$K_0 = 10$ and terminated the search once all detected levels reached 6 significant figures; this required up to $K = 31$.

At each depth, the algorithm requires us to look for the negative values of the objective function of (3.29). We can visualize the convergence by plotting $\log(|t^\star|)$, where $t^\star$ is the optimal value, versus the fixed energy E. Inverted 'spikes' in this plot show the zero crossings. As the intervals of positive t shrink with increasing K, two spikes seem to join around the exact value of the eigenstate energy, as shown in Fig. 3.8. The structure is always a double spike structure around each allowed value: two spikes can become so close to each other that the plot can no longer distinguish them. The numerical

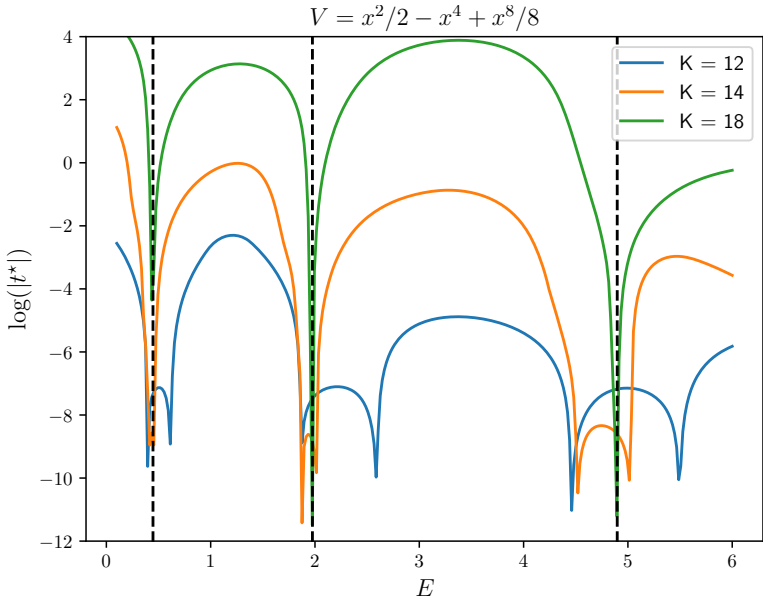

Figure 3.8: The (log of the) objective function evaluated over a range of energies for the potential (3.30). Exact energies (computed in *Mathematica* by FEM) shown as dashed lines. Results shown for $K = 12, 14, 18$.

estimates for the eigenenergies are shown in Table 3.1. This level of precision is beyond machine precision in *Mathematica*, though its implementation of a FEM eigensolver works much faster for this class of 1d problems. Specifically, evaluation of Mathematica's `NDEigensystem` to generate lowest 5 eigenenergies of the potential (3.30) took $\sim$ 1.54

n	Bootstrap	Uncertainty	*Mathematica* FEM
1	0.446987(5)	$\pm 2.86 \cdot 10^{-7}$	0.44698(8)
2	1.975515(7)	$\pm 2.06 \cdot 10^{-7}$	1.9755(2)
3	4.897587(3)	$\pm 2.55 \cdot 10^{-7}$	4.8975(9)
4	9.05144(00)	$\pm 6.13 \cdot 10^{-7}$	9.0514(4)
5	14.10082(3)	$\pm 1.76 \cdot 10^{-6}$	14.100(8)

Table 3.1: Energies for the potential (3.30) at $K = 30$ and rigorous bounds on absolute uncertainty, compared to the finite-element method (FEM) results.

seconds. Our implementation of the SDP bootstrap algorithm in *Python* took ~ 876 seconds to run from $K = 10$ to $K = 30$, generating the results above, and did not utilize any intelligent search strategy for zero crossings. The time for evaluation increases roughly exponentially in K, from ~ 12 sec for $K = 10$ to ~ 94 sec at $K = 30$.

As an additional point of performance comparison, one can also numerically diagonalize the Hamiltonian by writing it in the number (ladder operator) basis and truncating. This is a fundamentally variational method, so convergence will be monotonically downward toward the exact eigenvalues. To reproduce the precision of the bootstrap for this potential, this method required diagonalizing a matrix of size ~ 330, taking ~ 35 sec.

The data from each depth K is a set of valid energy intervals. It has been repeatedly observed that the widths of these intervals decreases exponentially in K. We find that result borne out again in Fig. 3.9. The convergence is exponential and uniform in slope across energy levels, at least asymptotically in K.

In the regime of constant exponential growth of Fig. 3.9, the approximate slope is ≈ -0.83; the average width of the allowed intervals decreases like $\bar{w}(K) \propto e^{-0.83K}$. Hence at $K' > K$, the ratio of widths goes like $e^{-0.83(K'-K)}$. Obtaining one more decimal digit of precision requires changing the size of the truncation to $K' = K + \log(10)/0.83 \approx K + 3$. This shows the power of the bootstrap approach: the number of significant digits scales approximately linearly with the depth K. This algorithm can be used to determine the

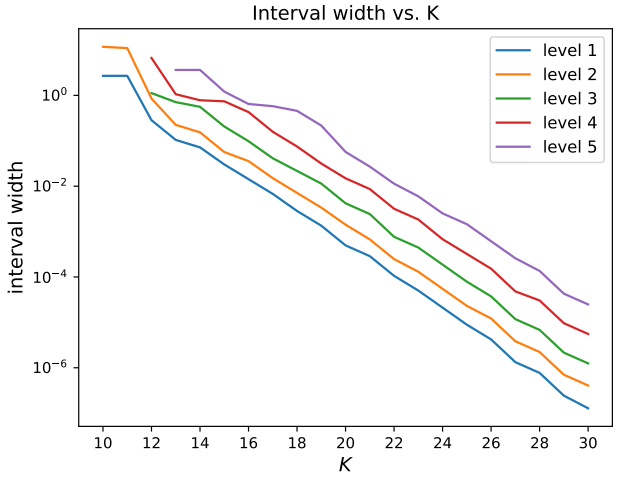

Figure 3.9: Width of allowed energy intervals vs. K, on a logarithmic scale.

energy spectrum of any real-line polynomial potential.

In the following chapter, we will study bootstrapping problems on domains with boundary, and will eventually adapt this algorithm to incorporate information about the boundary conditions of the state. The study of domains with boundary will require us to revisit many aspects of the bootstrap procedure laid out for real-line problems thus far.

Chapter 4

Bootstrap methods on domains with boundary

In its simplest form, the quantum mechanical bootstrap consists of two steps: given some Hamiltonian for a system, compute moment sequences associated to its eigenvectors, then check if those moment sequences are valid. How can we check if a moment sequence is 'valid'? Recall that this question is answered by the so-called classical moment problems. Given some interval $I \subseteq \mathbb{R}$, the moment problems address the question "given a real sequence a_n, does there exist a non-decreasing measure μ supported on I such that $a_n = \int_I x^n d\mu$?"

The three classical moment problems are those of Hamburger, Stieltjes, and Hausdorff, corresponding to the intervals $\mathbb{R}, \cong [0, \infty)$ and $[0, 1]$ respectively [101]. These are the three topological types of one-dimensional intervals, and each lead to slightly different positivity conditions on Hankel matrices, introduced and proven in Chapter 2.

For problems on the real line, we have seen the structure of the Hamburger problem: moment sequences $\langle x^n \rangle$ corresponding to positive measures on $\mathbb{R}$ are associated to a positive-semidefinite Hankel matrix M constructed as $M_{ij} = \langle x^{i+j} \rangle$. In this section, we

will turn our attention to problems on domains with boundary: the real half line and the real interval. Recall that the moment problem on the half line is addressed by the following theorem of Stieltjes:

Stieltjes, 1894. Let $\{a_n\}$ be a sequence of real numbers. The a_n correspond to the moments of a non-decreasing (normalizable) measure μ on , i.e. $a_n = \int_0^\infty r^n \, d\mu$, if and only if the matrices with elements $M_{ij} = a_{i+j}$, $\tilde{M}_{ij} = a_{i+j+1}, 0 \leq i, j \leq K-1$ are positive semi-definite for all K.

The notable difference between this result and the result for the moment problem on $\mathbb{R}$ is the positivity condition on the second matrix $\tilde{M}$, which introduces new constraints on the moments of half-line wavefunctions. However, there remain aspects of the bootstrap for half-line problems which are not obviously addressed by the moment recursion and positivity checks introduced thus far—essentially, the role and determination of boundary conditions.

To follow, we introduce and complete the half-line bootstrap for the hydrogen Hamiltonian. After, we address the Airy model. The results from the Airy bootstrap are intriguing as they betray some implicit assumptions about boundary conditions in the bootstrap. This naturally leads to more technical discussion of the data that we supply the bootstrap and allows us to generate the terms required to specify boundary conditions.

4.1 The hydrogen model

To begin, consider the hydrogen model with (radial) Hamiltonian

$$\hat{H} = \frac{1}{2}p_r^2 + \frac{\ell(\ell+1)}{2r^2} - \frac{1}{r}. \tag{4.1}$$

Here p_r obeys $[p_r, r] = -i$. As an aside, we invite the reader to properly define the radial momentum as a self-adjoint differential operator! We are working with unit mass and $\hbar = 1$. We have the general bootstrap eigenstate constraints

$$\langle[\hat{H}, \hat{\mathcal{O}}]\rangle = 0; \quad \langle\hat{H}\hat{\mathcal{O}}\rangle = \langle\hat{H}\rangle\langle\hat{\mathcal{O}}\rangle = E\langle\hat{\mathcal{O}}\rangle. \tag{4.2}$$

From this Hamiltonian and these constraints we obtain a recursion relation for the moments as before:

$$0 = 8mE\langle r^{m-1}\rangle + (m-1)[m(m-2) - 4\ell(\ell+1)]\langle r^{m-3}\rangle + 4(2m-1)\langle r^{m-2}\rangle. \tag{4.3}$$

The $m = 1$ case is the virial theorem, which gives the $\langle r^{-1}\rangle$ moment in terms of the energy:

$$E = -\frac{e^2}{2}\left\langle\frac{1}{r}\right\rangle. \tag{4.4}$$

This recursion relation closes given just the energy E; the search space is one dimensional. From a given energy E we can generate a moment sequence $\{\langle r^k\rangle\}_0^N$ for any $N > 0$.

Following again the naive algorithm, we choose values of the energy E, generate a moment sequence of some length, and apply the positivity conditions of the Stieltjes moment problem for a matrix of finite size K. This allows us to rule out energy values which do not correspond to eigenstates. The results, for different sizes K of the Hankel matrices, is shown in Fig. 4.1. For intervals which form around a given energy level, we can plot the convergence with K on a logarithmic plot and see that it is exponential in the matrix size K, as in Fig. 4.2. The flat portions which begin each curve represent the depths before which a given interval becomes disjoint. The addition of the second Stieltjes matrix is crucial for getting the bootstrap to pick up the $\ell = 0$ states, which are undetectable by the bootstrap if only the Hamburger positivity condition is used.

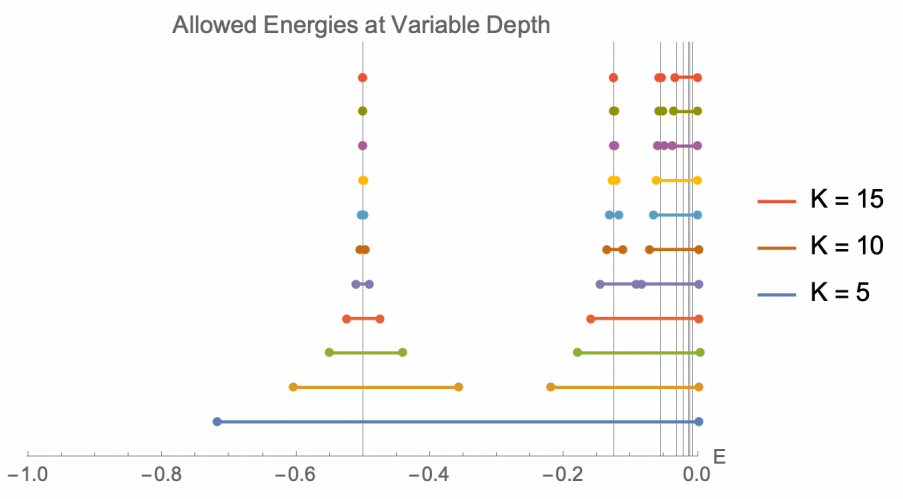

Figure 4.1: Allowed energies for the hydrogen bootstrap with $\ell = 0$, for sizes of Hankel matrix $K = 5, \ldots, 15$. Exact energies are in gray: in our units, they are $E_n = -1/2n^2$ for $n \geq \ell + 1$.

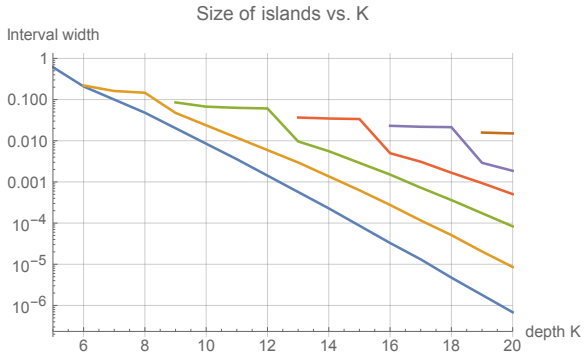

Figure 4.2: Interval width versus matrix size K on a logarithmic axis, with $\ell = 0$. Each line represents an interval which forms around an exact energy level and shrinks as K increases.

4.1.1 $\ell < 1$ and strange states

An outstanding question about the quantum mechanical bootstrap is what data it truly receives about the problem. For instance, the bootstrap is completely agnostic about the quantization of the angular momentum parameter ℓ, provided one forgets about the three-dimensional origin of the model. A spectrum exists for the radial Hamiltonian (4.1) for any (positive) value of the parameter ℓ.

When the azimuthal parameter ℓ is quantized, the solutions to the radial hydrogen problem are Laguerre polynomials with exponential decorating factors. Let us relax the quantization condition and consider the equation

$$-\frac{1}{2}f''(r) + \left[\frac{\ell(\ell+1)}{2r^2} - \frac{1}{r}\right] f(r) = (-E)f(r) \tag{4.5}$$

for arbitrary $0 < \ell < 1$ and with $r > 0, E > 0$. Multiplying this by r^2 brings it into a form similar to that of the hypergeometric differential equation. The general solution is expressed in terms of Whittaker's confluent hypergeometric functions:

$$f(r) = \alpha M_{k,\mu}(z) + \beta M_{k,-\mu}(z),$$

where the parameters are:

$$k = \frac{1}{\sqrt{2E}}, \qquad \mu^2 = (\ell + \frac{1}{2})^2, \qquad z = 2r/k.$$

Another set of solutions is given by the Whittaker M and W functions, but the basis above will work well for our purposes.

We require that the solution $f(r)$ is in $L^2(\mathbb{R}_+)$. This requires that solutions vanish at infinity. For real $z \to \infty$, the Whittaker M-function has leading order asymptotic expansions [102]

$$M_{k,\pm\mu}(z) \sim \frac{\Gamma(1 \pm 2\mu)}{\Gamma(\frac{1}{2} \pm \mu - k)} \mathrm{e}^{\frac{1}{2}z} z^{-k}. \tag{4.6}$$

The M-function diverges exponentially at infinity unless the gamma function in the denominator diverges as well. This would require

$$\frac{1}{2} \pm \mu - k = -n, \quad \text{where} \quad n \in \mathbb{N}. \tag{4.7}$$

Keeping this in mind, we can examine the behavior of these functions near the origin. Not all functions in the Hilbert space are finite at 0—they need only be normalizable. This means that we may have $f(r) = cz^s[1+\hat{\mathcal{O}}(z)]$ for $s > -1/2$ and still have a function which is locally L^2 at the origin. As $z \to 0$, the M-function behaves as

$$M_{k,\pm\mu}(z) = z^{\frac{1}{2}\pm\mu}[1 + \hat{\mathcal{O}}(z)]. \tag{4.8}$$

For $\mu > 0$ the $(+)$ branch is zero at the origin and is acceptable. If $1/2 < \mu < 1$, the $(-)$ branch is square-integrable but infinite at $r = 0$, which is also acceptable. But if $\mu \geq 1$, the $(-)$ branch will be non-normalizable.

The condition (4.7) is exactly a quantization condition. Let us consider first the $(+)$ branch. Rewriting in terms of physical parameters, it says that

$$1 + \ell + n = k = \frac{1}{\sqrt{2E}}$$

for some non-negative integer n. The physical energy is $E_{ph} = -E$ and is thus quantized by principal number $n > 0$ as

$$E_{ph}^{(+)} = -\frac{1}{2(n+\ell+1)^2}, \tag{4.9}$$

which is exactly the same as the classical rule for integral ℓ, simply continued to fractional values (note that n now starts at 0). For the $(-)$ branch of (4.7), we find the quantization rule

$$E_{ph}^{(-)} = -\frac{1}{2(n-\ell)^2} \tag{4.10}$$

for $n \geq 0$. Recall that this only corresponds to normalizable eigenfunctions in the regime $0 < \ell < 1/2$. Despite their normalizability, they are infinite at the origin. As a result

there are no inverse radial moments $\langle r^{-p} \rangle$, $p > 0$ which are defined for these solutions.

Bootstrapping $0 < \ell < 1$

Running a bootstrap for values $0 \leq \ell \leq 1$ gives an interesting regime in which to examine how the two Stieltjes matrices affect convergence and to see the signatures of the Whittaker functions. Fig. 4.3 displays bootstrap data for $K = 10$ at various values of ℓ, showing the allowed energy intervals vertically and checking only the Hamburger matrix $M_{ij} = \langle r^{i+j} \rangle$. When $\ell = 0$, checking the Hamburger matrix alone does not disallow

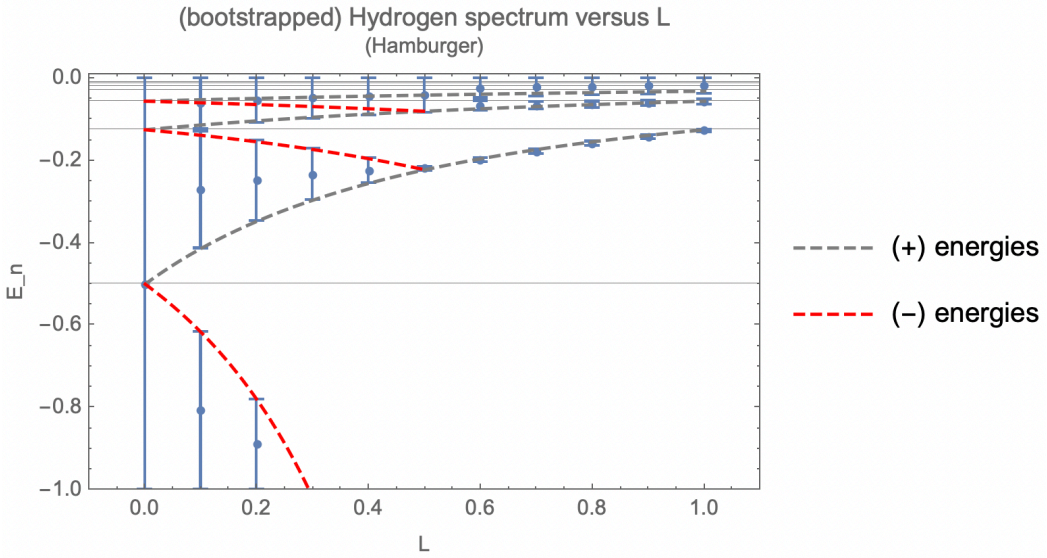

Figure 4.3: $K = 10$ bootstrap for various values of ℓ, using only the matrix $M_{ij} = \langle r^{i+j} \rangle$; allowed regions are the vertical blue intervals. One can see that convergence grows better as ℓ increases. Exact (hydrogen) energies in gray; Whittaker predictions in dashed gray, red.

any energy values. As ℓ increases to fractional values, the allowed intervals shrink and the positions of the "excited" intervals shift upwards, in accordance with perturbative expectations. Once $\ell = 1$ the Hamburger matrix works decently to bootstrap the excited states. Note that in the $\ell < 1/2$ regime, the bootstrap accepts any energy in between the two quantization rules, essentially detecting a superposition state of each branch of

eigenstates.

When we run the same experiment but use the positivity checks for both Stieltjes matrices (i.e. now including $\tilde{M}_{ij} = \langle r^{1+i+j} \rangle$), some interesting results emerge. First, the $\ell = 0$ states appear. There is a also a new, disjoint series of intervals that the bootstrap detects which decrease in energy as ℓ increases. These are precisely the states

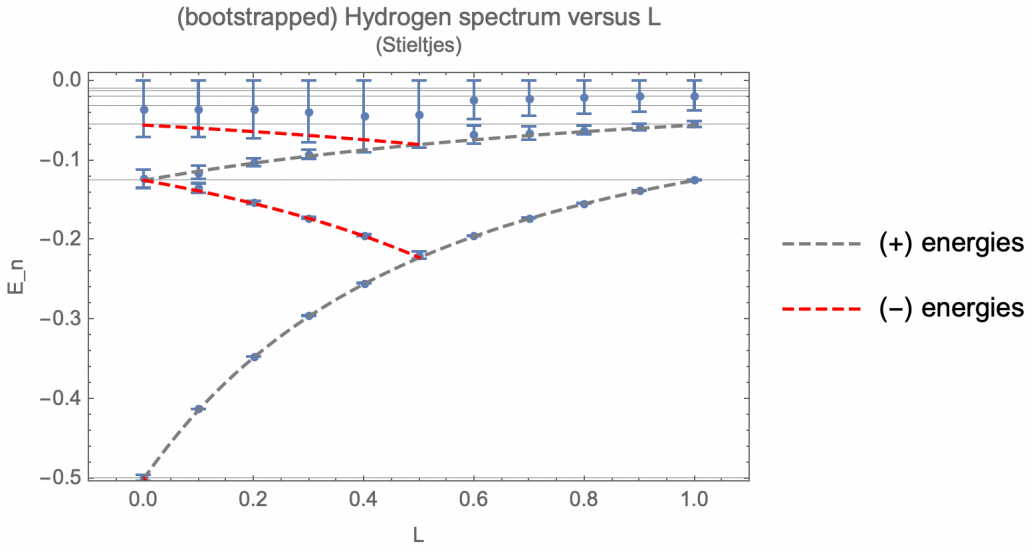

Figure 4.4: $K = 10$ bootstrap with both Stieltjes matrices $M, \tilde{M}$. There is a set of "states" which decrease in energy as ℓ increases, only while $0 \leq \ell \leq 1/2$.

with energies (4.10), which are infinite at the origin. We can eliminate them by adding another matrix to our positivity constraints.

Consider the matrix with elements $M'_{ij} = \langle r^{i+j-1} \rangle, 0 \leq i, j \leq K-1$. For any eigenstate accessible through the recursion, the $\langle r^{-1} \rangle$ moment is well-defined and proportional to the energy of the state by the virial theorem (this is implied by e.g. (4.3) with $m = 1$). Positivity of M' is thus another necessary condition for moment sequences derived from physical eigenstates of the hydrogen Hamiltonian.[1]

Finally, we can carry out a bootstrap where we check positivity of both Stieltjes

[1]The physical requirement here is that e.g. the moment $\langle V \rangle_\psi$ is well-defined for eigenstates ψ; this is not mathematically required for the pure eigenvalue problem.

matrices $M, \tilde{M}$ in addition to the matrix M' just introduced. Shown in Fig. 4.5, adding this additional positivity constraint eliminates the descending states visible for $\ell < 1/2$. While demanding positivity of this final matrix M' is reasonable within the context of

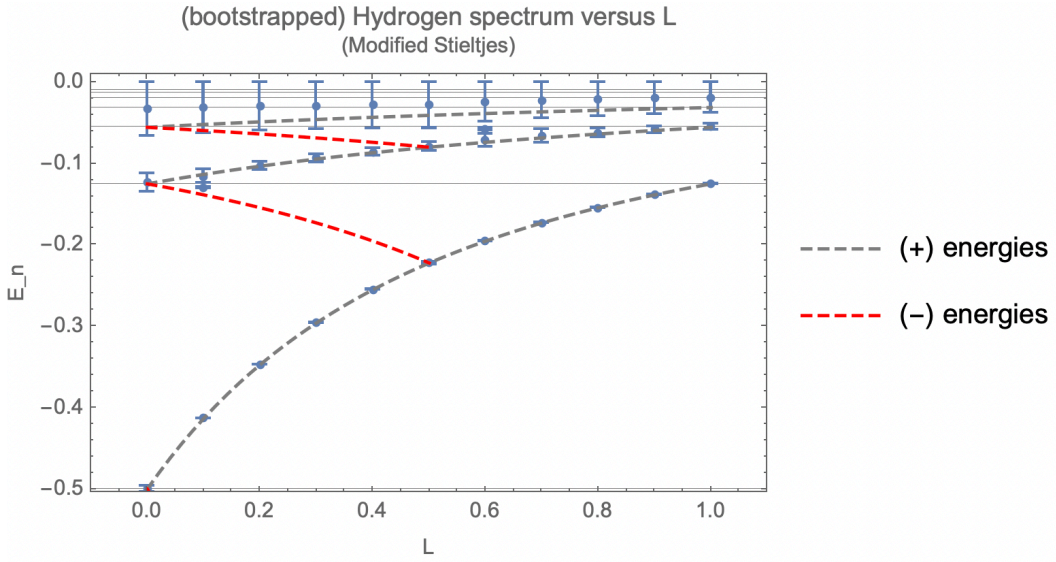

Figure 4.5: $K = 10$ bootstrap checking the three matrices $M, \tilde{M}, M'$. Spectrum flows upward as ℓ increases, as expected from perturbation theory. The bootstrap now does not detect the states (4.10).

quantum mechanics, from the Stieltjes problem point of view these states did correspond to acceptable probability measures. By enforcing that the first inverse moment $\langle r^{-1} \rangle$ is defined, we were able to impose a "soft" boundary condition on the state.

4.2 Bootstrapping the half line

The hydrogen problem shows that bootstrapping on the half line is not quite the same as bootstrapping on $\mathbb{R}$. Let us consider another problem from undergraduate quantum mechanics: the linear potential. This model is nice because like hydrogen, the recursion

for the model may be initialized by the energy E alone:

$$\langle x^m \rangle = \frac{1}{2m+1}\left[2mE\left\langle x^{m-1}\right\rangle + \frac{1}{4}m(m-1)(m-2)\left\langle x^{m-3}\right\rangle\right]. \tag{4.11}$$

We consider this problem on the half line, and carry out an algorithm identical to that of the hydrogen bootstrap, using the Stieltjes positivity check. The result is a bootstrap which converges nicely to the exact energies as computed by standard numerical techniques, as in Fig. 4.6. Notably, the bootstrapped spectrum corresponds to the exact energies of the system with *Dirichlet* boundary conditions for the wavefunctions: $\psi(0) = 0$. Why has the bootstrap selected this boundary condition versus a mixed or Neumann condition?

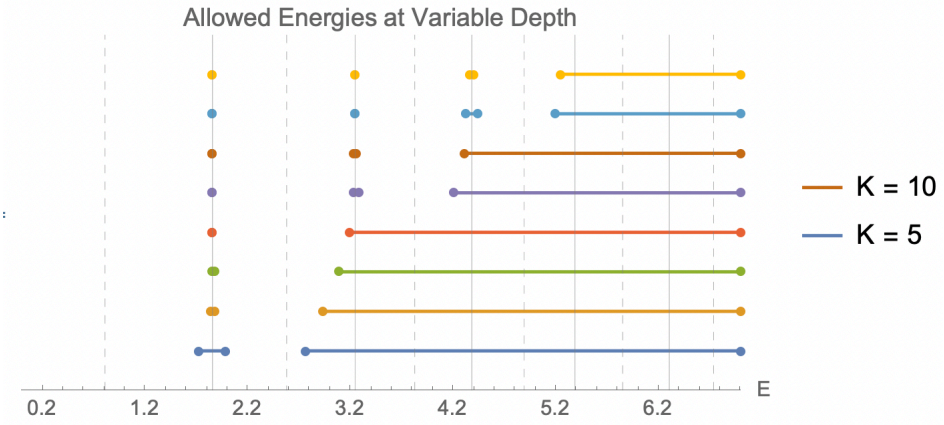

Figure 4.6: Numerical bootstrap for depths $5 \leq K \leq 12$ (increasing vertically) for the Airy model/linear potential. Intervals are energy values allowed at a given depth. Dashed vertical lines are the 'exact' energies for Neumann ($\psi'(0) = 0$) states and solid vertical lines are the Dirichlet ($\psi(0) = 0$) energies.

The answer is that because we have failed to specify boundary conditions at the origin, the recursion (4.11) is incomplete. The issue of boundary conditions in the bootstrap is subtle. The half line provides a good testing ground for dealing with the boundary conditions, as it is really not *a priori* clear what to do about the origin.

It turns out that the half line is rife with issues as a quantum mechanical system. We will introduce these issues and see that they are essentially related to questions of the domains of certain operators. In order to find a self-adjoint Hamiltonian, we will need to define some boundary conditions. We will see how these boundary conditions enter the bootstrap; there is quite a nice story about their origin. We will then revisit the linear potential.

4.2.1 Quantum mechanics on the half line

For simplicity, we will assume that "doing quantum mechanics" on the half line means solving the eigenvalue problem

$$-\frac{d^2\psi}{dx^2} + V(x)\psi = E\psi \tag{4.12}$$

for functions $\psi(x) \in L^2(\mathbb{R}_+)$ on the half line $x \geq 0$ and their eigenvalues E. In the usual quantum mechanical treatment, one would say that the Hamiltonian is the operator

$$\hat{H} = p^2 + V(x), \tag{4.13}$$

where the operators x, p obey the canonical relation $[x, p] = i$. We wish to determine the spectrum of $\hat{H}$. Of course, to serve as the physical energy operator of a system, the Hamiltonian should have only real eigenvalues; it must be self-adjoint. Textbooks would introduce this as the condition that $(\phi, \hat{H}\psi) = (\hat{H}\phi, \psi)$ for all states $\psi \in \mathcal{H}$. In a finite-dimensional Hilbert space, this is the condition of 'Hermiticity', and is equivalent to self-adjointness. But in the infinite-dimensional case we are interested in, the situation is more subtle.

Most operators in familiar one dimensional quantum mechanics are unbounded–

indeed, any Hamiltonian with arbitrarily large eigenvalues is unbounded. This means that for $\psi \in \mathcal{H}$, an unbounded operator A may map states out of the Hilbert space, i.e. $A\psi \notin \mathcal{H}$. To remedy this possibility, the definition of an unbounded operator A consists of how the operator acts on functions as well as a declaration of an operator domain $D(A)$, a dense subspace of $\mathcal{H}$. The domain $D(A)$ is the preimage of $\mathcal{H}$ under the operator A.

The required restriction of operator domains is just the familiar task of supplying boundary conditions to eigenvalue problems like (4.12). By supplying boundary conditions for the solutions, we eliminate some functions in the Hilbert space from the domain of consideration for the operator. The role of these operator domains has been extensively studied; see e.g. [103, 104, 105, 106].

Operator domains are also important for self-adjointness. Two conditions must be satisfied for an unbounded operator $\hat{H}$ with domain $D(\hat{H})$ to be self-adjoint. First, it must be *symmetric*, i.e.

$$(\hat{H}\phi, \psi) = (\phi, \hat{H}\psi) \qquad \forall \phi, \psi \in D(\hat{H}) \subset \mathcal{H}. \tag{4.14}$$

The second condition is that its adjoint shares the same domain: $D(\hat{H}) = D(\hat{H}^\dagger)$. In general, $D(\hat{H}) \subseteq D(\hat{H}^\dagger)$. Only when the domain of the operator coincides with the domain of its adjoint does the spectral theorem apply. We will consider two examples of these issues: the momentum operator on the half line and the Hamiltonian (4.13) on the half line.

No momentum on the half line?

Let us consider the operator $p = -i\partial_x$ acting on functions $\psi \in L^2(\mathbb{R}_+)$. The boundary conditions at infinity are already fixed by the Hilbert space. The operator p is symmetric

when $(p\phi, \psi) - (\phi, p\psi) = 0$. This places conditions on the domain $D(p)$:

$$(p\phi, \psi) - (\phi, p\psi) = 0 = \int_{\mathbb{R}_+} i\bar{\phi}'\psi + i\bar{\phi}\psi' = i\bar{\phi}(0)\psi(0), \tag{4.15}$$

where we have integrated by parts. This seems to suggest that we should define $D(p) = \{\psi \in L^2(\mathbb{R}_+) \mid \psi(0) = 0\}$, so that p is symmetric on $D(p)$. But what about $D(p^\dagger)$? By definition the adjoint satisfies $(p^\dagger\phi, \psi) = (\phi, p\psi)$ for $\psi \in D(p)$ and $\phi \in D(p^\dagger)$. As above we can write

$$(p^\dagger\phi, \psi) - (\phi, p\psi) = \int_{\mathbb{R}_+} i\bar{\phi}'\psi + i\bar{\phi}\psi' = i\bar{\phi}(0)\psi(0) = 0. \tag{4.16}$$

Because of the conditions on ψ, the above is true for any $\phi \in L^2(\mathbb{R}_+)$ which is finite at the origin. Thus, $D(p^\dagger) \neq D(p)$, and the momentum operator is not self-adjoint on $D(p)$.

One may wonder if we could suitably enlarge the domain of p so that $D(p^\dagger) = D(p)$. In fact, there is a theory of such 'operator extensions'. Given a symmetric, but not self-adjoint operator, it may be possible to extend the domain of definition so that the operator becomes self-adjoint. The existence of these self-adjoint extensions can be cleanly characterized in terms of deficiency indices: given a closed symmetric operator A, define two integers $n_\pm$ by

$$n_\pm = \dim \ \ker[i \mp A^*]. \tag{4.17}$$

Morally, this quantity measures 'how much' of the spectrum of A fails to be real, and hence how A fails to be self-adjoint. It can be shown that the operator A is self-adjoint if and only if $n_\pm = 0$, and that A has self-adjoint extensions if and only if $n_+ = n_-$ [104]. By explicitly computing the deficiency subspaces, one can follow a maze of theorems to explicitly construct self-adjoint extensions. A useful theorem of von Neumann states that for real potentials, the differential operator in (4.12) has equal deficiency indices $n_+ = n_-$.

In the case of the momentum operator, one can easily solve the equations $p\psi = -i\psi' = \pm i\psi$ in $L^2(\mathbb{R}_+)$ and realize that the deficiency subspaces are mismatched: $n_+ \neq n_-$. This shows that there is no suitable self-adjoint momentum operator on the half line. Trying to define such an operator can lead to various paradoxes [106]. Recently, the authors in [107] also considered these issues. They define a suitable momentum operator by passing to a cover of the Hilbert space. For our purposes, we are mostly concerned with the Hamiltonian, rather than the momentum alone.

Self-adjoint Hamiltonians

Despite not having a self-adjoint definition of momentum, we can define a domain on which the Hamiltonian (4.13) is truly self-adjoint. To construct this space we proceed essentially as before. The condition that the Hamiltonian $\hat{H} = -\partial_x^2 + V(x)$ is symmetric is

$$(\hat{H}\phi, \psi) - (\phi, \hat{H}\psi) = 0 = \int_{\mathbb{R}_+} -\bar{\phi}''\psi + \bar{\phi}\psi'' = \bar{\phi}(0)\psi'(0) - \bar{\phi}'(0)\psi(0). \tag{4.18}$$

This is satisfied if we require $\psi(0) + a\psi'(0) = 0$ (and similar for ϕ) for a constant $a \in \mathbb{C} \cup \{\infty\}$ (these linear, mixed boundary conditions are sometimes called 'Robin' conditions). Dirichlet conditions correspond to $a = 0$ and Neumann conditions to $a = \infty$. Let us consider this subset of $L^2(\mathbb{R}_+)$ as a candidate domain for $\hat{H}$. Is $\hat{H}$ self-adjoint on this domain?

As above, we can calculate $(\hat{H}^\dagger\phi, \psi) - (\phi, \hat{H}\psi)$ for $\psi \in D(\hat{H}),\ \phi \in D(\hat{H}^\dagger)$ and demand that the result vanishes. Doing so gives the condition

$$[\bar{\phi}(0) + a\bar{\phi}'(0)]\psi'(0) = 0 \quad \Longrightarrow \quad \phi(0) + \bar{a}\phi'(0) = 0. \tag{4.19}$$

This is exactly equivalent to the condition on the states $\psi \in D(\hat{H})$ provided the parameter

a is real. We can conclude that $\hat{H} = -\partial_x^2 + V$ is self-adjoint on the domain

$$D_a(\hat{H}) = \left\{\psi \in L^2(\mathbb{R}_+) \mid \psi(0) + a\psi'(0) = 0 \quad a \in \mathbb{R} \cup \{\infty\}\right\}. \tag{4.20}$$

We notice that there is a one-parameter family of such domains, indexed by the (dimensionful) extension parameter a. It remains to understand how confining ourselves to this domain will affect the recursion relations that generate the bootstrap. Indeed, the extension parameter a does represent a physical aspect of the system to which the bootstrap should be sensitive!

To illustrate the physical consequences [106], consider the free particle on ; $-\psi'' = E\psi$ with $\psi(0) + a\psi'(0) = 0$. The solutions with $E = k^2$ are forward and backward traveling plane waves:

$$\psi = Ae^{ikx} + Be^{-ikx}.$$

When we impose the boundary condition, the solution becomes

$$\psi = A\left(e^{-ikx} + Re^{ikx}\right); \qquad R = \frac{aik - 1}{aik + 1}.$$

We can interpret the (pure phase) R as a reflection coefficient, $R^*R = 1$. Physically, the interpretation is that the boundary conditions at the origin reflect waves with a phase shift $\arg R$ that depends on the extension parameter a. This suggests a relationship between Robin boundary conditions and scattering theory, one we will make precise in later sections.

Finally, we note that in the case of the moment problem/bootstrap on $\mathbb{R}$, these issues of operator domain are of less concern. The boundary conditions associated with $L^2(\mathbb{R})$ ensure that most familiar Hamiltonians are essentially self-adjoint. Basic theorems exist which guarantee that smooth, asymptotically confining potentials lead to self-adjoint

Hamiltonians in the obvious way [104].

4.3 Anomalies in the recursion

We have seen that for problems on the half line, finding a self-adjoint Hamiltonian required us to define a one-parameter family of domains $D_a(\hat{H})$. The bootstrap recursion should be sensitive to this entire family of physically inequivalent quantizations of the system.

To investigate these effects, let us consider the "0+1" dimensional version of Noether's theorem, which is usually introduced as Ehrenfest's theorem [108]. For an operator A and a Hamiltonian $\hat{H}$, Ehrenfest's theorem governs the time evolution of expectation values of the operator A in a state ψ:

$$\frac{d}{dt}\langle A\rangle_\psi = \left\langle \frac{\partial A}{\partial t} \right\rangle_\psi + i\langle [\hat{H}, A]\rangle_\psi. \tag{4.21}$$

When we derived the bootstrap recursion (e.g. as in [55]), we used the linear constraints $\langle [\hat{H}, \hat{\mathcal{O}}_i]\rangle = 0$ for some set of operators $\hat{\mathcal{O}}_i$, which are usually some monomial $x^n p^m$. This constraint is equivalent to setting (4.21) to 0, at least for operators without explicit time dependence. We are saying that the expectation value of these time-independent operators vanishes, which constrains us to eigenstates–or, more generally, time-independent density matrices. This is just the statement that in eigenstates, time evolution is just a pure phase rotation.

Given the discussion in the previous sections, the expression in (4.21) should ring some alarm bells. Specifically, the quantity $\langle [\hat{H}, A]\rangle_\psi$ is only well-defined if $\psi \in D(\hat{H}) \cap D(A)$. This is a very strong assumption! Without this assumption, one must be more careful. Let us assume ψ is an eigenstate of $\hat{H}$, so $\psi \in D_a(\hat{H})$ and $\hat{H}\psi = E\psi$. Then, due to the

eigenvalue equation, the following expression vanishes so long as $\psi \in D(A)$:

$$(\hat{H}\psi, A\psi) - (\psi, A\hat{H}\psi) = E(\psi, A\psi) - E(\psi, A\psi) = 0.$$

However, this is *not* equivalent to the quantity $(\psi, [\hat{H}, A]\psi)$. The commutator $[\hat{H}, A]$ algebraically generates a new operator. There is no guarantee that ψ is in the domain of this new operator. The correct relation is instead

$$(\hat{H}\psi, A\psi) - (\psi, A\hat{H}\psi) = 0 = (\psi, [\hat{H}, A]\psi) + \langle(\hat{H}^\dagger - \hat{H})A\rangle_\psi. \tag{4.22}$$

The first term is the algebraic commutator extended to $D(\hat{H})$. But there is now an extra term $\mathcal{A} \equiv \langle(\hat{H}^\dagger - \hat{H})A\rangle_\psi$. This modification to the Ehrenfest theorem has been noticed before in the literature [105, 106]. It is dubbed an 'anomaly', which is an appropriate term for a number of reasons. Firstly, like the chiral anomaly in gauge theory, it is a total derivative term. It also appears as an additive modification to the 'normal' Ehrenfest theorem (4.21); one can consider this a 0+1-dimensional anomalous Ward identity. Dealing with operator domains is genuinely a quantum effect that alters conservation equations—an anomaly.

Note that $\mathcal{A} = 0$ when A keeps $D(\hat{H})$ invariant, as $\hat{H}^\dagger = \hat{H}$ on $D(\hat{H})$ by construction. But this is often not the case. By using the constraint $\langle[\hat{H}, \hat{\mathcal{O}}]\rangle_\psi = 0$, we were unwittingly extending the algebraic commutator to the whole space $D(\hat{H})$. For the bootstrap program, the correct constraint to use is (4.22). One should evaluate the commutator $[\hat{H}, A]$ algebraically and evaluate the anomaly term $\mathcal{A}$ for states $\psi \in D(\hat{H})$.

4.3.1 A correct recursion

Let us apply these new ideas to generate a complete recursion for bootstrapping the positional moments on the half line. Including the anomaly, the bootstrap recursion is generated by the following constraint on operators $\hat{\mathcal{O}}$ in energy eigenstates $\psi \in D_a(\hat{H})$, which we take to be real:

$$0 = (\psi, [\hat{H}, \hat{\mathcal{O}}]\psi) + \langle (\hat{H}^\dagger - \hat{H})\hat{\mathcal{O}}\rangle_\psi. \tag{4.23}$$

Let us take the Hamiltonian to be $\hat{H} = p^2 + V(x)$ and our first trial operator as $\hat{\mathcal{O}}_1 = x^n$. The algebraic commutator is

$$[\hat{H}, \hat{\mathcal{O}}_1] = [p^2, x^n] = -2inx^{n-1}p - n(n-1)x^{n-2},$$

where we will always 'normal order' x in front of p. We can evaluate the anomaly by explicitly integrating by parts:

$$\begin{aligned}
\mathcal{A}_1 = \langle (\hat{H}^\dagger - \hat{H})x^n\rangle_\psi &= \int_{\mathbb{R}_+} -\psi'' x^n\psi + \psi\partial_x^2(x^n\psi) \\
&= -\int_{\mathbb{R}_+} \psi'' x^n\psi + [\psi\partial_x(x^n\psi) - \psi' x^n\psi|_0^\infty + \int_{\mathbb{R}_+} \psi'' x^n\psi \\
&= -\lim_{x\to 0} nx^{n-1}\psi^2 \\
\mathcal{A}_1 &= -\delta_{n,1}\psi(0)^2.
\end{aligned}$$

As promised, the anomaly is a surface term, picking up a dependence on the state's boundary conditions. The result is a modified constraint which will help build the recursion:

$$0 = 2in\langle x^{n-1}p\rangle_\psi + n(n-1)\langle x^{n-2}\rangle_\psi + \delta_{n,1}\psi(0)^2. \tag{4.24}$$

We can proceed the same way using the trial operator $\hat{\mathcal{O}}_2 = x^n p$. The algebraic commutator is

$$[\hat{H}, \hat{\mathcal{O}}_2] = -2inx^{n-1}p^2 - n(n-1)x^{n-2}p + ix^n V'(x),$$

while the anomaly term may be evaluated to yield

$$\mathcal{A}_2 = i\delta_{n,1}\psi(0)\psi'(0).$$

The result is another modified constraint:

$$0 = 2in\langle x^{n-1}p^2\rangle_\psi + n(n-1)\langle x^{n-2}p\rangle_\psi - i\langle x^n V'(x)\rangle_\psi - i\delta_{n,1}\psi(0)\psi'(0). \tag{4.25}$$

To generate the full recursion relation, we use (4.24), (4.25) and the eigenvalue equation:

$$\langle x^{n-1}p^2\rangle_\psi = E_\psi\langle x^{n-1}\rangle_\psi - \langle x^{n-1}V(x)\rangle_\psi. \tag{4.26}$$

The result is the following recursion relation for problems on the half line, with boundary conditions $\psi(0) + a\psi'(0) = 0$ in a given state:

$$\begin{aligned} 0 = 2nE_\psi\langle x^{n-1}\rangle_\psi + \frac{1}{2}n(n-1)(n-2)\langle x^{n-3}\rangle_\psi \\ - 2n\langle x^{n-1}V\rangle_\psi - \langle x^n V'\rangle_\psi + \delta_{n,2}\psi_0^2 + \delta_{n,1}\frac{\psi_0^2}{a}, \end{aligned} \tag{4.27}$$

where $\psi_0 \equiv \psi(0)$. By including the anomaly terms, the recursion is now sensitive to the choice of operator domain for the Hamiltonian. We see that the recursion (4.11) that we used for bootstrapping the linear potential omitted both of these contact terms, which amounted to setting $\psi_0 = 0$; a specific choice of operator domain. That is why the results uncovered only the Dirichlet energy spectrum! In the next section, we will revisit the

Airy problem and apply these results to the numerical bootstrap.

As as a final comment, consider the $n = 1$ case of the recursion (4.27) which gives us the virial theorem:

$$E_\psi = \langle V \rangle_\psi + \frac{1}{2}\langle xV'(x) \rangle_\psi + \frac{1}{2}\psi_0\psi_0'.$$

There is now an anomalous contribution to the energy, one which vanishes in the case of either pure Dirichlet or Neumann boundary conditions. Interestingly, this contribution persists when $V = 0$. Let us consider this free particle on a half line. The recursion suggests there should be a state with energy

$$E_a = -\frac{1}{2a}\psi_0^2.$$

This state is created by the boundary conditions. It is also exactly the same as the energy of a state bound in an inverted delta function potential on $\mathbb{R}$ (see Appendix A, also [106]).

This gives us some physical insight to the situation regarding the anomaly: the boundary conditions at the origin are like adding a delta function source. This delta function source must come with a dimensionful parameter, e.g. a scale, for the Hamiltonian to be dimensionally consistent. The free particle on the half line does not have translation invariance, but it does have dilatation, or scale, invariance. In the quantum theory, the boundary conditions introduce a dimensionful parameter, breaking the classical scale invariance of the system. This is thus the simplest possible example of a conformal anomaly.

4.3.2 Revisiting the Airy model

Let us consider the linear potential again, this time using the anomaly-corrected recursion (4.27). Our recursion is thus

$$\langle x^n \rangle = \frac{1}{2n+1}\left[2nE\langle x^{n-1}\rangle + \frac{1}{2}n(n-1)(n-2)\langle x^{n-3}\rangle + \delta_{n,2}\psi_0^2 + \delta_{n,1}\frac{\psi_0^2}{a}\right].$$

In the case of Dirichlet boundary conditions $\psi_0 = a = 0$, both contact terms vanish and we are left with the recursion (4.11). This gave us a one-dimensional search space $\{E\}$ which correctly yielded the Dirichlet spectrum. In the case of Neumann conditions $a \to \infty$, one of the contact terms persists while the other vanishes, and the recursion depends also on ψ_0.

We can consider the case of Neumann BCs as a two-dimensional bootstrap search space $\{E, \psi_0\}$. By borrowing the methods used earlier for the double well potential, we can perform the numerical bootstrap by searching for points which pass the positivity checks in the (E, ψ_0) plane. This bootstrap should recover both the Dirichlet and Neumann spectra (and no others); allowed islands which form along the axis $\psi_0 = 0$ should do so at the Dirichlet energy levels.

The result is shown in Fig. 4.7. The bootstrap correctly finds the Dirichlet levels and the Neumann levels, while not returning results for states with mixed boundary conditions: this is expected as we did not include both contact terms. To find the mixed spectra, we could increase the dimension of the search space once more, bootstrapping the free parameters $\{E, \psi_0, \psi_0'\}$ (bootstrapping a would require $a \in [0, \infty)$ which is computationally undesirable). In this way we can fully specify the desired boundary conditions for any problem on the half line via the recursion (4.27).

To demonstrate that the bootstrap can correctly find the full Robin boundary conditions, we can perform a low-resolution search for positivity in the 3d space of $\{E, \psi_0, \psi_0'\}$

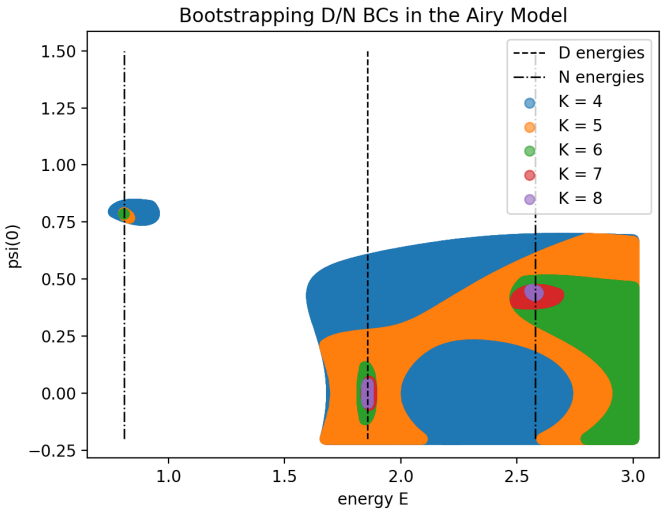

Figure 4.7: Bootstrapping the Dirichlet and Neumann spectra by passing to a search space of dimension two, with free parameters E, ψ_0.

then project down into the $\{E, a\}$ plane by taking $a = -\psi_0/\psi_0'$. We can analytically compute the dependence of the eigenvalue E on the parameter a. The normalizable solution of $-f'' + xf = Ef$ is $f \propto \mathrm{Ai}(x - E)$. So we should have $a(E) = -\mathrm{Ai}'(-E)/\mathrm{Ai}(-E)$. The results are shown in Fig. 4.8. Due to the larger dimension of the search space, getting numerically satisfactory results is computationally intensive, at least done in the most naive, brute-force way. But the 'experimental' data clearly conforms with our analytical expectations. This verifies that the anomalous contributions in the recursion do correctly account for the Robin boundary conditions.

With the theory and examples presented in this section, we see how boundary conditions enter algebraically into the bootstrap. With the ability to account for arbitrary mixed boundary conditions on half line problems, we will later proceed to both develop the SDP formulation of the algorithm for half-line domains and apply these ideas to the determination of one-dimensional scattering amplitudes.

However, before moving on to applications, we will consider the final type of one-dimensional interval: the finite interval $[a, b]$. As discussed earlier, the moment problem

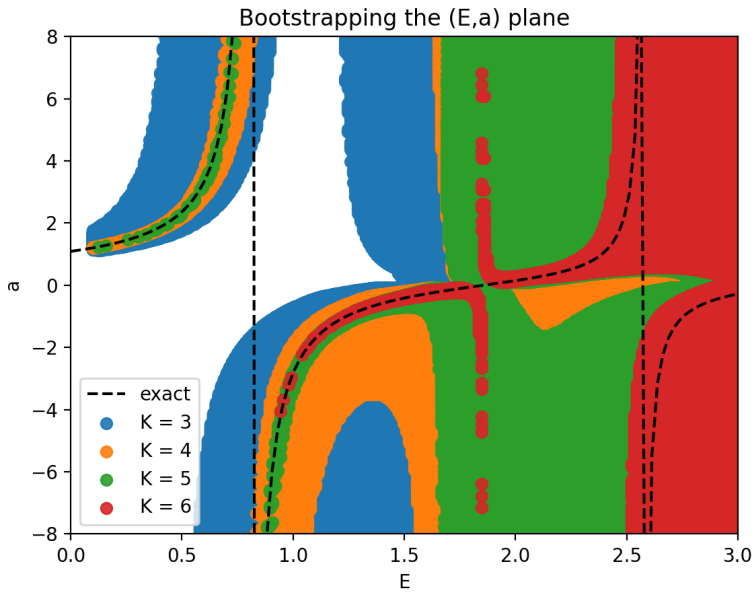

Figure 4.8: Projecting a 3d bootstrap into the (E, a) plane. While numerically sparse, the bootstrap data agrees with the analytical predictions for the Robin boundary conditions.

on a finite interval is that of Hausdorff, and the finite interval is also where well-known theorems of Sturm & Liouville and Floquet are at our disposal. In the next section, we develop and test the bootstrap approach to problems on periodic intervals and see how the theory of anomalies developed here affects the outcomes of our numerical experimentation.

4.4 Bootstrapping band structure

Let us start with a free particle on a circle $\theta \equiv \theta + 2\pi$. The Hamiltonian is given by

$$\hat{H} = -\frac{1}{2}\partial_\theta^2 + V(\theta). \tag{4.28}$$

We are interested in understanding how the bootstrap approach leads to properties of the spectrum of the particle on the circle for arbitrary V.

Suppose we have an eigenstate of $\hat{H}$. To this state, we associate a normalized measure $|\psi(\theta)|^2 d\theta \geq 0$. Again, this can be thought of as a unitarity constraint: probabilities for intervals are positive and normalized.

Consider a complex, differentiable periodic function $f(\theta)$ as a (normal) operator in the quantum system. The general quantum mechanical bootstrap constraint is that $\langle \hat{\mathcal{O}}^\dagger \hat{\mathcal{O}} \rangle \geq 0$ for all operators. In particular, this applies to f. Because of the periodicity, the operator admits a Fourier expansion,

$$f(\theta) = \sum_{n=-\infty}^{\infty} a_n \exp(in\theta). \tag{4.29}$$

It follows that $\langle f(\theta)^\dagger f(\theta) \rangle \geq 0$. Expanding this condition, we get that

$$\sum_{n,m} a_m^* a_n \langle \exp(i(n-m)\theta) \rangle \geq 0 \tag{4.30}$$

for all L^2 normalizable sequences a_n. In particular this is true for all truncations to a finite set of the a_n, $-K \leq n \leq \tilde{K}$. We get this way a quadratic form of size $(K + \tilde{K} + 1) \times (K + \tilde{K} + 1)$ which is both a Hermitian matrix and is also positive definite. This form is given by

$$T = \begin{pmatrix} 1 & \langle \exp(i\theta) \rangle & \langle \exp(2i\theta) \rangle & \dots \\ \langle \exp(-i\theta) \rangle & 1 & \langle \exp(i\theta) \rangle & \ddots \\ \langle \exp(-2i\theta) \rangle & \langle \exp(-i\theta) \rangle & 1 & \ddots \\ \vdots & \ddots & \ddots & \ddots \end{pmatrix}. \tag{4.31}$$

We also have that $T \succeq 0$. This is a special case of a Toeplitz matrix. This positivity condition is a classical result referred to as the trigonometric moment problem.[2] Its

[2]Like the Hamburger or Stieltjes moment problem, positivity of this matrix for all sizes guarantees

sufficiency was first proven in 1911 by Toeplitz and Carathéodory [109]. We did not address this specific moment problem in Chapter 2 as it describes measures on a complex domain, the unit circle in $\mathbb{C}$.

We can immediately notice some constraints implied by this positivity condition. For example, by looking at any 2×2 block with two entries on the diagonal, we find that

$$\begin{pmatrix} 1 & \langle \exp(i(n-m)\theta) \rangle \\ \langle \exp(i(m-n)\theta) \rangle & 1 \end{pmatrix} \succeq 0. \tag{4.32}$$

This produces the obvious inequality

$$|\langle \exp(i(n-m)\theta) \rangle|^2 \leq 1. \tag{4.33}$$

If we specialize to even potentials, we can assume that $\psi(\theta) = \pm\psi(-\theta)$ so that odd functions in θ have vanishing expectation value. Under those conditions, we can replace $\langle \exp(i(n-m)\theta) \rangle \to \langle \cos((n-m)\theta) \rangle$ and the Toeplitz matrix becomes real symmetric.

Actually, there is a modification we can make to the standard Toeplitz positivity condition, one which is a stronger but still necessary condition. Let $\hat{\mathcal{O}} = \sum a_n e^{in\theta}$ as before. Since the operators $1 \pm \cos(\theta)$ are positive semidefinite on the circle, the following operators are well-defined and unique:

$$\hat{\mathcal{O}}_\pm = \sqrt{1 \pm \cos(\theta)} \sum_n a_n e^{in\theta}.$$

These operators are related to the operator $\hat{\mathcal{O}}$ as

$$\hat{\mathcal{O}}^\dagger \hat{\mathcal{O}} = \frac{1}{2} \left(\hat{\mathcal{O}}_+^\dagger \hat{\mathcal{O}}_+ + \hat{\mathcal{O}}_-^\dagger \hat{\mathcal{O}}_- \right).$$

that the sequence $\{\langle e^{in\theta} \rangle\}$ is the moment sequence of a unique positive measure.

On general grounds, we should still have $\langle \hat{\mathcal{O}}_{\pm}^{\dagger} \hat{\mathcal{O}}_{\pm} \rangle \geq 0$ in any state. Each of these defines a positivity condition on a matrix whose entries are slightly altered from that of the standard Toeplitz matrix (4.31). Specifically, their matrix elements are

$$T_{nm}^{\pm} = \langle e^{i(n-m)\theta} \rangle \pm \frac{1}{2} \langle e^{i(n-m+1)\theta} \rangle \pm \frac{1}{2} \langle e^{i(n-m-1)\theta} \rangle. \tag{4.34}$$

Clearly $2T_{nm} = T_{nm}^{+} + T_{nm}^{-}$. Positivity of both $T^{\pm}$ implies positivity of the matrix (4.31) but not necessarily the other way around. Checking positivity of the matrices with elements given by (4.34) is in this sense a stricter condition than simply checking positivity of (4.31). Indeed, using this twofold positivity check improves the convergence of the bootstrap, as we verified for ourselves. One may heuristically think that the standard Toeplitz matrix construction associates to some initial data a point in the cone of positive semidefinite matrices, while this modified procedure associates endpoints of a line whose midpoint is the standard Toeplitz matrix. Since the cone of positive matrices is convex this line lies fully within the cone. The line is more likely to leave the cone than the point under perturbation of the initial data.

The general bootstrap problem on the circle is then the following: find a recursion relation for the Fourier modes of the measure $\langle \exp(i(n-m)\theta) \rangle$ at fixed energy E, expressed in terms of some finite amount of data (parameters). Next, solve the recursion relation and check for positivity at various sizes of the matrix T, or of both $T^{\pm}$. As we increase the size of the matrix, our previous results are still valid, so we can only shrink the allowed parameter space. If the parameter space has shrunk enough, we have 'solved' the problem to some precision and ideally we obtain a discrete spectrum for E.

4.4.1 The free particle

To understand how the bootstrap works, we should first study the free particle on the circle, with Hamiltonian

$$\hat{H}_0 = \frac{p^2}{2}. \tag{4.35}$$

If we solve this system, we are supposed to get

$$E = \frac{n^2}{2}, \tag{4.36}$$

for $n \in \mathbb{Z}$, corresponding to 2π-periodic wavefunctions. Consider first that on energy eigenstates we have $\langle[\hat{H}_0, \hat{\mathcal{O}}]\rangle = 0$ as usual. We now take $\hat{\mathcal{O}} = \exp(in\theta)$ and find

$$[\hat{H}_0, \exp(in\theta)] = n\exp(in\theta)p + \frac{n^2}{2}\exp(in\theta). \tag{4.37}$$

From here we obtain the constraint

$$\langle \exp(in\theta)p\rangle = -\frac{n}{2}\langle\exp(in\theta)\rangle. \tag{4.38}$$

As an aside, from $\hat{\mathcal{O}} = p$ we find that $\langle p^2\rangle \geq 0$, so that the bootstrap produces only positive energy. Similarly, if we use $\hat{\mathcal{O}} = \exp(in\theta)p$, we get that (after using that $p^2 = 2E$)

$$2En\langle\exp(in\theta)\rangle - \frac{n^3}{4}\langle\exp(in\theta))\rangle = 0. \tag{4.39}$$

This is a direct constraint on the expectation values of the Fourier modes; there is no recursion. There are two types of solutions.

First, there is $\langle\exp(in\theta))\rangle = 0$. In this case the Toeplitz matrix is the identity and is

trivially positive. Secondly, there are possible solutions where $\langle \exp(in\theta) \rangle \neq 0$ so long as

$$E = \frac{n^2}{8}. \tag{4.40}$$

If we first compare with (4.36), the quantization seems to be off: it is as if an integer n is allowed to be a half integer also. We can ask: are we supposed to consider the first type of solutions where $\langle \exp(in\theta) \rangle = \delta_{n,0}$ for all non-trivial n? If we follow the bootstrap philosophy, the answer should be an unequivocal yes. They correspond to a constant measure. The only constraint is $E \geq 0$.

What is the meaning of these solutions? Clearly, $p \simeq \sqrt{2E}$ would be continuous. Nowhere in the commutations relations used to generate the consistency conditions is it specified that the spectrum of p is quantized. All we know is that the potential is periodic, but we don't know that the period is 2π. This was only implicit in the choice of mode functions. We could just as well be on a covering of the circle and the bootstrap would not change, except that now additional values of n that are not integers would also be allowed. If we allow for this possibility, what the bootstrap has produced is a continuous value of p and we have the band structure of the particle on a circle. There is a momentum p, and a quasimomentum $p \mod (\Pi)$ where Π is the minimal momentum in the dual torus of the circle. In this case $\Pi = 1$.

Now let us again examine the second type of solutions where for some integer n (and also $-n$) , $\langle \exp(in\theta) \rangle = C \neq 0$. For all other $|m| \neq n$, we have $\langle \exp(im\theta) \rangle = 0$. The

Toeplitz matrix then has a positive definite submatrix of the form

$$M = \begin{pmatrix} 1 & C & 0 & \dots \\ C^* & 1 & C & \ddots \\ 0 & C^* & 1 & \ddots \\ \vdots & \ddots & \ddots & \ddots \end{pmatrix}. \tag{4.41}$$

This system is very similar to a discrete second order difference operator with Dirichlet boundary conditions

$$\Delta = \begin{pmatrix} 2 & 1 & 0 & \dots \\ 1 & 2 & 1 & \ddots \\ 0 & 1 & 2 & \ddots \\ \vdots & \ddots & \ddots & \ddots \end{pmatrix}. \tag{4.42}$$

The operator Δ is positive and gapless in the large matrix limit. We can do a change of basis where the 1 outside the main diagonal acquire random phases, which can be chosen to be constant. We have that

$$M \simeq |C|\Delta + (1 - 2|C|)\mathbf{1}. \tag{4.43}$$

In the infinite size limit we get that because Δ is gapless, $(1 - 2|C|) \geq 0$. That is, we find a bound $|C| \leq 1/2$. At finite size, $|C| > 1/2$, it is like having a negative mass squared term on a lattice. We can get positivity of the matrix with bounds that approach $|C_{\max}| \to 1/2$. The tachyon can be stabiliized by finite size effects, where the smallest eigenvalue of Δ is of order $1/K^2$.

Consider the wave functions $\psi(\theta) \propto \cos(n\theta+\phi)$ where n is an integer or a half integer. One can check that $|\psi|^2$, properly normalized, saturates the bound $|C| = 1/2$ with a specific phase for C. They are allowed states in the quantum system and the bootstrap

is consistent that fact: all solutions that pass the bootstrap bounds are allowed physical states. What can we do now with states where $|C| < 1/2$? The interpretation is that the measure μ we get is a convex combination of two allowed bootstrap solutions for different angles. This indicates that the bootstrap solutions we have found analytically are compatible with arbitrary density matrices for a system with two levels. A mixed state measure would be a convex combination of two pure-state measures.

These combinations usually depend on three parameters. In this case, we only get a two parameter space, so one can not resolve completely the density matrix problem just from the probability measure μ. The extremal bounds are pure states and the ones in the middle of the disk can be either mixed states or pure states. The non-trivial solutions to the bootstrap in this case indicate a double degeneracy. They occur at quasimomentum $q = (p \mod \Pi) = 0 = -q$ and at $q = (p \mod \Pi) = \Pi/2 \equiv -q$; the symmetric points in the band occur where both interfering wave functions have the same quasimomentum.

4.4.2 Self-adjointness on the interval

Given that the inclusion of anomaly terms allowed us to specify boundary conditions for the half line bootstrap, one is tempted to ask if the same can be said for bootstrapping problems on the interval. Our approach so far does not allow us to specify the quasimomentum, so we can only in theory detect energy bands. Other work [64, 56] came to the same conclusion, and tried new methods to obtain the full dispersion relation.

Here, we will analyze the problem on an interval using the same approach as in the previous sections: by precisely defining operator domains and analyzing the presence of possible anomaly terms. We find that unlike the half line, the recursion is insensitive to a large family of inequivalent boundary conditions on the interval. These families of boundary conditions have been studied in multiple contexts [106, 104], and essentially

correspond to the theory of Floquet exponents, or, to a condensed matter theorist, the Bloch quasimomentum.

Operator domains

In the following, we will work over the Hilbert space $\hat{H} = L^2[0,1]$ with the additional assumption that the states ψ are smooth. However, we will not assume the states are real. Consider first the momentum operator $p = -i\partial_x$. It is symmetric when

$$(\psi, p\phi) - (p\psi, \phi) = 0 = \bar{\psi}_1\phi_1 - \bar{\psi}_0\phi_0,$$

where we use e.g. $\phi_x \equiv \phi(x)$. One choice of a symmetric domain is Dirichlet boundary conditions $\psi_1 = \psi_0 = 0$. However, it is not hard to see that in the case of Dirichlet boundary conditions, $D(p^\dagger)$ will not be constrained by any boundary conditions, and hence $D(p) \subset D(p^\dagger)$; p will fail to be self-adjoint. However, symmetricity of p is also achieved when $\phi_1 = e^{i\theta}\phi_0$ for all states in the domain $D(p)$. These are 'twisted' boundary conditions, and include the periodic and anti-periodic sectors. Furthermore, it can be shown that p is self adjoint on this domain. Hence, there is a family of suitable self-adjoint domains for p

$$D_\theta(p) = \left\{\psi \in \hat{H} \text{ smooth} \mid \psi_1 = e^{i\theta}\psi_0,\ \psi_0 \neq 0\right\}. \tag{4.44}$$

The situation is somewhat similar for the Hamiltonian $\hat{H} = p^2 + V = -\partial_x^2 + V$. The condition for symmetricity of $\hat{H}$ is

$$(H\phi, \psi) - (\phi, H\psi) = 0 = \left(\bar{\phi}\psi'\right) - \bar{\phi}'\psi\Big|_0^1.$$

This is satisfied by Dirichlet boundary conditions. It is also satisfied if for $\forall\psi \in D(H)$ we have $\psi, \psi' \in D_\theta(p)$. However, in contrast to the momentum operator, both choices here

will furnish a self-adjoint domain $D(H) = D(H^\dagger)$, as one can check by simply taking $\psi \in D(H)$ and $\phi \in D(H^\dagger)$ in the above. In conclusion, there is another one parameter family "plus one" of self-adjoint domains for $\hat{H}$:

$$D_\theta(H) = \left\{ \psi \in \hat{H} \text{ smooth} \mid \psi_1 = e^{i\theta}\psi_0,\ \psi_1' = e^{i\theta}\psi_0' \text{ or } \psi_1 = \psi_0 = 0 \right\}. \tag{4.45}$$

The physical difference between the twisted and Dirichlet boundary conditions is that of periodic potentials and the infinite square well. Let us focus on the former, and assume that we are imposing the twisted condition on our states. Note that with the Bloch ansatz $\psi_k(x) = e^{ikx}f(x)$, where f is periodic, the state ψ_k and all its derivatives are in the twisted sector of $D_\theta(H)$.

Anomalies?

Now that we have defined our operator domains, it is natural to investigate whether there are anomaly terms that will modify the bootstrap recursion. Recall that the anomaly-corrected constraint we use is

$$0 = (\psi, [\hat{H}, \hat{\mathcal{O}}]\psi) + \langle (H^\dagger - H)\hat{\mathcal{O}} \rangle_\psi. \tag{4.46}$$

We will consider the twisted sector $D_\theta(H)$. The anomaly term vanishes whenever $\hat{\mathcal{O}}D_\theta(H) \subseteq D_\theta(H)$. Consider the operator $A_n = e^{2\pi i n x}$. We can verify that for $\psi \in D_\theta(H)$, the state $\phi = A_n\psi \in D_\theta(H)$ also:

$$\phi_1 = e^{2\pi i n}\psi_1 = e^{i\theta}\psi_0 = e^{i\theta}\phi_0.$$

Consider also the momentum operator $p = -i\partial_x$. Letting $\phi = p\psi$ for $\psi \in D_\theta(H)$, we have

$$\phi_1 = -i\psi_1' = -ie^{i\theta}\psi_0' = e^{i\theta}\phi_0,$$

so that $\phi \in D_\theta(H)$ as well. As a result, all the operators $A_n, p, A_n p$ leave the domain invariant, and hence do not contribute anomalies. These are the operators needed to create a recursion for the moments $t_n = \langle e^{2\pi i n x} \rangle_\psi$, which is what we based our previous analysis on. For these choices of operators, we did not omit any anomaly contributions.

4.4.3 The Mathieu problem

We now turn to applying these ideas to a particle moving in an inverted cosine potential on the circle. The Hamiltonian we use is

$$\hat{H} = \frac{p^2}{2} + V(\theta) \equiv \frac{p^2}{2} - 2a\cos(\theta).$$

The time independent Schrödinger equation takes the form

$$\left[-\frac{1}{2}\frac{d^2}{d\theta^2} - 2a\cos(\theta)\right]|\psi\rangle = E|\psi\rangle,$$

which is equivalent to the classical Mathieu equation after a change of variables:

$$\frac{d^2y}{dx^2} + (A - 2q\cos 2x)y = 0.$$

We would like impose periodic boundary conditions $\psi(\theta) = \psi(\theta + 2\pi)$. This will turn the Schrödinger equation into a Sturm-Liouville problem and hence quantize the energy E. Unfortunately, as discussed previously, the naive bootstrap system does not do that—there are no constraints in the moment recursion enforcing periodic boundary conditions or even sensitive to twisted boundary conditions. Instead, we should expect to get a band structure for the potential.

The Fourier coefficients of the periodic wave function satisfy a recursion relation and

some exact solutions of the corresponding equation are known (see [110] and references therein). It is not clear that the more general problems of the band structure are solved analytically.

Recursion relation between moments

As described previously, we are interested in trigonometric moments $t_n = \langle e^{in\theta} \rangle$, and we compute their commutators with various elements of the Hamiltonian. In particular the algebraic relations imply, with $V(\theta) = -2\alpha\cos(\theta) = -\alpha(e^{i\theta} + e^{-i\theta})$

$$[V(x), e^{in\theta}p] = \alpha e^{i(n+1)\theta} - \alpha e^{i(n-1)\theta}.$$

Using $\langle [\hat{H}, \hat{\mathcal{O}}] \rangle = 0$ and $\langle \hat{H}\hat{\mathcal{O}} \rangle = E\langle \hat{\mathcal{O}} \rangle$ for arbitrary operators $\hat{\mathcal{O}}$ in energy eigenstates, we obtain a moment recursion for the trigonometric moments (recall $t_n \equiv \langle e^{in\theta} \rangle$):

$$0 = -\frac{n^3}{4} t_n + 2nEt_n + \alpha(2n+1)t_{n+1} + \alpha(2n-1)t_{n-1}. \tag{4.47}$$

This is consistent with our previous analysis at $\alpha = 0$. We can turn this around on its head to obtain an expression for the moment t_{n+1}:

$$t_{n+1} = \frac{1}{\alpha(2n+1)} \left[\left(\frac{n^3}{4} - 2nE \right) t_n - \alpha(2n-1)t_{n-1} \right]. \tag{4.48}$$

Notice that since the potential is even, the wavefunctions squared can be chosen to be even. This means the measures from which the moments are extracted are all even. Some special cases of the recursion relation are:

- $n = 0$; gives $t_1 = t_{-1}$, which shows directly that $\langle \sin(\theta) \rangle = 0$.

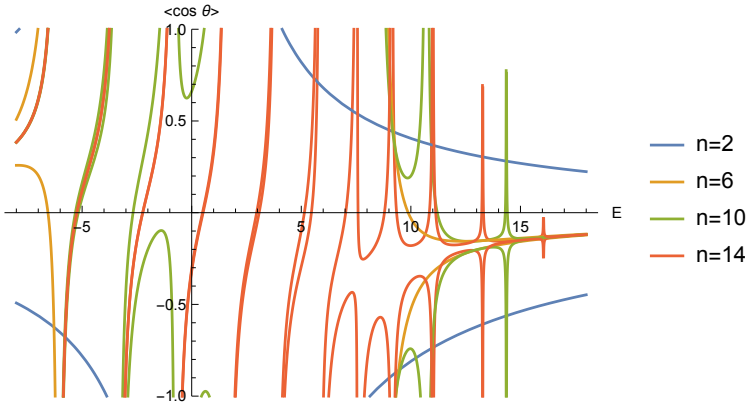

Figure 4.9: Bounds on t_1 from $t_n = \pm 1$ at different values of the energy. Calculations done with $a = 4$.

- $n = 1$; gives

$$t_2 = \frac{1}{3\alpha}\left[\left(\frac{1}{4} - 2E\right) t_1 - \alpha\right],$$

  where we are taking $t_0 = 1$. This shows that the search space is two dimensional: $S = \{E, t_1\}$, for example.

Moreover, as we argued at the beginning of the section, the bootstrap for 2×2 matrices implies that $t_1 \in [-1, 1]$, and also that $t_n \in [-1, 1]$. The first constraint gives a bound on the search space for t_1. The latter bound can be used as a simplified bootstrap, where we only check the bounds on the t_n without determining full positivity. This can help narrow the search space. Because t_n ends up being a linear function of t_1 at fixed energy, we can obtain bounds on t_1 by solving $t_n(E, t_1) = \pm 1$, to obtain bounds $t_1^{\pm}(E, n)$. The allowed values must be between these two solutions. This can be done more generally in periodic problems, where one would obtain linear constraints on the initial data.

Bound on t_n for various n are shown in Figure 4.9. As can be seen, the allowed values of $t_1 = \langle \cos(\theta) \rangle$ converge rapidly to very shallow strips, more or less nested between each other. Here we are already starting to see the appearance of many bands and, when we take the last value $\langle \cos(14\theta) \rangle$ into account, convergence to a narrow strip at high values

of E.

In Fig. 4.9, curves are shown that clearly go to un-physical values $t_1 \to \pm\infty$. These are poles in the energy denominators that appear when solving for $t_n = \pm 1$ for t_1. At those values, one is in a gap of energy. At least from this point of view, for this two dimensional problem, one sees the appearance of gaps in the spectrum relatively easily.

This type of "simplified bootstrap" where one checks simple bounds on t_1 seems very effective at narrowing the search space more generally and would be interesting to explore further. Passing all tests for the various t_n might even give the band structure exactly, which would be easier than checking numerically for positive definiteness of large matrices.

Mathieu Bootstrap

Now we display our results for bootstrapping the potential $V(x) = -2a\cos(x)$ using the trigonometric moment approach and recursion described previously. The algorithmic structure is extremely similar to that of the double well; we use here a grid search algorithm and check the positivity constraints at every point considered within the search space. We searched a range of values for the potential strength a in the region of the $E, \langle\cos(x)\rangle$ plane which is expected to contain the bound states: $E \in [-2a, 2a]$ and $\langle\cos(x)\rangle \in [-1, 1]$. There is no reason, in principle, why we could not extend the energy range to reach above the maximum of the potential. However, the behavior of the parameter islands changes drastically when $E > 2a$, and so we neglect to pursue this.

Fig. 4.10 shows a set of example bootstrap data for $a = 4$. In contrast to the double well problem, the bootstrap converges to curves, rather than points, in the $(E, \langle\cos(x)\rangle)$ plane. To get a sense of the convergence, we can extract from the data of Fig. 4.10 the maximum and minimum energy values of each island. These will be upper and lower bounds, respectively, on the exact energy bands. As K increases, one can see these

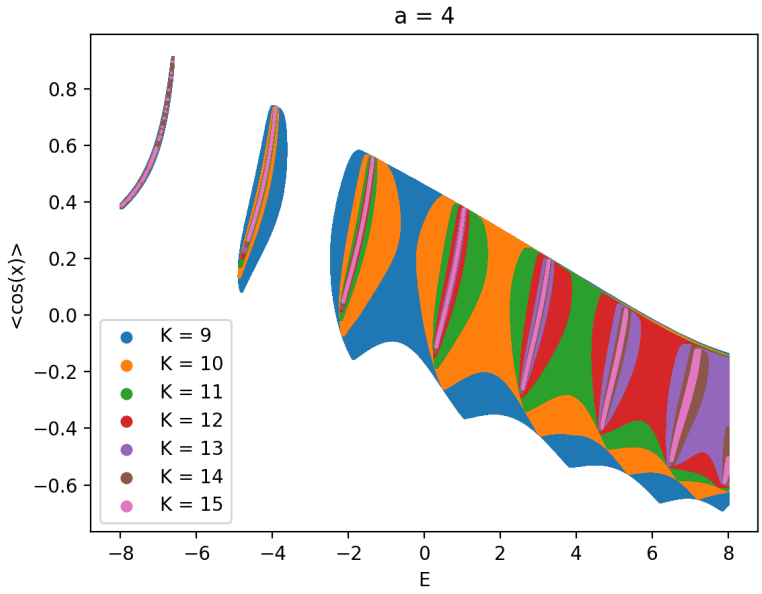

Figure 4.10: Example data from the Mathieu bootstrap. At high depths, the islands become curves. One can see numerical artifacts due to insufficient resolution appearing in the ground state.

bands form, shrink, and approach a constant width as the islands approach curves of finite length. This is shown in Fig. 4.11. As the bands form they quickly approach a width which persists to higher depth. Finally, we can characterize the way the bands change

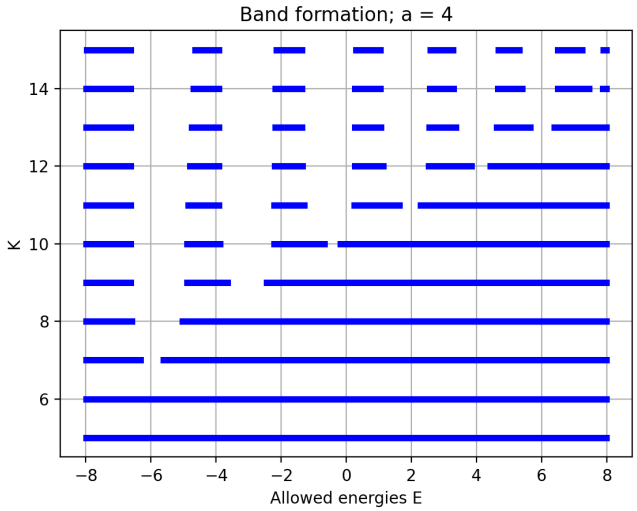

Figure 4.11: Allowed energy values versus depth K. Bands form and converge to limiting values.

with the potential strength a. As a increases, the potential well admits more and more bound states. We can approximate the energies of the low lying states by assuming an approximate harmonic oscillator at the bottom of the potential. The squared frequency at the bottom of the well is $\omega^2 = 2a$. For the case above, the energies of the bands should roughly be given by $E_k \simeq -2a + (\frac{1}{2} + k)\omega$. In the case in the figure, these are split by $\omega = 2\sqrt{2}$ and start at $E_0 \simeq -7$. This is roughly observed. Additional perturbative corrections from the full cosine potential are expected and are negative in first order perturbation theory. Because the bands are somewhat thick, tunneling effects that determine the band structure are important as well.

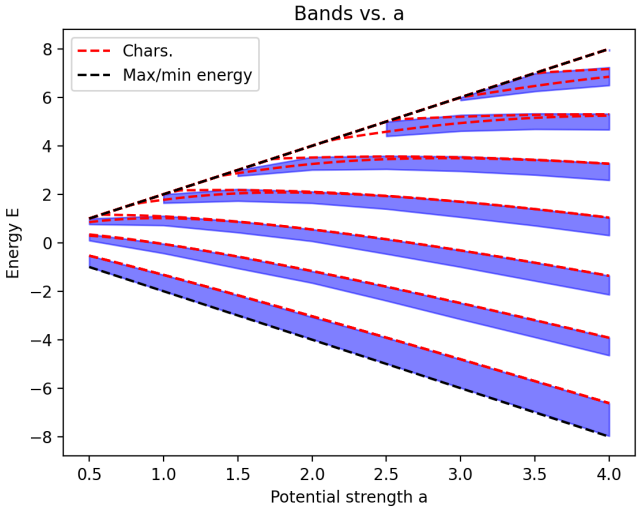

Figure 4.12: Bands versus potential strength a. Bands were selected using the highest value of K with well-conditioned data. This ranges from $K = 8$ for $a = 0.5$ to $K = 14$ for $a \geq 3.5$. Convergence is slower for larger values of a. The harmonic approximation is included in red.

Dispersion relations

Our results so far for the Mathieu problem give continuous segments in the $(E, \langle\cos(\theta)\rangle)$ plane. The general theory of second order differential equations state that there can be at most two linearly independent solutions with the same energy. Because the notion

of quasimomentum is conserved, when two states with different quasimomentum have the same energy, it turns out that they have opposite quasimomentum. The only cases where that does not happen is if one is at a symmetry point of quasimomentum: when $q = p \mod (\Pi) \equiv -q$. In figure 4.13 we show the band structure for the free particle in the circle. The bands have (all) the energy values for different quasimomentum. It

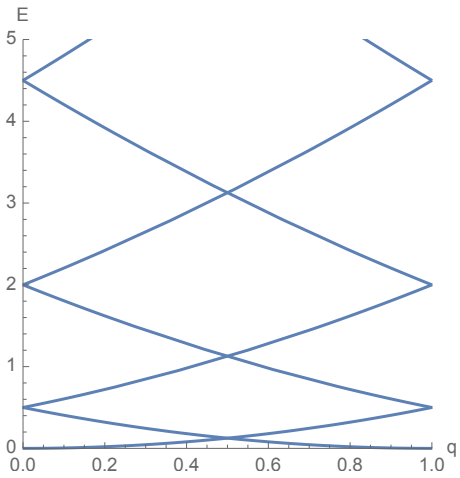

Figure 4.13: Band structure versus quasimomentum for a free particle

is exactly when curves interset that there is a double degeneracy, and when our theory results produced non-trivial density matrices.

Once we add the potential as a perturbation, quasimomentum is conserved, but not momentum. States that are degenerate in both quasimomentum and energy are usually split by the perturbation and there is level repulsion around those values (the levels, or bands, are usually said to hybridize). This opens up gaps in the spectrum at values of $E \sim n^2/8$, for n integer. The maxima and minima of the bands will end up at symmetric points of the quasimomentum. Hence, we can determine by the bootstrap method the spectrum of the periodic or antiperiodic wavefunctions: we concentrate on the endpoints of the bands.

We can test this idea for small values of a, particularly, considering the pole structure

that appears in figures like 4.9. For example, if we take $a = 0.1$ as a small parameter, for example, we find that there are poles in the eigth term of the sequence at $E \simeq 0.494024, 1.12503, 2.00051, 3.12553, 4.50048, 6.12541, 8.00402$, extremely close to the crossings at $E = n^2/8$, for $n = 2, 3, 4, 5, 6, 7, 8$. This shows that the hybridization of levels is taking place exactly where it should by perturbation theory arguments.

For other states, determining q is much harder. The values $q, -q$ are degenerate and that fact is not apparent from the measure on the circle directly. We known that $\exp(iq) \equiv \exp(ip)$, so in principle we can determine an even function of q, $\cos(q) = \cos(p)$. This also works in expectation values.

Unfortunately, since p is unbounded above as an operator, a series truncation of $\cos(p)$ will have large discrepancies at large p. Considering that the probability of measuring a given value of p compatible with q is finite, if these are sufficiently suppressed for high values of p, one might be able to use this method to obtain and approximate value of q. The series of the expectation value of $\cos(p)$ would be obtained from a recursion relation of the expectation values of the even powers of p. These expectation values include contributions from high p and are prone to in principle large errors. This same problem was discovered in [56].

There is another way to address this problem—we can also study the band structure on a longer spatial period of size s times larger. That would compress the value of $\Pi \to \tilde{\Pi} = \Pi/s$. There would then be more crossings in the band structure at fixed a. If we add a small perturbation on $\cos(\theta/s)$, these new crossings will again hybridize and open small gaps. The location of these small gaps could then be used to extract the different values of the quasimomentum with respect to $\tilde{\Pi}$. Indeed, the bootstrap at those exact points would allow non trivial expectation values of $\cos(m\theta/s)$ for some integer m, exactly like what we had in the free particle case: one should be able to detect the non-trivial density matrix structure at those values. The implementations of these

computations are beyond the scope of the present work.

4.5 Bootstrapping scattering problems

For many applications of the quantum mechanical bootstrap to work, the moments of the probability distribution need to be finite, but the scattering problem does not have this property. The essential idea of this section is that the scattering behavior of a potential may be determined by solving a related family of bound-state problems with the same potential, a family parametrized by the boundary conditions at some location. One places a geometric cutoff in the far scattering region and then solves the bound-state problem with all the possible boundary conditions at that cutoff. To determine the scattering phase, one uses the same boundary condition to match to the asymptotic (plane-wave) wavefunction. In this asymptotic region, if the potential is not constant, we supplement the plane-wave solution by a WKB approximation to the desired order of precision.

To follow, we describe how one can determine scattering phase shifts using any numerical eigen-energy algorithm. In particular, these include the semidefinite programming (SDP) bootstrap algorithm developed earlier, now applied to the real half-line. This is similar in spirit to the program of determining scattering data by the energy spectrum at finite volume, which can be realized by a lattice computation [111].

To begin, consider a one-dimensional quantum system with a one-sided potential such that $V(x) = 0$ for $x \leq 0$ and $V \to \infty$ as $x \to \infty$ and with the Hamiltonian given by

$$H = -\partial_x^2 + V(x).$$

Physically, one understands that waves come in from $x = -\infty$, reflect off the potential

barrier, and return to $x = -\infty$ with a phase shift $\delta(E)$ depending on the incident energy E. In this one-dimensional, one-sided system, this phase shift completely specifies the S-matrix and hence the physics of scattering.

Let $R(E) = \exp(i\delta)$ be the reflection coefficient for waves with energy $E = k^2$. One has

$$\psi(x) = A\left[e^{ikx} + R(E)e^{-ikx}\right]; \quad x \leq 0. \tag{4.49}$$

Imagine placing a hard boundary at $x = 0$ and enforcing there a Robin boundary condition

$$\psi(0) + a\psi'(0) = 0 \implies a = -\frac{\psi(0)}{\psi'(0)}. \tag{4.50}$$

Here a, the Robin parameter, is real 'plus infinity'-valued; the point $a = \infty$ corresponds to the Neumann condition. As before the variable a parametrizes self-adjoint extensions of half-line Schrödinger operators [104].

On the right hand side $x \geq 0$, the boundary condition (4.50) defines a self-adjoint Hamiltonian and therefore a discrete spectrum of energies which changes continuously with a. Each value gives a spectrum $E_n(a)$ which may be inverted to give a function $a(E)$. One then matches the value of the wavefunction and its derivative at the boundary $x = 0$. This gives a direct relationship between the reflection coefficient $R(E)$ and the Robin parameter $a(E)$:

$$R(E) = \frac{ika(E) + 1}{ika(E) - 1}; \quad k = \sqrt{E} > 0. \tag{4.51}$$

One can therefore extract the S-matrix by solving a succession of bound state problems for different values of the Robin parameter a. Just as bound states can be considered as a suitably interfering set of plane waves, the data of plane wave scattering are equivalent to a continuous family of bound states.

In this section we demonstrate this approach to determining the scattering phase shift of numerous potentials. We do so by applying the semidefinite programming bootstrap algorithm as well other numerical methods to determine the energy spectrum for half-line problems with arbitrary Robin conditions, and from there to extract the expected reflection coefficients. We demonstrate the consistency of this approach by comparing the numerics to physical expectations for scattering. Finally, we use WKB methods to extend the approach to potentials which are not constant on the scattering region but that are instead slowly varying in the asymptotic regime and for which $V(x) < k^2$ in the $x < 0$ region. We show as an example that we can numerically reproduce the reflection coefficient of the zero-mode Liouville theory by this approach.

4.5.1 The half-line semidefinite algorithm

Earlier in this work we described how to formulate the one-dimensional quantum mechanical bootstrap as a semidefinite program. We showed how this could be applied to determine the spectrum of a polynomial potential of arbitrary degree on the real line. The generalization of this approach to half-line problems is straightforward, though one must include the anomaly terms introduced in Section 4.3 to properly handle the boundary conditions.

Take a potential $V(x)$ on the real half-line $x \geq 0$ and with a general Robin boundary condition at the origin $x = 0$, so that $\psi_0 + a\psi_0' = 0$, writing $\psi_x \equiv \psi(x)$. The only nonzero

anomalies are given by[3]

$$\mathcal{A}[nx^{n-1}] = -\frac{1}{M}\psi_0^2\delta_{n,1}, \tag{4.52}$$

$$2i\mathcal{A}[xp] = -\frac{1}{M}\psi_0\psi_0', \tag{4.53}$$

$$2i\mathcal{A}[p] = \frac{1}{M}\left(\psi_0'\right)^2 + 2\psi_0^2(E - V(0)). \tag{4.54}$$

The last of the anomalies appears in a constraint on expectation values of the operator $\hat{\mathcal{O}} = p$ as:

$$0 = -\langle V'(x)\rangle + 2i\mathcal{A}[p]. \tag{4.55}$$

This is a quantum-corrected version of Newton's second law which now includes an anomalous contribution from the boundary condition. With a polynomial potential $V = \sum^d c_m x^m$ and Robin boundary conditions at $x = 0$, this lowest-level constraint allows one to determine the boundary value ψ_0^2 in terms of the other moments and the energy E:

$$\psi_0^2 = \left[2(E - c_0) + \frac{1}{a^2 M}\right]^{-1} \cdot \sum_{m=1}^{d} 2mc_m\langle x^{m-1}\rangle, \tag{4.56}$$

where we have additionally used the relation $\psi_0' = -\psi_0/a$.

One can therefore express all the nonzero anomalies as linear combinations of moments $\langle x^k\rangle$ of order $k \leq d-1$. Higher moments $\langle x^k\rangle$ with $k \geq d$ can then be computed recursively using the constraints $\langle[\hat{H}, \hat{\mathcal{O}}]\rangle = 0$, $\langle\hat{H}\hat{\mathcal{O}}\rangle = E\langle\hat{\mathcal{O}}\rangle$. Like in the real line case, the higher moments may be written as linear functions of the $d-1$ primal moments $\langle x\rangle, \langle x^2\rangle, \ldots, \langle x^{d-1}\rangle$. Their coefficients will depend (non-linearly) on the energy E and the Robin parameter a.

The formulation and solution of the SDP then proceeds as described in Section 3.3,

[3]If the boundary condition were at some $x \neq 0$, the anomalies would continue to persist at higher orders in the recursion.

with the salient modification being the required positivity of two $K \times K$ moment matrices:

$$M_{ij} = \langle x^{i+j} \rangle, \; M'_{ij} = \langle x^{1+i+j} \rangle; \quad 0 \leq i, j, \leq K-1. \tag{4.57}$$

which are the necessary positivity conditions associated with the Stieljtes moment problem.

One maximizes the minimal eigenvalue of both of these matrices simultaneously, defining the optimization problem

$$\begin{aligned} &\text{maximize} \quad t \\ &\text{subject to} \quad \begin{bmatrix} M & 0 \\ 0 & M' \end{bmatrix} - t \, \mathrm{Id} \succeq 0, \end{aligned} \tag{4.58}$$

at fixed energy E and Robin parameter a. This is a linear semidefinite program with d primal variables $(t, \langle x \rangle, \ldots, \langle x^{d-1} \rangle)$ written in the linear-matrix-inequality form. Pairs (E, a) are deemed physically allowable at size K if the optimal objective $t^\star$ is positive. The convergence property of the bootstrap ensures that if a pair is unphysical at some depth K it will continue to be unphysical at all higher matrix sizes.

It should be noted that the *Mathematica* function `NDEigensystem` now supports Robin (or generalized Neumann) boundary values. At the level of machine precision, this finite element-based algorithm runs orders of magnitude more efficiently than the SDP algorithm described here, which runs on a multiple-precision solver [100]. As a demonstration of the application to half line problems, some of the data in the following sections is generated via the bootstrap algorithm. However, the discussion of the scattering phenomenology and role of the Robin parameter is independent of the algorithm used. It depends only on being able to numerically solve the spectrum of a one-sided differential eigensystem with a Robin boundary condition.

4.5.2 Bootstrapping pure reflection

In the case of pure reflection, the quantity of interest is the reflection coefficient. In terms of the wavenumber $k = \sqrt{E} > 0$ and Robin parameter a it is given by

$$R(k) = \frac{ika + 1}{ika - 1} = e^{i\delta(k)}. \tag{4.59}$$

The phase shift is the complex argument of $R(k)$; using the identity

$$\arg \frac{1 + it}{1 - it} = 2 \tan^{-1}(t), \tag{4.60}$$

one may write the phase shift $\delta(k)$ as

$$\delta(k) = 2 \tan^{-1}(ka). \tag{4.61}$$

By determining $a(E)$ one has determined the phase shift, and hence all the information about scattering off the one-dimensional, one sided potential.

The half-harmonic wall

In the case of a half-harmonic potential wall one can compute the function $a(E)$—and therefore the phase shift—exactly; we compare this to data obtained by solving a succession of bound-state problems using the SDP algorithm described previously.

To be precise, let $V(x) = x^2$ for $x \geq 0$ and zero otherwise. Consider the half line $x \geq 0$ where the Schrödinger equation is

$$-\psi''(x) + x^2\psi(x) = E\psi(x) \tag{4.62}$$

in units where $\hbar = 2m = 1,\ \omega = 2$. The general solution is given by parabolic cylinder

functions $U(a, z)$ (see chapter 12 in [102]) as

$$\psi(x) = c_1 U(-E/2, \sqrt{2}x) + c_2 U(E/2, i\sqrt{2}x). \tag{4.63}$$

Asymptotically, one finds that only the solution with real argument is normalizable as $x \to \infty$. Up to a formal normalization constant, the feasible solution is

$$\psi(x) \sim U(-E/2, \sqrt{2}x). \tag{4.64}$$

The values of the function U and its derivative at zero are known; to construct the Robin function $a(E)$ we take their ratio. This no longer depends on the normalization and is given by

$$a(E) = -\frac{\psi(0)}{\psi'(0)} = \frac{1}{2}\frac{\Gamma\left(\frac{1}{4} - \frac{E}{4}\right)}{\Gamma\left(\frac{3}{4} - \frac{E}{4}\right)}. \tag{4.65}$$

This function already contains all the spectral information of the harmonic oscillator. The full harmonic potential on $\mathbb{R}$ is even, so all states are of odd or even parity. These states satisfy Dirichlet (D) or Neumann (N) conditions at the origin $x = 0$ respectively. Therefore, the odd states of the harmonic oscillator should correspond to $a = 0$ and the even states to $a = \infty$.

The Robin function (4.65) is zero precisely when the gamma function in the denominator diverges and infinite when the numerator diverges. This leads to two quantization rules for the energies E_n depending on the boundary condition in question:

$$E_n = \begin{cases} 3 + 4n; & \text{(D)}, \\ 1 + 4n; & \text{(N)}, \end{cases} \tag{4.66}$$

for $n \geq 0$ in each. Together these rules describe the entire harmonic spectrum, which is

at $E_n = 2n + 1$ for $n \geq 0$ in our units.

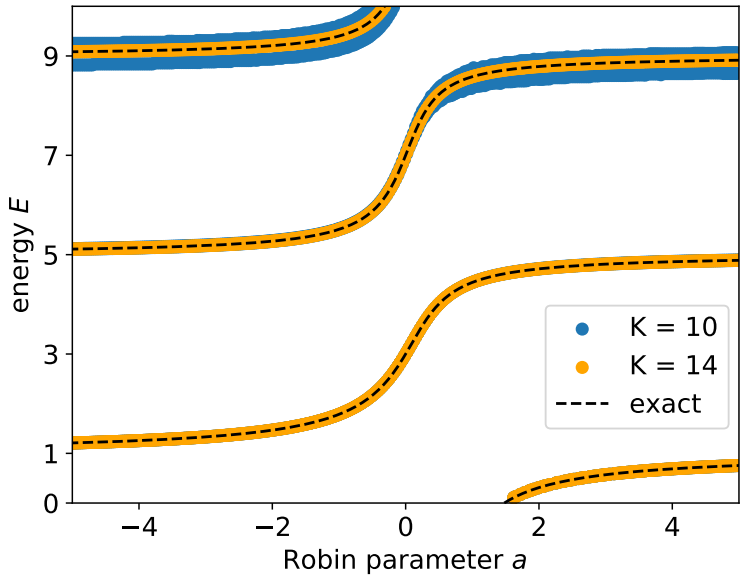

Figure 4.14: Bootstrapped harmonic spectrum versus Robin parameter for two depths $K = 10,\ 14$. At higher energies the intervals of positivity are larger; their size shrinks as K increases. The exact relation (4.65) is shown in black.

We may compare the function $a(E)$ determined here to the bootstrap results. Using the SDP algorithm described in the previous section, we determine the first few harmonic energy levels $E_n(a) \in [0, 10]$ for a range of Robin parameter values $a \in [-5, 5]$. We then invert the spectrum $E_n(a)$ to find the (single-valued) function $a(E)$. These data and the exact curve are shown in Fig. 4.14, showing excellent agreement.

Resonant scattering

The function $a(E)$ contains information not just about bound states but also metastable ones. Consider the Hamiltonian

$$\hat{H} = p^2 + \frac{1}{2}x^2(x-3)^2 \tag{4.67}$$

on the half line $x \geq 0$. This potential has a (local) minimum at $x = 3$ where $V = 0$. Such a local minimum will tend to confine states for a short amount of time, with tunneling to $x < 0$ leading to metastability.

It is generally known that bound and metastable states are reflected in the analytic structure of the S-matrix or, in our case, the reflection coefficient [108]. In the complex E plane, bound states correspond to purely imaginary poles in the upper half-plane and metastable states to poles in the lower half plane.

The signatures of these metastable poles are reflected in the phase shift $\delta(E)$, and in particular its derivative. Let such a metastable pole occur at $E_m = E_0 - i\Gamma$ where $\Gamma > 0$ is the *width* of the metastable state; its characteristic lifetime in the time-dependent picture. Near $E \approx E_m$, the reflection coefficient $R(E)$ should reflect this singular structure and be a pure phase. On general grounds, this implies that near E_m one has

$$R(E) \approx \frac{E - E_0 - i\Gamma}{E - E_0 + i\Gamma}. \tag{4.68}$$

The phase shift is $\delta = \arg R$; with the identity (4.60) one finds that the derivative of $\delta(E)$ near the resonant energy $E_m = E_0 - i\Gamma$ behaves as

$$\delta'(E) \approx \frac{2\Gamma}{(E - E_0)^2 + \Gamma^2}, \tag{4.69}$$

forming a Lorentz/Cauchy distribution centered at E_0 with width Γ. In the context of decay widths, this is often referred to as the Breit-Wigner distribution, and is studied in numerous texts [112, 108].

As before, the phase shift may be numerically determined by the spectral flow of $\hat{H}$ for various values of the Robin parameter a, with the results shown in Fig. 4.15. Here, we do the numerics using the *Mathematica* function `NDEigensystem` to solve for the lowest three

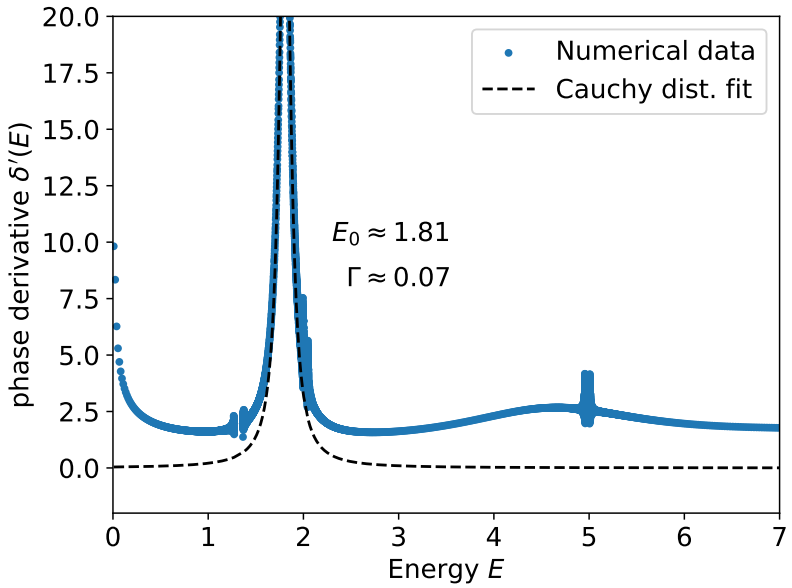

Figure 4.15: A strong energy resonance in the phase shift for a potential with metastable states. A regression to a Cauchy distribution is included in black. In blue, the transformation of spectral numerical data.

eigenstates of the potential (4.67) at a range of Robin parameter values $a \in [-20, -20]$. We invert the spectrum to obtain the function $a(E)$, then construct the phase shift using Eqn. (4.61) and its derivative numerically, using a spline interpolation to decrease noise. An energy resonance is clear in Fig. 4.15, corresponding to the existence of a metastable state of the potential and consistent with physical expectations.

4.5.3 Liouville scattering

The potentials considered in the previous sections are unique and hand-picked in that they are identically zero on the negative real axis. This allows an exact solution of the Schrödinger equation in the $x < 0$ region and subsequent matching of boundary conditions to extract the phase shift from dependence of the Robin parameter on the energy.

In many situations, the potential may be nonzero but slowly-varying and weak at

large negative x. This is the case for the exponential potential which famously arises as the potential in the semiclassical Liouville theory [113, 114]. To be precise, after canonical quantization the zero-mode Hamiltonian is

$$\hat{H}_0 = \frac{p^2}{2} + 2\pi\mu e^{2bx}, \tag{4.70}$$

ignoring any zero-point energy. From the perspective of the fundamental dilaton field this Hamiltonian follows by considering spatially uniform solutions: the 'mini-superspace' approximation. We are not concerned with the physical origin of the theory so much as applying the tools of the previous section to the one-sided exponential potential.

The Schrödinger equation corresponding to the Hamiltonian (4.70) is

$$-\frac{1}{2}\psi''(x) + 2\pi\mu e^{2bx}\psi(x) = \frac{k^2}{2}\psi(x), \tag{4.71}$$

where now we use the dispersion $E = k^2/2$. This is solved by a linear combination of Bessel functions whose properties are well-known. By demanding regularity at $x = \infty$ and matching to the plane wave ansatz (4.49), one find that the reflection coefficient $R(k)$ is given by

$$R(k) = -(\pi\mu/b^2)^{-ik/b}\frac{\Gamma(1+ik/b)}{\Gamma(1-ik/b)} \tag{4.72}$$

We will reproduce this, at least approximately, by combining the bound-state approach with a WKB approximation to the wavefunction. One sets a boundary and solves a one-sided bound state problem with Robin boundary condition on the right-hand side of the boundary, as before. Placing the boundary at some modestly large, negative position L then ensures that the semiclassical (WKB) approximation is valid and accurate to the left of the boundary, at least for potentials which smoothly go to zero. This is certainly true for the exponential potential $V = e^{2bx}$, which, along with its derivative, goes to zero

very quickly as $x \to -\infty$. For our purposes, we need a regime where $k^2 \gg V(x)$ and that V varies slowly on the scale of k (any feature of V needs to occur on a region that is long compared to the local wavelength $1/k(x) \sim 1/k$).

The WKB wavefunction

Any wavefunction can be written in the form

$$\psi(x) \propto \exp(\lambda(x) + i\omega(x)). \tag{4.73}$$

In the WKB approximation, the functions $\lambda(x)$, $\omega(x)$ (modulating the amplitude and phase, respectively) are expanded in powers of the formally small parameter $\hbar$ as

$$\omega(x) = \frac{1}{\hbar} S_0(x) + \hbar S_2(x) + \hat{\mathcal{O}}(\hbar^3), \tag{4.74}$$

$$\lambda(x) = S_1(x) + \hbar^2 S_3(x) + \hat{\mathcal{O}}(\hbar^4). \tag{4.75}$$

The functions $S_n(x)$ satisfy a hierarchy of equations found by substituting the ansatz (4.73) into the Schrödinger equation and solving order-by-order in $\hbar$. In particular, the lowest-order correction $S_0(x)$ solves the eikonal equation

$$[S_0'(x)]^2 = 2(E - V(x)). \tag{4.76}$$

If one takes $V \to 0$ in this equation, one finds $S_0(x) = \pm\sqrt{2E}x = \pm kx$, reproducing the free plane-wave solution seen earlier.

Because the potential is real, on general grounds the semiclassical (WKB) wavefunction is given by the linear combination

$$\psi_{scl} = Ae^{\lambda(x)}e^{i\omega(x)} + Be^{\lambda(x)}e^{-i\omega(x)}. \tag{4.77}$$

The data of the reflection coefficient $R(k)$ is contained in the asymptotic relative normalization of these two solutions: roughly the ratio B/A as $x \to -\infty$. The semiclassical wavefunction interpolates between the asymptotic limit, where the S-matrix is defined, and a finite value $L < 0$, where the potential is slowly varying. Here where the WKB approximation is valid we place a boundary at $x = L < 0$. On the right-hand side, one defines a bound state problem with Robin boundary condition

$$\psi(L) + a_L \psi'(L) = 0. \tag{4.78}$$

Solving this determines a spectrum $E_n(a_L)$ which is subsequently inverted to obtain a function $a_L(E)$ as described in the previous section.

By continuity of the wavefunction and its derivative at the point $x = L$, the semiclassical wavefunction should define the same Robin parameter:

$$a_L = -\frac{\psi_{scl}(L)}{\psi'_{scl}(L)}. \tag{4.79}$$

Substituting the equation (4.77), one can determine a relation between the ratio of coefficients B/A of the semiclassical wavefunction and the Robin parameter a_L at finite L:

$$B/A = -e^{2i\omega(L)} \frac{1 + a_L\lambda'(L) + ia_L\omega'(L)}{1 + a_L\lambda'(L) - ia_L\omega'(L)}, \tag{4.80}$$

where the a_L, $\lambda(x)$, and $\omega(x)$ all implicitly depend on the energy E.

On the other side of the domain, relating the reflection coefficient R to the ratio B/A requires another matching formula. Define the angle θ_0 as the limit

$$\theta_0 \equiv \lim_{x \to -\infty} \omega(x) - kx, \tag{4.81}$$

recalling that here $k = \sqrt{2E}$. This limit is finite in general due to the known asymptotic behavior of the function $S_0(x)$, which dominates the expansion of the function $\omega(x)$ at large negative x. With this angle appearing as a decorating phase, the asymptotic reflection coefficient is

$$R_{scl}(k) = -e^{-2i\theta_0} e^{2i\omega(L)} \frac{1 + a_L\lambda'(L) + ia_L\omega'(L)}{1 + a_L\lambda'(L) - ia_L\omega'(L)}. \tag{4.82}$$

Taking the argument of this function yields the WKB-corrected phase shift as a function of the wavenumber $k = \sqrt{2E}$:

$$\delta_{scl}(k) = -\pi + 2\tan^{-1}\left(\frac{a_L\omega'(L)}{1 + a_L\lambda'(L)}\right) + 2(\omega(L) - \theta_0) \mod 2\pi. \tag{4.83}$$

The WKB approximation may then be carried out to any order in calculating the functions $\omega(x)$ and $\lambda(x)$ to determine increasingly accurate expressions for the phase shift.

As the potential $V \to 0$, one finds that $\lambda' \to 0$ while $\omega' \to k$. In this limit one also has $\omega(L) - \theta_0 \to kL$. This limit reproduces the expression (4.61) for a boundary at $x \neq 0$. In this way the zero-order WKB approximation reduces to the results determined earlier.

We note that there is a calculational trade-off in the location of the cutoff L. As one takes $L \to -\infty$ and the potential weakens in strength, the WKB approximation grows increasingly accurate. However, the bound state problem, defined on $[L, \infty)$, has low-lying eigenenergies with wavelengths of order $|L|$, which in turn are the only states for which this matching procedure determines the physics of scattering. One therefore must balance accuracy of the WKB approximation with the range of wavenumbers k for which the phase shift may be approximately determined.

The exponential potential

As a demonstration, we show the accuracy of the WKB approach to approximating the scattering phase (4.72), setting $\mu = 1/2\pi$ and $b = 1$ for definiteness. First, one can explicitly compute the lowest-order WKB functions $S_n(x)$, from which the amplitude and phase modulation may be constructed. Defining the semiclassical momentum

$$p(x) = \sqrt{2(E - V(x))} = \sqrt{2(E - e^{2x})}, \tag{4.84}$$

the first four WKB functions $S_n(x)$ are given by:

$$S_0(x) = p(x) - k \tanh^{-1}\left(\frac{p(x)}{k}\right), \tag{4.85}$$

$$S_1(x) = -\frac{1}{2}\log p(x), \tag{4.86}$$

$$S_2(x) = \frac{2E + 3e^{2x}}{24\sqrt{2}p(x)^3}, \tag{4.87}$$

$$S_3(x) = \frac{p''(x)}{8p(x)^3} - \frac{3p'(x)^2}{16p(x)^4}. \tag{4.88}$$

The correction S_0 is by far the largest in absolute numerical terms and increases in size as $x \to -\infty$. A large phase is to be expected, as the eikonal or first-order WKB approximation is equivalent to a saddle-point or stationary phase path integral.

Most applications of the WKB method include only the first two corrections $S_0,\ S_1$. Indeed we find that these corrections are more than sufficient to reproduce the exact phase shift law (4.72) by solving bound-state problems and applying the approximation of Eqn. (4.83). These data are shown in Fig. 4.16 along with the exact curve for a boundary at $L = -5$.

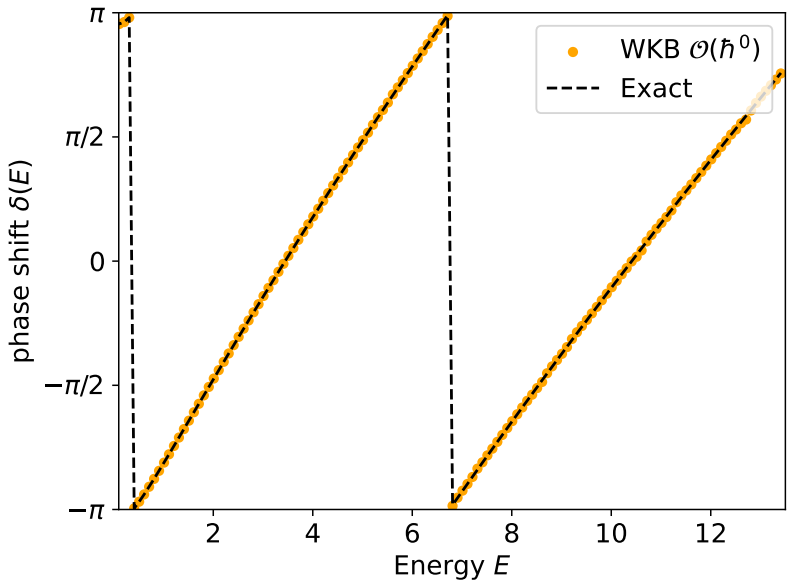

Figure 4.16: Phase shift due to reflection off the exponential potential reconstructed with the first-order WKB approximation (orange) compared to the exact result (dashed, black). With a boundary at $L = -5$, we solve the bound state problem on the right to define the Robin function $a_L(E)$. In blue, the naive application of Eqn. (4.61) with $a_L(E)$. In orange, the correction functions $S_0(x)$, $S_1(x)$ give the approximate semiclassical phase shift with good accuracy.

4.5.4 Discussion: bootstrapping domains with boundary

With the analysis of scattering phenomena from the perspective of the bootstrap, we have addressed and developed the application of these methods to essentially all basic Schrödinger problems in one dimension. The key insight was the identification of the way boundary conditions enter algebraically into the moment recursion relations. The incorporation of the anomaly terms allowed us to generalize the naive and semidefinite bootstrap algorithms to new domains with arbitrary boundary conditions.

The goal of these developments is to provide a framework for analyzing more complex quantum mechanical systems through a bootstrap approach. We did see that certain aspects the state were insofar out of reach, i.e. the Bloch quasimomentum. Understanding how the bootstrap may become sensitive to this parameter, or proving that it cannot, would be an interesting direction for further work.

Additionally, our discussions so far have focused exclusively on polynomial potentials. This is because the algebra of x, p naturally contains only polynomials in x, and this algebra leads to closed recursions for the positional moments x^n. The present methods would gain significantly more generality if the ideas could be extended to rational potentials $V(x) = p(x)/q(x)$ where $q(x) \neq 0$. The bootstrap methods so far are essentially problems of polynomial optimization, where the polynomial degree is increased at each depth by the moment recursion. The similar problem of rational optimization has been studied in the mathematical literature [87]. If these methods could handle arbitrary rational potentials, through e.g. Pade approximants one could bootstrap to arbitrary precision almost any potential regardless of functional form.

Chapter 5

Bootstrap methods in spin chains

In this chapter we bring the bootstrap program full circle by attempting to use it to extract numerical conformal data from critical quantum spin chains. Unlike the conformal bootstrap, we do this by studying finite-size spin chains at criticality and regressing their properties—energy and correlation functions—with the known, universal finite-size behavior. This work is directly inspired by the preliminary investigations along these lines carried out in [70], which extended the bootstrap program in high energy theory to many-body systems. Having addressed most familiar one-dimensional Schrödinger systems, we consider the graduation to one-dimensional spin systems as the capstone to this work's investigation of bootstrap methods in $1 + 1d$ quantum systems.

We construct hierarchies of non-commutative optimization problems and solve them to determine conformal weights and central charges for two spin chains where the conformal data is exactly known: the (integrable) tranverse-field Ising model and the (non-integrable) self-dual axial next-nearest-neighbor Ising (ANNNI) model. With the correct setup, the approach can yield good numerical results in the integrable Ising model. We then apply these same approaches to the non-integrable model, which has multiple phases associated to three different emergent CFTs, to see how the approach may generalize.

Our investigations reveal that there exist significant challenges to reliably estimating these data in generic spin systems and that the convergence of these methods is still not fully understood. Other methods for the extraction of conformal data, such as the lattice modes and periodic uniform matrix product states approach of [115, 116, 117], at present provide a more robust solution to determining CFT spectra from critical spin systems. However, the approach taken by these works relies on an exact or approximate diagonalization of the full Hamiltonian. The power of the semidefinite approach is its ability to study only correlations of operators in the state while remaining agnostic to the state itself.

5.1 Bootstrapping ground states

Determining the ground state of a quantum mechanical system is a canonical example of a difficult but convex optimization problem. Usually, 'solving' a quantum system is understood to be the problem of determining a state $|\psi\rangle$ in a physical Hilbert space $\hat{H}$ subject to the constraints of unitarity, $\langle\psi|\psi\rangle = 1$, and any dynamical relations furnished by the Hamiltonian $\hat{H}$. One understands operators as mapping states to other states. However, one may also view the problem algebraically. The data of the generic quantum mechanical problem may be restated as an algebra of observables $\mathcal{A}$ (which act on the Hilbert space) and a set of linear functionals $\omega_\psi : \mathcal{A} \to \mathbb{R}$ which represent the physical states. Here, one views states as acting on operators.

Ground state problems are traditionally approximated using the variational principle. The variational principle relies on the fact that given any normalizable state $|\psi\rangle$, the true ground state energy of the system E_0 provides a global lower bound on the expectation value of the Hamiltonian in this state: $\langle\hat{H}\rangle_\psi \geq E_0$. Any particular variational approach describes a recipe for constructing a well-parametrized state that hopefully gives one a

close upper bound on the true energy. It is informally similar to bootstrap methods in the sense that it requires a well-informed guess which is then bounded by general constraints on the ground state energy.

Formally, the bootstrap and variational approaches represent dual simplifications of the same fundamental, exact optimization problem. To make this precise, consider an interacting quantum system with many degrees of freedom. Any physical state defines, or is equivalently defined by, a Hermitian positive semidefinite (PSD) density operator $\rho \succeq 0$. The ground state of a system with Hamiltonian $\hat{H}$ is the optimum $E^\star$ of the convex optimization problem

$$\begin{aligned} \text{minimize} \quad & \text{tr}(\rho \hat{H}), \\ \text{subject to} \quad & \rho \succeq 0;\ \text{tr}(\rho) = 1, \end{aligned} \tag{5.1}$$

where the optimization occurs over the positive semidefinite (PSD) cone of all physical density matrices, defining a semidefinite program (there is additionally a Hermiticity constraint $\rho^\dagger = \rho$ which we take to be implicit in the semidefinite constraint throughout) [86]. While formally simple, this optimization problem generically contains an exponential number of degrees of freedom in the physical size of the system. For example, if the system is composed of N qubits, a generic density matrix is specified by $\mathcal{O}(2^{2N})$ parameters all coupled by the semidefinite constraint, making a direct solution of (5.1) infeasible for all but the smallest systems.

In order to make the program computationally tractable, one must somehow simplify the semidefinite constraint. Broadly speaking, there are two ways to do this: by either restricting or enlarging the feasible domain (recall that the feasible domain is the set of optimization variables where the constraints are satisfied). The variational approach restricts the feasible domain and views the problem in terms of states. Any variational

ansatz—matrix product states, projected entangled-pair states—is a parametrization of a set of density matrices ρ_θ by a linear or at worst polynomial (in the system size N) set of parameters θ. These states are usually constructed to be PSD and normalizable and hence the problem (5.1) becomes the much smaller optimization problem

$$\begin{aligned} \text{minimize} \quad & \operatorname{tr}(\rho_\theta \hat{H}), \\ \text{subject to} \quad & \rho_\theta \succeq 0;\ \operatorname{tr}(\rho_\theta) = 1, \end{aligned} \tag{5.2}$$

over the variational parameters. However, depending on the parametrization chosen, the problem may no longer be convex; it can be stored in memory, but determining the optimal choice of parameters may require finely-tuned non-linear optimization methods like stochastic gradient descent.

The price of this parametrization is that the optimum $E_\theta^\star$ of the program (5.2) gives only an upper bound on the true ground state energy: $E_\theta^\star \geq E^\star$. This is because any sub-exponential parametrization of states ρ_θ necessarily covers only a strict subspace of the entire physical Hilbert space $\mathcal{H}_\theta \subset \mathcal{H}$. Good ansatze will offer a sharp upper bound, but the feasible domain will (almost) never extend to cover the exact ground state.

While the variational approach restricts the feasible domain to the space of variational parameters, bootstrap methods instead *relax* the semidefinite constraint by enlarging the feasible domain. Informally, this means enforcing positivity only on some submatrix of the entire density matrix ρ. This can be realized as follows. The semidefinite constraint $\rho \succeq 0$ is equivalent to the positivity of $\operatorname{tr}(\rho\hat{\mathcal{O}}) \geq 0$ for all positive semidefinite operators $\hat{\mathcal{O}} \succeq 0$ in the observables algebra $\mathcal{A}$, a subset we can call $\mathcal{A}_+$. To relax the constraint, one enforces this positivity condition on only a subset of such operators $\mathcal{S} \subset \mathcal{A}_+$, defining

the semidefinite program

$$\begin{aligned} &\text{minimize} && \mathrm{tr}(\rho \hat{H}), \\ &\text{subject to} && \mathrm{tr}(\rho \mathcal{S}_i) \geq 0;\ \mathrm{tr}(\rho) = 1. \end{aligned} \tag{5.3}$$

Whereas in the variational approach we optimized over a subspace of the physical Hilbert space, our relaxed constraint now means we are optimizing over a larger Hilbert space which contains possibly unphysical states: $\{\mathrm{tr}(\rho\mathcal{S}) \geq 0\} \supset \{\mathrm{tr}(\rho\mathcal{A}) \geq 0\}$. Therefore, the optimum $E^\star_{\mathcal{S}}$ of the program (5.3) always give a lower bound on the true optimum: $E^\star_{\mathcal{S}} \leq E^\star$.

The bootstrap and the variational principle are in this sense dual approximations of the same fundamental optimization problem. While the challenge in the variational approach is the selection of a "good" variational ansatz (a subset of states), the challenge in the bootstrap approach is the selection of a "good" subset of operators $\mathcal{S}$ on which to enforce the positivity constraint.

5.2 The many-body bootstrap

With the general motivation in mind, let us formalize the setup of interest. We consider a finite quantum spin chain on N sites. In principle we can consider any number of dimensions but we confine ourselves to one spatial dimension throughout this work. To each site n is associated a finite set of operators $\{\hat{\mathcal{O}}^{(i)}_n\}$ which collectively form an algebra $\mathcal{A}$ over the entire chain. In the case of a spin-1/2 chain, one has the Pauli matrices I, X, Y, Z at each site, and the algebra is $\mathbb{R}^{\otimes 4N}$ as usual. Let $\mathrm{span}(\mathcal{B}) \subset \mathcal{A}$ be some subspace which contains the Hamiltonian; regarding the basis $\mathcal{B}$ as a vector of operators one may write

$$\langle \hat{H} \rangle = c^T \langle \mathcal{B} \rangle, \tag{5.4}$$

for some (complex) vector c. Here, the expectation value should be viewed as a linear functional $\langle\cdot\rangle : \mathcal{A} \to \mathbb{C}$ on the operator algebra; the space of such maps is the domain of the optimization. This functional is exactly analogous to the functional $L_{\mathbf{y}}(\cdot)$ used to define the Lasserre hierarchy in Chapter 2.

For any set of operators $\mathcal{B}$, we construct the moment matrix M, a $|\mathcal{B}| \times |\mathcal{B}|$ Hermitian matrix with elements

$$M_{ij}(\mathcal{B}) = \langle \mathcal{B}_i^\dagger \mathcal{B}_j \rangle. \tag{5.5}$$

The relaxed density matrix constraint of (5.3) is equivalent to a matrix positivity condition on $M(\mathcal{B})$:

$$M(\mathcal{B}) \succeq 0. \tag{5.6}$$

This positivity condition is the same as that which appears in the classical moment problem [101, 87] and in most if not all of the previous literature on the bootstrap program outside of CFT. This constraint is required by unitarity and is generically contained within, if not equivalent to, the positivity constraints which form the convergent relaxations (2.32) of the non-commutative polynomial optimization problem (2.31).

There may be other physical constraints. For example, if we wish to consider only energy eigenstates (which includes the ground state), one has the linear constraints

$$\langle [\hat{H}, \hat{\mathcal{O}}] \rangle = 0. \tag{5.7}$$

for any operator $\hat{\mathcal{O}}$. Earlier chapters, on the bootstrap in Schrödinger quantum mechanics, uncovered additional anomalous constraints both linear and semidefinite which encode boundary conditions or other limiting information about the states under consideration. Other possible additions may include constraints on the entropy or variance of states and observables [48, 38]. We note that since these systems have finite-dimensional

Hilbert spaces, Hamiltonians need only be Hermitian in order to be essentially self-adjoint.

The bootstrap problem for the ground state energy is therefore the following semidefinite program: given an operator basis $\mathcal{B}$ and Hamiltonian $\hat{H}$, solve

$$\begin{aligned} \text{minimize} \quad & \langle \hat{H} \rangle = c^T \langle \mathcal{B} \rangle, \\ \text{subject to} \quad & M(\mathcal{B}) \succeq 0; \ \langle [\hat{H}, \mathcal{B}_i] \rangle = 0. \end{aligned} \tag{5.8}$$

A key idea of the approach is that of hierarchies. By considering increasingly large operator bases $\mathcal{B}$, the result of the optimization problem (5.8) approaches the exact value, coinciding when $\mathcal{B} \cong \mathcal{A}$ or when certain conditions on the rank of the optimal M are met [46]. Formally, for a flag of subspaces

$$\{1\} \subset \text{span}(\mathcal{B}_1) \subset \text{span}(\mathcal{B}_2) \subset \cdots \subset \mathcal{A}, \tag{5.9}$$

one has $E^\star_{\mathcal{B}_1} \leq E^\star_{\mathcal{B}_2} \leq \cdots \leq E^\star$. The semidefinite constraint at level 2 contains that at level 1 and so on. This hierarchy allows one to construct increasingly large programs the optima of which grow increasingly close to the correct value of the objective function [44]. Note that we are considering here a less structured hierarchy of bases rather than the hierarchy of 'word' lengths used to construct the set of relaxations in (2.32). If the bases in the hierarchy are chosen correctly, one may even be guaranteed exponential convergence toward the exact value in the size of the basis chosen [49]. In principle the correlation functions—the matrix elements of $M(\mathcal{B})$—should also approach their exact value, but their convergence properties are not as well understood and experimentally appear weaker than those of the objective function. This latter notion of convergence is not addressed in the works studying convergent relaxations, which focus on the the objective function.

5.2.1 Related work in condensed matter and quantum information theory

We quickly review in a bit more detail the related approaches to semidefinite methods in spin chains described in the introduction. Early work [24] studied fermionic systems and considered only two-body density matrices, which in the case of fermionic ground states of electronic systems, provides a decent variational ansatz. While this "reduced density matrix" theory leveraged semidefinite programming, it was a variational approach rather than a bootstrap approach, with the variational parameters being matrix elements of the two-body reduced density matrix.

Some time later, Barthel & Hubener and Mazziotti [118, 37] systematized the semidefinite approach, defining a hierarchy of problems of the form (5.8) and providing lower bounds on the energy of various spin systems. In [37], considering any spin system algebra as being comprised of Jordan-Wigner fermion ladder operators, the authors consider a flag of subspaces given by (the span of) normal-ordered monomials of ladder operators of increasing degrees $k, k+1, \ldots$. Each of these subspaces defines, after taking expectation values, a set of e.g. k-point Green's functions, and the hierarchy of such subspaces provides successively better estimates of the ground state energy. Considering the fermion algebra as the Banach space of observables, the work [37] defined exactly the hierarchy of relaxations proposed as a generalization of Lasserre's non-commutative hierarchy in [44].

While the ground state energy problem is already QMA-hard, Barthel & Hubener note that consideration of the Green's functions is related to another QMA-hard problem, the so-called representability problem. Given some k-point operator $\hat{\mathcal{O}}^{(k)} = a_{i_1}^\dagger \cdots a_{i_m}^\dagger a_{i_{m+1}} \cdots a_{i_k}$, the exact k-point Green's function is given by $G_k(\hat{\mathcal{O}}) = \mathrm{tr}(\rho \hat{\mathcal{O}}^{(k)})$ where ρ is the exact density matrix of the entire system. Given access only to ostenisble numerical values

of $G_k(\hat{\mathcal{O}})$ for various operators $\hat{\mathcal{O}}$, determining whether these values are consistent with being derived from a global physical state ρ is QMA-complete.

To evade this, the authors note that the condition $G_k(\hat{\mathcal{O}}) = \mathrm{tr}(\rho\hat{\mathcal{O}}^{(k)})$ for a global state is not equivalent to but requires that

$$G_k(X^\dagger X) \geq 0 \tag{5.10}$$

for any operator X. Not all positive semidefinite $\hat{\mathcal{O}}_+$ operators have such a representation $\hat{\mathcal{O}}_+ = X^\dagger X$, but any such operator $X^\dagger X$ is positive semidefinite. This is therefore exactly a 'sum-of-squares' relaxation of the general Green's functions positivity constraint, relating the approach to the theory of polynomial positivity addressed earlier in this work.

Subsequent works [38, 43] construct different hierarchies of operator bases but rely on the same positivity conditions and the notion of semidefinite relaxations; some introduce slightly different formulations of the ground energy problem which nonetheless provide lower bounds to the optimum [42, 52]. More recently, modifications of these types of semidefinite methods introduce aspects of renormalization [39] and clustering of operators [40]. In these works, the authors are able to compute the ground state of numerous spin systems to great accuracy including the Hubbard model, which, due to the fermion sign problem, is known to be difficult for Monte Carlo methods.

The central focus of all these works is the computation of the ground state energy. While technically a QMA problem, many results (including ours) indicate that especially for translation-invariant systems, semidefinite methods quite quickly and easily give good estimates of the ground state energy, i.e. within a few percent error, even in relatively naive setups. However, the computation of ground state correlations via semidefinite methods is much less studied. In [38], the authors demonstrate that semidefinite meth-

ods give values of the spin-spin correlation function which qualitatively agree with density matrix renormalization group (DMRG) results. However, qualitative agreement is insufficient if one's goal is the accurate extraction of conformal data via this method.

The topic of computing and bounding correlations by semidefinite or bootstrap methods has recently received some specific attention. The review [50] addressess a number of problems in quantum information and gives a good overview of how semidefinite and related methods can be applied to qubit systems. A pair of papers by Fawzi et al. [48, 49] go a step further and provide 'certified' algorithms for bounding expectation values of arbitrary observables in the ground state of a quantum system potentially at nonzero temperature. These works provide a concise and complete description of the relevant optimization problems and associated constraints, and even offer some proofs of the exponential convergence of these methods observed in certain cases. They address directly the issue of correlation functions and use their algorithm to produce rigorous bounds for the ground state correlators. However, for the size of optimization problem constructed, the obtained bounds are again far too weak for the analysis of conformal data, as we verified in our own numerical experimentation.

5.3 The transverse-field Ising model

To study the issue of determining correlations in spin systems by semidefinite methods, we now turn to the canonical example of a spin chain with a CFT limit: the transverse-field Ising model. It is a one-dimensional (plus time) spin chain on N sites. The operator algebra $\mathcal{A}$ has 4^N elements: the four Paulis $\{I, X, Y, Z\} = \{I, \sigma^a \mid a = x, y, z\}$ at each site and their tensor products. They obey the standard algebraic relations

$$[\sigma_i^a, \sigma_j^b] = 2i\varepsilon^{abc}\sigma_j^c\delta_{ij} \qquad \text{(no sum over } j\text{)}. \tag{5.11}$$

We use the Hamiltonian

$$\hat{H} = -\sum_{j=1}^{N} [X_j X_{j+1} + hZ_j] \tag{5.12}$$

with periodic boundary conditions $N + 1 \equiv 1$. The Hamiltonian is translation-invariant which means the ground state is translation invariant (in particular, $\mathbb{Z}_N$ invariant). We will use this symmetry to reduce the number of optimization variables. As is well known, in the thermodynamic limit $N \to \infty$ at $h = 1$, the theory describes a free fermion compactified on the circle. This conformal field theory has central charge $c = 1/2$.

A specific program is specified by an operator basis $\mathcal{B}$, which we view as a vector of operators. We will consider a number of different operator bases and observe each of their convergence properties, but we begin with a very simple choice: define

$$\mathcal{B}_0 = \{I\} \cup \{X_i, Y_i, Z_i \mid i = 1, \ldots, N\}. \tag{5.13}$$

The moment matrix $M(\mathcal{B}_0)$ is constructed as

$$M(\mathcal{B}_0) = \langle \mathcal{B}_0 \mathcal{B}_0^\dagger \rangle \succeq 0, \tag{5.14}$$

and is therefore a $(3N+1) \times (3N+1)$ matrix for this particular choice of operator basis. Its matrix elements are correlation functions which will act as the optimization variables of the semidefinite program. Many of these matrix elements are linearly dependent either due to algebraic relations between the operators in $\mathcal{B}_0$ or by invariance of the functional $\langle \cdot \rangle : \mathcal{A} \to \mathbb{R}$ under translation and potentially other discrete symmetries.

To handle these equalities, we write the relevant semidefinite program in the linear matrix inequality (LMI) form, which is customarily regarded as the dual formulation.

This regards the matrix $M(\mathcal{B}_0)$ as a linear combination of matrices, i.e.

$$M(\mathcal{B}_0) = F_0 + x_1 F_1 + x_2 F_2 + \cdots , \tag{5.15}$$

where the F_i are numerical, Hermitian matrices, and the x_i are unique correlation functions: $\langle X \rangle, \langle X_1 Y_3 \rangle, \langle Z_1 Z_2 \rangle$, etc. For a given operator basis, the construction of the x_i, F_i is independent of the objective function. In practice, this means that semidefinite solvers can cache matrix factorizations, leading to increased speed at runtime.

5.3.1 Computational implementation

To flexibly construct many different semidefinite programs, we used the `OpenFermion` package from Google Quantum AI [119]. This Python package defines efficient Pauli and fermionic algebra objects and includes routines for exact diagonalization, Trotterization, etc. We use these native objects to define elements of the algebra of observables $\mathcal{A}$.

Operators in $\mathcal{A}$ are generically linear combinations of products of Pauli matrices. Products are then encoded as N-length strings: $\langle X_1 \rangle = XIII \cdots I$, $\langle Z_1 Z_3 \rangle = ZIZII \cdots I$, and so on. To take advantage of translation invariance, we define a cyclic invariant hash function which takes as input a string of length N and outputs an integer hash value invariant under cyclic shifts of the string. In general, the hash function should be constructed to be invariant under symmetries of the ground state. In the periodic BC case each unique hash value corresponds to the orbit of a given correlation function under $\mathbb{Z}_N$ translation acting on the operators and becomes an optimization variable x_i of the semidefinite program. The number of such (dual) variables n_d depends on the number of sites, the length of the operator basis, and any special algebraic relations that may exist between elements of the basis. Operator bases must be chosen so that $\langle \hat{H} \rangle$ may be written as a linear combination of the optimization variables x_i.

A semidefinite program for any spin chain ground state is therefore specified by a Hamiltonian $\hat{H}$ and an operator basis $\mathcal{B}$; the algebraic relations are automatically computed to determine the x_i. Finally, one defines the optimization problem

$$\begin{aligned} \text{minimize} \quad & \langle \hat{H} \rangle = \textstyle\sum_{i=1}^{n_d} c_i x_i, \\ \text{subject to} \quad & M(\mathcal{B}_0) = F_0 + \textstyle\sum_{i=1}^{n_d} x_i F_i \succeq 0. \end{aligned} \tag{5.16}$$

At this point, one may choose to add extra constraints. Outside of enforcing symmetries like cyclic or translation invariance on the expectation values, there are two types of constraints one can generically add to the ground-state problem. Both types are considered and utilized in the "certified" algorithms of Fawzi et al. [48, 49]. The first are eigenstate constraints of the form

$$\langle [\hat{H}, \hat{\mathcal{O}}_i] \rangle = 0. \tag{5.17}$$

These apply in any energy eigenstate, and essentially state that time evolution for the states in question is trivial. The second are unique to the ground state and state that any perturbation to the state raises the energy:

$$\langle \hat{\mathcal{O}}_i^\dagger [\hat{H}, \hat{\mathcal{O}}_i] \rangle \geq 0. \tag{5.18}$$

We experimented in multiple instances with including these constraints in the optimization, but find that they rarely affect the outcome for SDPs written in terms of spin variables. This behavior was also noted by Lawrence [70]. However, the equality constraints appear to be crucial for constructing fermionic SDPs. Note that the inclusion of these constraints may require new operators to be added to the basis (and therefore more optimization variables), which can in practice diminish the performance of the solver.

Once the problem is constructed in this fashion, we use the the `cvxpy` package with

MOSEK to solve the SDP [120, 121]. While we experimented with using sparse matrix data structures, we did not find that these increased the performance and sometimes even slowed down the internal compilation of the SDP. Compilation was slow in general. This issue could be addressed by working directly with a command-line SDP solver [100], some of which are natively adapted to parallel processing and handling extremely large problems. This would require manually converting complex to real variables and writing/reading IO files, but would avoid slowdowns in `cvxpy` compilation.

5.3.2 Choosing an operator basis

For a fixed Hamiltonian and system size N, the computational implementation of the bootstrap takes in an operator basis $\mathcal{B}$ and outputs numerical approximations of the energy and any ground-state correlation functions contained in the (optimized) moment matrix $M(\mathcal{B})$. These can be numerically extracted and subsequently compared to the known, exact values.

To understand the performance of the method, we consider four different operator bases. The first is the basis of one-site operators $\mathcal{B}_0$ with size $3N+1$. To go one step up in the hierarchy, we define

$$\mathcal{B}_1 = \mathcal{B}_0 \cup \{\sigma_1^a \sigma_2^b \mid a, b = x, y, z\}. \tag{5.19}$$

So far, the hierarchy $\mathcal{B}_0 \subset \mathcal{B}_1$ is similar to that proposed in [38], but at level $\mathcal{B}_1$ we anchor each nearest-neighbor two-point function at site 1, resulting in a basis of size $|\mathcal{B}_1| = 3N+10$. At the proximate level, consider all nearest-neighbor two-point functions, taking

$$\mathcal{B}_2 = \mathcal{B}_0 \cup \{\sigma_1^a \sigma_n^b \mid a, b = x, y, z;\ n = 2, \ldots, N\}. \tag{5.20}$$

This basis is much larger, with size $|\mathcal{B}_2| = 12N + 1$.

Finally, we consider a special basis: that of the Jordan-Wigner fermion ladder operators. Recall that the JW fermion operators $c_i, c_i^\dagger$ are constructed of long strings of Paulis:

$$c_i = \frac{1}{2} \prod_{j=0}^{i-1} [-Z_j] \, (X_i - iY_i), \tag{5.21}$$

$$c_i^\dagger = \frac{1}{2} \prod_{j=0}^{i-1} [-Z_j] \, (X_i + iY_i). \tag{5.22}$$

We use these operators to define the fermion basis

$$\mathcal{B}_F = \mathcal{B}_0 \cup \{c_i, c_i^\dagger \mid i = 1, \ldots, N\}, \tag{5.23}$$

where the basis $\mathcal{B}_0$ is included so that all two-point correlation functions of interest can be (easily) obtained from the program optimum. Since the Ising Hamiltonian is known to be quadratic in this basis, we should expect that the fermion basis yields the best results, similarly to the harmonic oscillator system in the Schrödinger bootstrap. Of course, its introduction here relies on our prior analytical knowledge that the system has an exact free-fermion description.

While these operators obey fermion algebraic relations, they are still fundamentally written in terms of spin variables. One can instead construct SDPs which use the JW fermions as algebraic primitives. While this approach can work well to determine the ground state, it becomes very difficult to extract local spin correlation functions from the fermion description. For interacting fermionic Hamiltonians, the two-point spin correlation functions are necessarily highly non-local in the JW fermions, making fermionic primitives impractical for estimating correlation functions from optimality.

5.3.3 Results: bootstrapping Ising

Ground state energy

We begin by considering the Ising Hamiltonian (5.12) for a range of values of the transverse field h. The bases $\mathcal{B}_0, \mathcal{B}_1, \mathcal{B}_2$ contain operators which capture more local dynamics of the spin chain; the fermion basis $\mathcal{B}_F$ instead contains operators which are very non-local in the sense that they involve Pauli operators over many sites of the system. At criticality $h = 1$, the system contains strong long-range correlations. It is

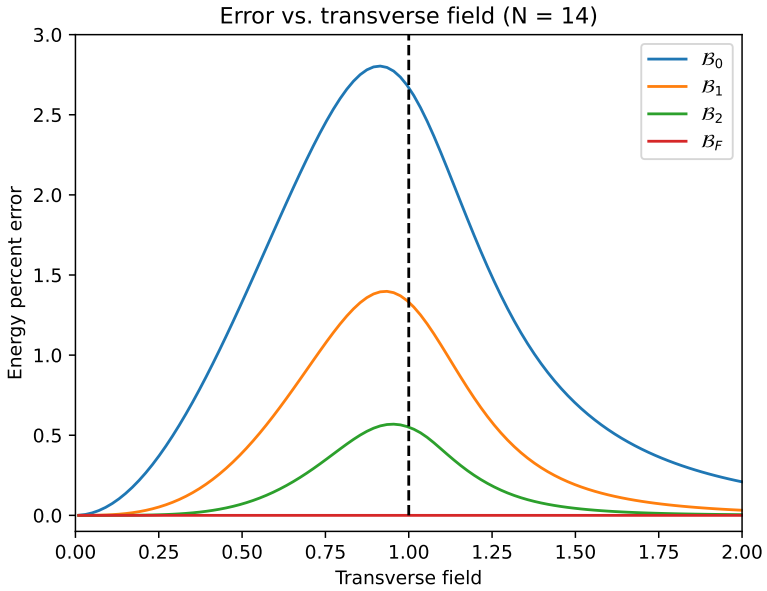

Figure 5.1: Percent error vs. transverse field for the four operator bases described in the previous subsection. The critical point $h = 1$ is demarcated.

therefore unsurprising that the bases constructed of local operators have their largest percent errors near the critical point. This is reflected in Fig. 5.1, shown for a system with $N = 14$ sites, where the fermion basis results in an essentially exact answer, likely deviating by only floating-point and solver error.

Note that even the simplest basis $\mathcal{B}_0$ already gives an approximate ground state energy within a few percent error of the known, exact value. Since $\mathcal{B}_0 \subset \mathcal{B}_1 \subset \mathcal{B}_2$,

one is guaranteed that the approximated energy increases in fidelity as one moves up the hierarchy. However, these increases may be of vastly differing magnitude relative to the increase in the size of the basis and the associated computational time. While the bases $\mathcal{B}_0, \mathcal{B}_1$ define SDPs solved in only a matter of seconds, the bases $\mathcal{B}_2, \mathcal{B}_F$ may take multiple minutes to reach optimality. The time taken to solution versus the system size N is tracked below in Fig. 5.2. Regardless of the basis under consideration, the size of

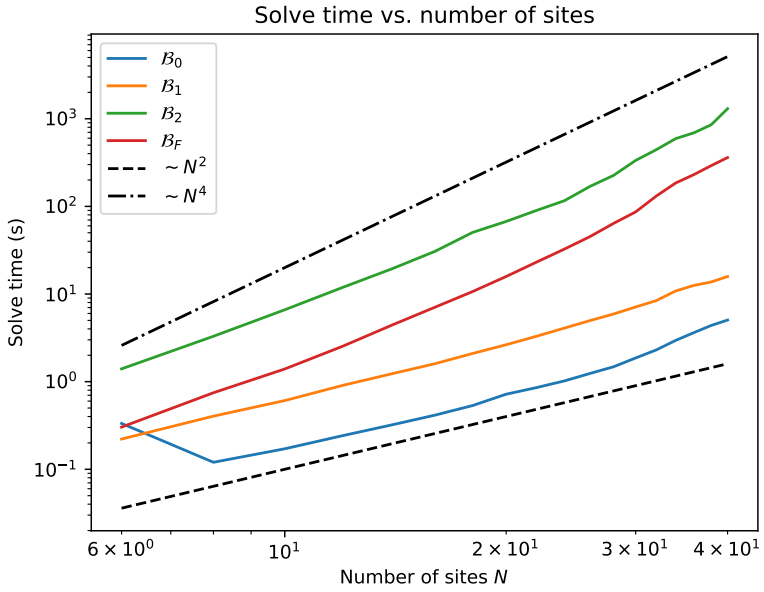

Figure 5.2: Time to optimality for each operator basis and over a range of system sizes; scaling comparison curves are included for solve time proportional to N^2, N^4.

the basis grows linearly in the system size N, and the number of dual variables grows at worst like N^3. At a fixed value of the transverse field, we observe that the energy error, as function of the system size, plateaus quickly (around $N \sim 20$) for each basis to a constant value.

These results confirm what has been found numerous times in the literature: the bootstrap method, a set of semidefinite relaxations, yields good accuracy in predicting the finite-size ground state energy of the spin chain even for small operator bases at most linear in the size of the system N. We note that many previous works make very detailed

choices of operator bases; experimentally, we find generically that one and two-point operators do quite well to estimate the energy of translation-invariant nearest-neighbor Hamiltonians.

Magnetization

An important question for numerical methods in many-body systems is whether they can reliably detect phase transitions. At the quantum critical point $h = 1$, the transverse-field Ising model displays a second-order phase transition; the magnetization $\langle Z \rangle$ has a discontinuous second derivative $\partial_h^2 \langle Z \rangle$ with respect to the transverse field h. In any finite-size system, there is technically no phase transition: the second derivative of the magnetization should display a large but finite spike at the quantum critical point.

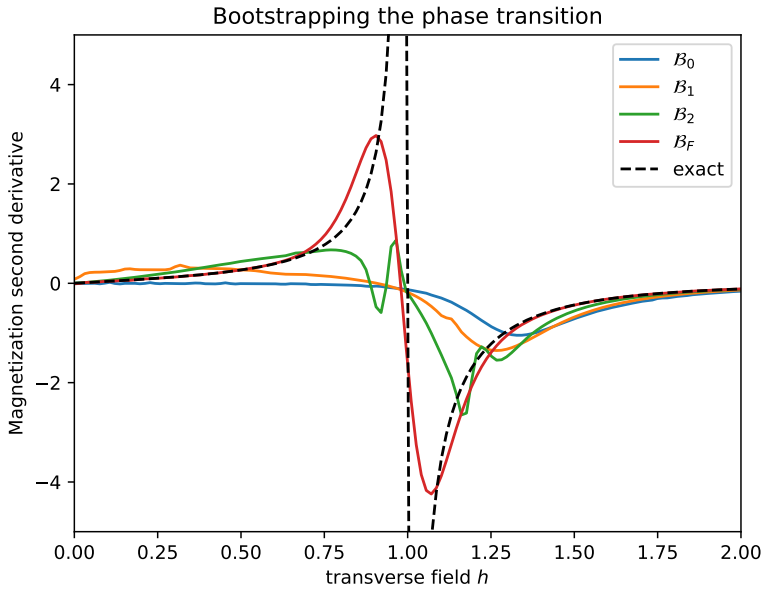

Figure 5.3: The second derivative of the magnetization $\partial^2 \langle Z \rangle / \partial h^2$ with respect to the transverse field h, with the exact curve shown in black, dashed. The fermion basis detects the divergence, but the other bases show much less sensitivity.

Computing the magnetization by SDP methods is the first test of the bootstrap's ability to compute correlation functions. Since the magnetization enters directly into the

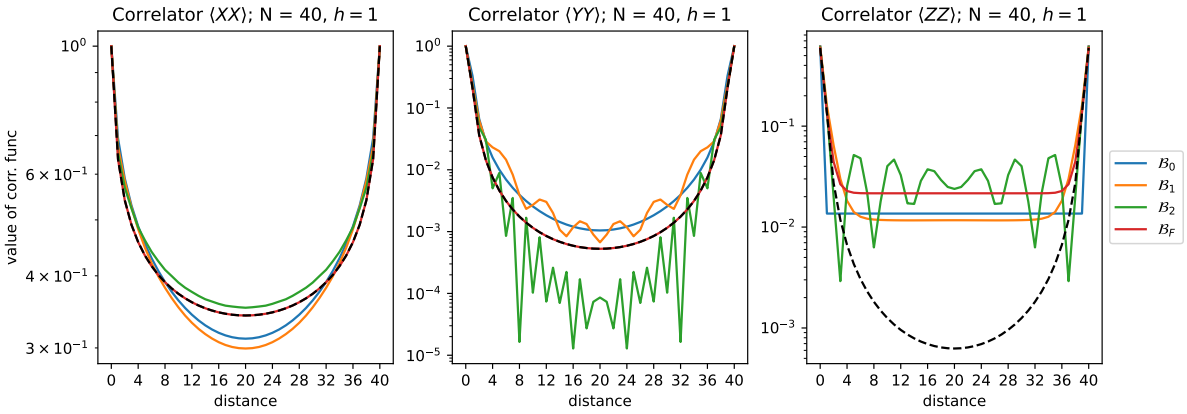

Figure 5.4: Correlation functions (in particular, their absolute value) as estimated from the optimal values of the SDP, compared with the exact expressions (black, dashed). While basic qualitative agreement is achieved for the XX correlator, the estimates of the others are not good.

Hamiltonian, whereas most two-point functions serve effectively as slack variables, the expectation should be that the bootstrap performs well in computing this quantity.

In Fig. 5.3, we compute the second derivative of the magnetization $\partial^2\langle Z\rangle/\partial h^2$ exactly and by SDP with the four operator bases introduced earlier. The fermion basis clearly detects the phase transition, and the complete two-point function also displays some sensitivity. Most bases display a distinct asymmetry about the critical point, a behavior also evident in the energy error versus transverse field of Fig. 5.1.

Correlation functions

We turn now to the spin-spin correlation functions. With the goal of determining conformal scaling dimensions from the critical spin chain, we must study the connected correlation functions $\langle X_1X_{1+n}\rangle^c, \langle Y_1Y_{1+n}\rangle^c, \langle Z_1Z_{1+n}\rangle^c$ at criticality as functions of n. For the transverse-field Ising model, exact expressions for these quantities at finite N are known and are reproduced in the Appendix. For each of the bases $\mathcal{B}_0, \mathcal{B}_1, \mathcal{B}_2, \mathcal{B}_F$ under consideration, we compute the exact correlation functions and compare these to the approximate values obtained at optimality of the program (5.16). These comparisons are

pictured in Fig. 5.4.

The results make it clear that, as previously observed in [38, 48], the SDP relaxations can give values for the correlation functions which *qualitatively* agree with the exact results. Small deviations in the values are magnified by the logarithmic scale on the plot. However, the qualitative agreement of Fig. 5.4 is in general not sufficient to obtain accurate results for the scaling dimensions, which depend in a detailed way on the large separation region. In this regime, the expectation values are small, but not small enough.

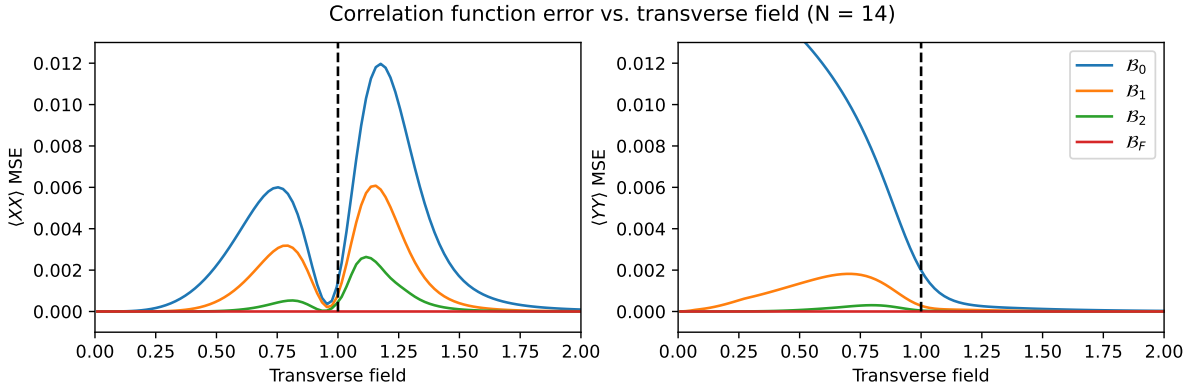

Figure 5.5: Correlation function mean squared error (MSE) versus transverse field for the $\langle XX \rangle$, $\langle YY \rangle$ correlation functions. While each basis in the hierarchy improves the overall error, the error profile across phases of the model is much more nontrivial than the error profile observed for the energy estimate.

To study in more detail the error associated to the correlation function estimates, we can consider the mean-squared-error across all connected correlators $\langle XX \rangle, \langle YY \rangle, \langle ZZ \rangle$ for each basis versus the transverse field h, shown in Fig. 5.5. We compute the squared error e.g. $|\langle X_1 X_{1+n} \rangle_{\text{exact}} - \langle X_1 X_{1+n} \rangle_{SDP}|^2$ and average over all distances n and over all 3 connected correlation functions. The nontrivial error profile shows that convergence to the correct correlation functions happens in less predictable fashion compared to the error seen in the energy estimates and, interestingly, has a local minimum near the quantum critical point. The correlation error also approaches zero in every basis as we move into the ordered phase $h \to \infty$.

5.3.4 Determination of conformal data

To extract conformal dimensions from the $N \to \infty$ limit of the critical spin chain, we have to compare our numerical estimates to correlation functions of the 2D CFT compactified on the cylinder. For a conformal field $\phi(z, \bar{z})$ on the complex z plane, the scaling dimension $\Delta_\phi = h + \bar{h}$ is defined by the two-point function as

$$\langle \phi(z, \bar{z}) \phi\,(z', \bar{z}') \rangle \sim (z - z')^{-2h} (\bar{z} - \bar{z}')^{-2\bar{h}}. \tag{5.24}$$

Following Cardy [122], we consider the conformal mapping $w = (L/2\pi) \log z$ which takes the plane to a finite strip of width L. We are primarily interested in the equal-time correlators; with $w = t + i\sigma$ with $\sigma \in [0, L]$, the correlation function at two equal-time points (σ_1, σ_2) is given by

$$\langle \phi(\sigma_1) \phi(\sigma_2) \rangle \sim \sin \left(\frac{\pi(\sigma_2 - \sigma_1)}{L} \right)^{-2\Delta_\phi}. \tag{5.25}$$

Therefore, to use the (finite) spin-chain correlation functions to compute Δ_ϕ, one should regress to the expression

$$\langle X_1 X_{1+n} \rangle \sim \sin(\pi n/N)^{-2\Delta_X}. \tag{5.26}$$

Strictly speaking, the critical spin chain/CFT correspondence is only valid in the $N \to \infty$ limit. Therefore, one should investigate the finite-size correlation functions at large system size N and with $n \gg 1$, where the long-distance behavior is more reliably reflective of the physics of the conformal theory. In practice, this means using a short-distance cutoff and only considering values of the correlation function at $n \gtrsim 5$ for system sizes of order $N \sim 40$.

The results of this procedure for the $\langle X_1 X_{1+n} \rangle$ correlator are included in Table 5.1 with $N = 40$ and considering $5 \leq n \leq 35$. As is well known, with the Hamiltonian

basis	exponent estimate	% error
$\mathcal{B}_0$	0.2008	60.661
$\mathcal{B}_1$	0.2133	70.712
$\mathcal{B}_2$	0.1404	12.3439
$\mathcal{B}_F$	0.1248	0.1994

Table 5.1: Estimates of the critical exponent $\Delta_X = 1/8 = 0.125$ from the SDP correlation functions for each basis and the associated percent error, computed here with $N = 40$ and a cutoff of 5 sites on each side.

(5.12) at criticality the X operator becomes the spin field with conformal dimension $\Delta_X = 0.125 = 1/8$ in the thermodynamic limit. From the results, it is clear that the fermionic basis provides the best estimate of the scaling dimension. When these estimates are extracted only by regressing against the SDP correlation functions, there is no way to extract rigorous error bounds or even confidence intervals, at least from a single run of the program. Interestingly, the error in the estimates from bases $\mathcal{B}_0, \mathcal{B}_1$ increases with the system size N, even when modulating the cutoff.

The correlation functions and the energy also permit an estimation of the central charge of the conformal theory. The ground-state energy of a critical spin chain has well-known finite-size scaling properties with respect to the system size N [122, 123]. In particular, one has

$$e_0^{(N)} \equiv E_0^{(N)}/N \sim e_0 - \frac{\pi c}{6N^2} + \mathcal{O}(N^{-3}), \tag{5.27}$$

where e_0 is the ground state energy density per site in the thermodynamic limit $N \to \infty$ and c is the central charge. In general, the dimensions in Eqn. (5.27) are not exactly correct. That is, they depend on the speed of light in the lattice theory; we call the lattice speed of light v by abuse of notation. In general, one must do a normalization step to compute the effective speed of light in order for the parameter c in (5.27) to be equal (in dimensions and value) to the CFT central charge. An example of this type of normalization procedure is handled in [117].

Given an estimate of the critical exponent Δ_X, we can directly estimate the effective speed of light from the numerical SDP. The procedure goes as follows. For an operator with scaling dimension Δ, the unequal time continuum correlation function depends on the speed of light v as

$$\left\langle \mathcal{O}(0,t)\mathcal{O}(x,0)^\dagger \right\rangle \propto \frac{1}{(x^2 - v^2t^2)^\Delta}. \tag{5.28}$$

The idea is to take time derivatives of this expression to extract factors of v and regress an estimate for the speed of light directly from the correlators; the details of the manipulations are worked out in Appendix C. For an operator on a lattice of size N, one finds

$$\frac{\langle \ddot{\mathcal{O}}(0,0)\mathcal{O}(x,0)^\dagger \rangle}{\langle \mathcal{O}(0,0)\mathcal{O}(x,0)^\dagger \rangle} = \frac{-2\pi^2 v^2 \Delta}{N^2 \sin(\pi x/N)^2}, \tag{5.29}$$

where we consider a ratio of correlation functions so that any unphysical normalization of the field/operator does not enter into this expression. To evaluate the time derivative on the left hand side we can use the algebraic structure of the time evolution: $\ddot{\mathcal{O}} = -[\hat{H}, [\hat{H}, \mathcal{O}]]$.

Let us carry out this procedure for the X field with the Hamiltonian (5.12) at criticality. From the operator algebra one finds

$$\langle \ddot{X}_1 X_{1+n} \rangle = 4\langle X_1 X_{1+n} \rangle - 4\langle Z_1 X_2 X_{1+n} \rangle - 4\langle Z_1 X_N X_{1+n} \rangle. \tag{5.30}$$

We must choose an operator basis which will give us access to numerical estimates of these three-point functions. To this end, we use an extension of the fermion basis $\mathcal{B}_X = \mathcal{B}_F \cup \mathcal{B}_2$ and solve the resulting SDP on a chain of length $N = 20$; this problem already has ~ 7.5k optimization variables and takes about 60 seconds to solve. From the result, we first regress the connected $\langle XX \rangle$ correlator to obtain an estimate of the scaling dimension Δ_X; we find $\Delta_X \simeq 0.12412$.

Next, we compute the SDP estimates of the ratio $-\langle \ddot{X}_1 X_{1+n}\rangle / \langle X_1 X_{1+n}\rangle$ over distances $3 \leq n \leq 17$, using a short-distance cutoff to ensure we are in the regime of validity of the expression (5.29), and regress to the right-hand side of (5.29) to determine v. With our scaling dimension estimate, we find $v \simeq 2.02$. This is in line with the known analytical results, where the fermionic representation of the Ising Hamiltonian gives a dispersion relation with exact lattice speed of light $v_{exact} = 2$. In this case, one technically need not regress the entire expression against x, but doing so ensures that the results should replicate for any given value of the position.

Finally, we can use all these estimates to address the issue of the central charge. The dimensionally consistent finite-size scaling law says that for a lattice of size N, one has at leading order

$$e_0^{(N)} \sim e_0 - \frac{\pi c v}{6N^2}. \tag{5.31}$$

Using the same basis $\mathcal{B}_X$, we solve the SDP over a range of system sizes $N = 12, \ldots 20$ and regress the energy density estimates to the scaling law above, using our estimated speed of light. Doing so yields $e_0 \simeq -1.27323$ and $c \simeq 0.4967$. Comparing to the exact values, the estimate of the thermodynamic energy density is exact to less than 1 part in 10^{-5} and the central charge estimate is within 1% error.

The analysis of this section demonstrates that in principle, SDP relaxations of exact ground state problems can be used to estimate scaling dimensions and central charges of CFTs arising from critical spin chains. However, doing so with high fidelity depends strongly on one's choice of operator basis. In numerical experiments, we found that using composite bases like $\mathcal{B}_0 \cup \mathcal{B}_F$, $\mathcal{B}_1 \cup \mathcal{B}_F$ instead of the large basis $\mathcal{B}_X = \mathcal{B}_2 \cup \mathcal{B}_F$ gave essentially unusable results for the speed of light regression (the difficult part of the procedure), despite furnishing good estimates of the scaling dimension Δ_X. For non-integrable models, determining a sufficiently good operator basis may be extremely

difficult, and may push the memory requirements of the semidefinite solver beyond what is reasonable for laptop-based computation.

5.3.5 Non-invertible symmetries

At criticality, the transverse-field Ising model exhibits a non-invertible symmetry: the Kramers-Wannier duality. This strong/weak duality transformation maps the transverse field term to the nearest-neighbor term in the Hamiltonian. In particular, it implies the following equality of expectation values at criticality:

$$\langle X_j X_{j+1} \rangle \sim \langle Z_j \rangle. \tag{5.32}$$

This duality is part of the physics but is in no way specified or enforced in the construction of the SDP. By studying how these correlation functions approach or diverge from one another near the critical point, we can better understand how and if the SDP can detect non-trivial aspects of the physics. To test whether the SDP results respect this symmetry, we plot the absolute difference between the values of these correlators as obtained at optimality for each operator basis considered here and across a small range of values of the transverse field centered around the critical point $h = 1$.

The duality works as follows. We can fix the subalgebra of operators $K_{2j} = X_j X_{j+1}$ and $K_{2j-1} = Z_j$ (that is, we do not include the individual X_j in the algebra). For this case, the individual K anticommute with their nearest neighbors and commute with the rest. The subalgebra generated by the K_n has an automorphism $K_n \to K_{n+1}$ that leaves the Hamiltonian invariant at criticality; this is the non-invertible symmetry. A two point function operator $X_j X_k$ is a non-trivial operator in the algebra of the K, defined by

$$X_j X_k = K_{2j} K_{2j+2} \dots K_{2k-2}, \tag{5.33}$$

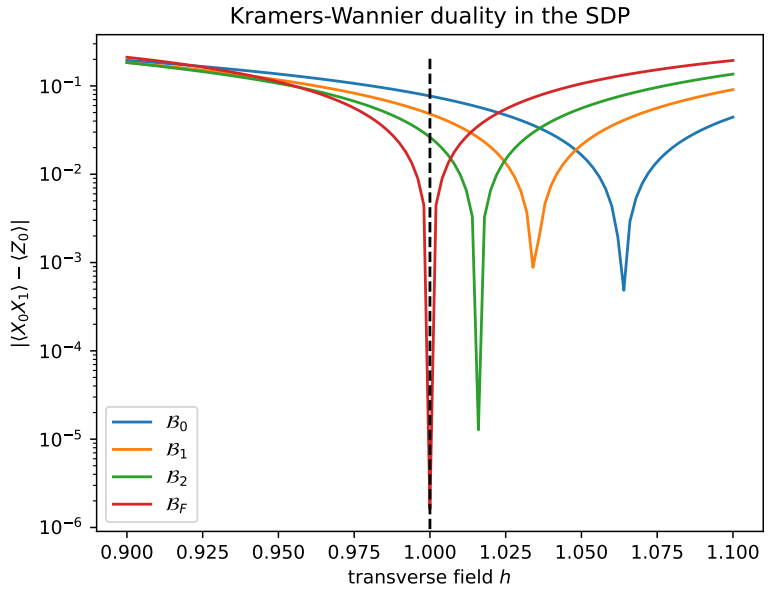

Figure 5.6: Testing whether Kramers-Wannier duality holds in the Ising model SDP at optimality. Only the fermion basis obtains the correct result. Interestingly, the other bases seem to approximately reach the dual point at values of the transverse field slightly away from criticality. As the bases grow in size, the self-dual point approaches the quantum critical point, denoted in black.

which in the algebra of the K is a non-local chain. When we use the duality, the bilocal operator gets mapped to the non-local chain $K_{2j+1} \dots K_{2k-1} = Z_{j+1} \dots Z_k$.

Notice that if one uses only local and bilocal operators in the basis of correlators for the SDP, the sub-operator basis for the optimization does not have the images of the operators under the duality. Expectation values of operators related to each other in this way by the Kramers-Wannier duality should be identical to each other and if the equations are sufficiently symmetric between the operators that are related to each other, the SDP solvers tend to find such symmetric solutions. The equations for the solver can not see the symmetry directly: it is blind to the knowledge of the non-local operators in the local and bilocal basis. To ameliorate this problem, one needs to include non-local operators from the beginning, like $Z_{j+1} \dots Z_k$ perhaps with additional decorations at the endpoints. Indeed, the fermions obtained by the Jordan-Wigner transformation

are optimal as they transform very simply into each other under the Kramers-Wannier duality and also allow one to write the Hamiltonian easily. This explains why only the fermion basis is able to see the duality in Figure 5.6.

5.3.6 Open boundary conditions in the bootstrap

One nice feature of the bootstrap approach, noted and applied in multiple works [70, 69, 55], is that it may still theoretically be applied to systems in the thermodynamic (or large N) limit $N = \infty$. In particular this is true for the spin systems we consider here.

There are three classes of boundary conditions we can consider for the spin chain bootstrap and each have different symmetries. In practice, this means different sets of boundary conditions will cause different sets of expectation values to be identified when constructing the set of optimization variables. The first class of boundary conditions are periodic on a chain of length N (which is what we have used up until this point) with Ising Hamiltonian

$$\hat{H}_C = -\sum_{j=1}^{N} X_j X_{j+1} - h\sum_{j=1}^{N} Z_j; \quad X_{N+1} \equiv X_1. \tag{5.34}$$

With periodic boundary conditions, expectation values are grouped by their $\mathbb{Z}_N$ orbits, a $\mathcal{O}(N)$ reduction in the number of unique optimization variables. We can also consider the class of open boundary conditions on a chain of length N; the Hamiltonian becomes

$$\hat{H}_O = -\sum_{j=1}^{N-1} X_j X_{j+1} - h\sum_{j=1}^{N} Z_j. \tag{5.35}$$

Note that this system is not translation invariant, and so there is no immediate grouping of expectation values. Finally, we can consider the thermodynamic limit of the system

$N \to \infty$. Here we have translation invariance and we use as the objective function the energy density, as in [70]:

$$\hat{h}_j = -X_j X_{j+1} - hZ_j. \tag{5.36}$$

Each of these boundary conditions define SDPs with vastly differing numbers of optimization variables. In particular, consider the basis $\mathcal{B}_2$ consisting of all one-point operators and all nearest-neighbor two-point operators in a system of size $N = 20$ (240 operators). The open BC SDP has 24720 optimization variables, the thermodynamic limit SDP has 4305 variables, and the periodic BC SDP has only 1242 variables. This results in an extreme difference in speed and memory requirements at runtime. Fig. 5.7 shows the

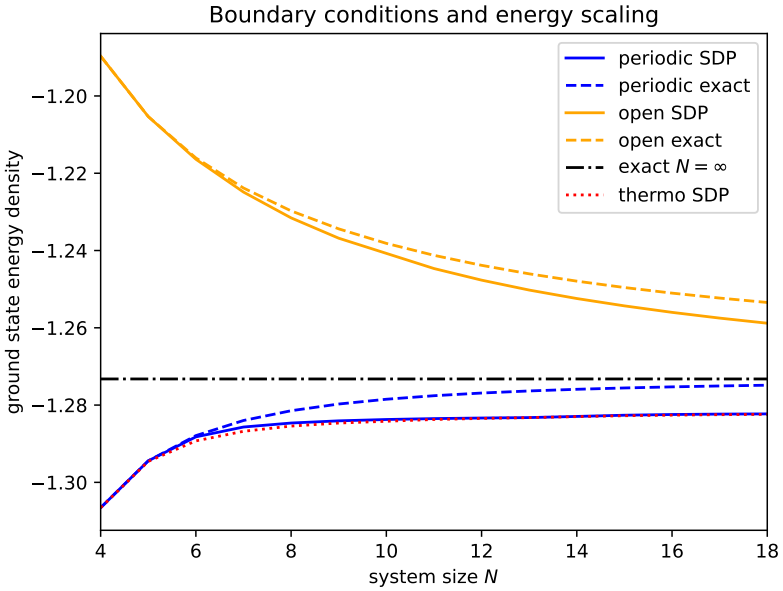

Figure 5.7: Energy density scaling with system size for Ising SDP results with periodic, open, and thermodynamic boundary conditions. Results from exact diagonalization are shown as dashed lines. Notably, the thermodynamic limit SDP appears to essentially reproduce the periodic SDP results.

results of solving these three classes of Ising SDP over a range of system sizes with the basis $\mathcal{B}_2$ (a function of system size). The results of exact diagonalization are shown as dashed lines. The open BC find the correct physical behavior, providing a good bound

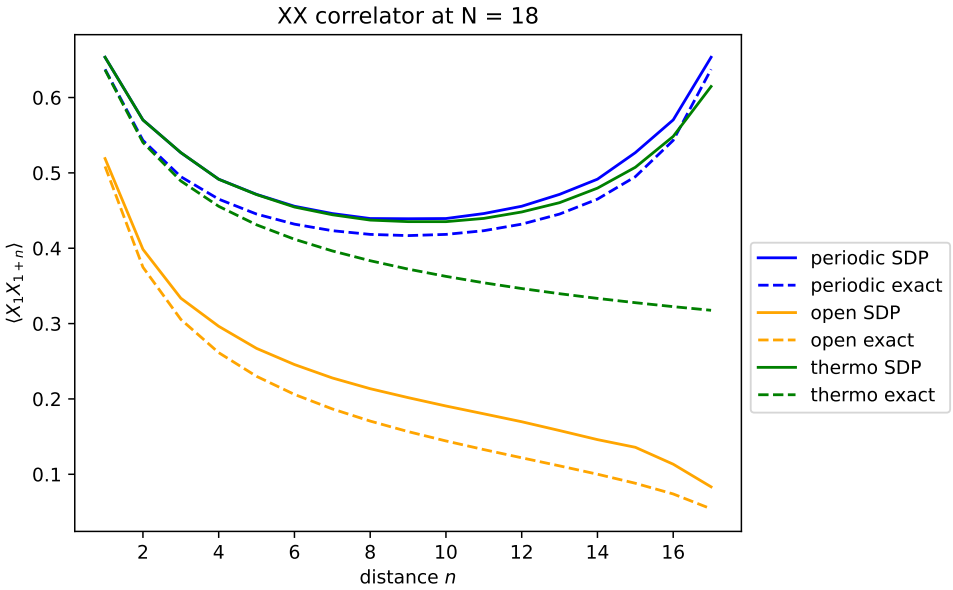

Figure 5.8: Comparison of $\langle XX \rangle$ correlation function values obtained for the basis $\mathcal{B}_2$ constructed for a system of $N = 18$ sites by each class of SDP: periodic, open, and thermodynamic. While the periodic and open results qualitatively reproduce the desired physical behavior, the thermodynamic SDP results appear to approximately (though not exactly) reconstruct cyclic invariance of the correlation function.

for the exact solution of the open system. However, the thermodynamic SDP appears to reconstruct the results of the periodic SDP and with a steeper computational cost.

To understand better the convergence of the periodic and translation-invariant thermodynamic SDPs, we can compare the optimal values of the connected $\langle XX \rangle$ correlation function for the same basis at system size $N = 18$, shown in Fig. 5.8. Notably, the translation-invariant thermodynamic SDP appears to reproduce a quasi-periodic behavior. To understand why this is, one must consider exactly what information the SDP sees about the system as defined by its objective function and constraints. In the periodic and thermodynamic SDPs, the objective functions are identical (up to a multiplicative factor) by translation/cyclic invariance. While the periodic SDP enforces cyclic invariance directly, the thermodynamic SDP sees only translation invariance. The only information the thermodynamic SDP has about the system 'size' is contained in the basis of operators

used to construct the moment matrix.

The translation-invariant SDP enforces approximate translation invariance due to implicit symmetries in the way the problem is specified. Clearly, the physical results of any SDP should be invariant under certain permutations of the operator basis, which have no physical meaning. Permutations acting on the operator basis $\mathcal{B}$ induce an action by conjugation of the moment matrix $M = \langle \mathcal{B}\mathcal{B}^\dagger \rangle$. The moment matrix, constructed of expectation values, is only invariant under this conjugation if the permutation is compatible with the operator algebra and symmetries of the state functional (and therefore the algebraic relations between matrix elements of M).

Consider a basis of X_i for $i = 1, \ldots, N$ and Y_i for sites $i = 1, \ldots, K$. If $K = N$, we have an exact reordering symmetry $i \to N - i + 1$, i.e. space parity. This symmetry leaves all translation-invariant moment matrix elements invariant, and so any optimal result of the SDP will also (approximately) have this symmetry. Therefore, even a problem without explicitly enforced cyclic symmetry may approach a cyclic symmetry at optimality as a consequence of discrete symmetries in the problem grammar. Testing this behavior with the basis just described, one sees that the translation-invariant SDP approximately finds periodicity for $K \geq N/2$, but does not find periodicity for $K < N/2$. That periodicity appears at $K = N/2$ is no accident and is a consequence of translation invariance coupled with the reordering symmetry. Future work, beyond the scope of this thesis, should investigate the relationship between permutation actions on the operator basis and the symmetries obeyed (or enforced) on the linear functional used to build the moment matrix.

These results contrast existing statements that the thermodynamic SDP, with an N-finite basis, is computing an approximation of the system with open boundary conditions. The open system has no translation invariance due to the boundary conditions and hence receives a completely different objective function, leading to the physically expected

result. In contrast, exactly what system the thermodynamic SDP is solving depends on discrete 'gauge' symmetry in the definition of the operator basis and construction of the moment matrix.

One can also ask why the SDP solver prefers this translation symmetric solution? The answer is clear: the Casimir energy at criticality is negative, so the periodic solution has lowest energy. In practice, this means that when studying systems at criticality, one must always assume that one is not in the thermodynamic limit. Instead, one needs to study the system at finite volume and include finite size corrections. This usually makes it harder to compute critical exponents: one ends up having information only of half the size of the system.

Discussion: transverse-field Ising SDP

Investigating the bootstrap approach to the transverse-field Ising spin chain reveals that while convergence to the correct ground-state energy happens quickly and efficiently even for small operator bases, the convergence of the off-diagonal elements of the moment matrix $M(\mathcal{B})$ is highly nontrivial and to date not well-understood. While convergence properties of the objective function are known in the literature, we are at present unaware of any mathematical results that describe in detail the convergence of off-diagonal elements of the LMI-type semidefinite program defined by (5.16). In the mathematical setting, these elements do not have the direct physical interpretation that they do in the bootstrap.

Even when the energy estimate is with a few percent error, the estimates of the correlation functions can be quite inaccurate. Fundamentally, the "correlation functions" that do not enter into the objective function are really just slack variables for the SDP; intepreting them literally risks conflating the true correlation functions of the system with optimization variables which obey only a small subset of the constraints satisfied

by the system's true correlators. Only when using a physically-informed basis—that of the Jordan-Wigner fermion operators—does the method present a solid attempt at computing interesting physical quantities. However, this basis is constructed with the understanding that it describes the model in terms of its integrable variables, where the integral is the fermion parity [124]. Extending the present method to non-integrable models without these integral charges may fail if the task is accurate computation of the ground-state correlations.

5.4 A non-integrable model

Having now addressed an integrable model, where our extra physical information informed our approach, we now turn to analyzing a non-integrable model and observing the performance of semidefinite methods as benchmarked against the exact diagonalization results.

Following the outline of Milsted and Vidal [117], we consider the axial next-nearest-neighbor Ising (ANNNI) model with Hamiltonian

$$\hat{H}_{ANNNI} = -\sum_{j=1}^{N} \left[X_j X_{j+1} + Z_j + \gamma X_j X_{j+2} + \gamma Z_j Z_{j+1} \right]. \tag{5.37}$$

This model was introduced and studied in [125, 126, 127] and presents interesting physical behavior in the context of our previous investigation of the Ising model: at various values of γ it describes three different emergent CFTs. Furthermore, the Jordan-Wigner description of the model is a theory of interacting fermions. We will see how the bootstrap SDP method performs both in producing the correct energies and correlation functions as obtained by exact diagonalization.

To do this, we will use some modified, larger operator bases. In particular, we will

consider the basis $\mathcal{B}_2$ and the combined bases $\mathcal{B}_F^{(i)} \equiv \mathcal{B}_i \cup \mathcal{B}_F$, where the $\mathcal{B}_i$ are defined as before. These bases take advantage of the performance of the fermion operators in constraining the results near the Ising point while also hopefully producing higher-fidelity representations of the correlation functions, as we saw was necessary to estimate the lattice speed of light in the Ising model. To begin, in Fig. 5.9, we plot the percent

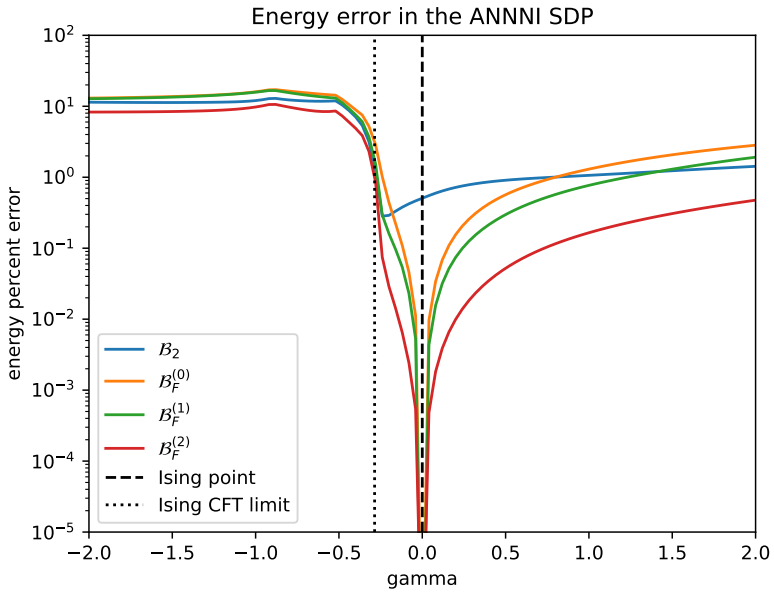

Figure 5.9: Energy error from SDP estimates of the ANNNI model ground state as a function of the parameter γ. The Ising point and associated free fermion theory is shown as a dashed line; the near-exact performance of the fermion basis is a clear signal of the integrability of the model. Below the Ising CFT threshold $\gamma \geq -0.285$ (dotted), the SDP error plateaus to a constant and large value.

error of the SDP versus exact diagonalization results for the model (5.37) at system size $N = 12$. One can clearly see the Ising point in the error curve: at the point where the system is integrable, the energy becomes heavily constrained and the error in the estimate essentially saturates at floating-point precision. A distinct decrease in the energy error is also visible moving from left to right at $\gamma \approx -0.285$, where the model begins to admit an emergent Ising CFT description. To the left of this boundary, the error plateaus to a relatively large value (and remains there for more negative values of the parameter γ).

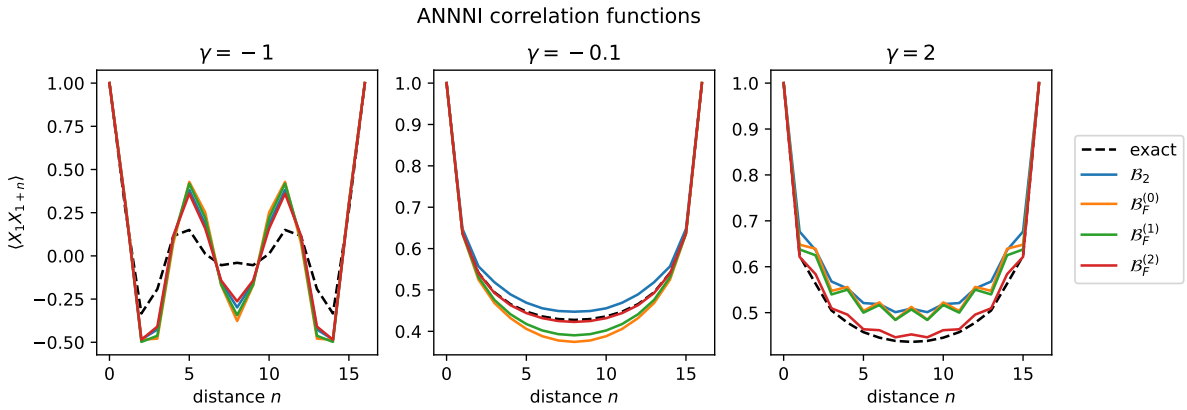

Figure 5.10: Comparing exact diagonalization versus SDP estimates of the correlation function $\langle XX \rangle$ ($N = 16$) in three regimes of the ANNNI model phase diagram: $\gamma = -1, -0.1, 2$. Unsurprisingly, the largest basis does best. The SDP results are worst in the $\gamma < -0.286$ regime, consistent with the results seen in the energy estimation.

It is not clear to us why the performance of the SDP is so poor on the left side of this threshold.

To better understand the predictions being made by the model, we can examine the results obtained for the connected $\langle XX \rangle$ correlation function at values of γ in each regime of interest: we consider $\gamma = -1, -0.1, 2$. Again, while qualitative adherence to the exact values is observed, smaller bases clearly struggle to accurately reproduce the correlation functions. The agreement is worst in the regime below the Ising CFT threshold, where the energy error had plateaued to a constant and macroscopic value. The best-performing basis $\mathcal{B}_F^{(2)}$ contains all nearest-neighbor two-point operators in the theory as well as all single-site Jordan-Wigner fermions. While it does well nearer to the Ising point, discrepancies are clearly visible as we move away from $\gamma = 0$. At $\gamma = 2$, the best-performing basis considered thus far gives an estimate of the XX scaling dimension $\Delta_X \simeq 0.114$, amounting to $\sim 8\%$ error.

We would like to be able to estimate central charges from the finite-size scaling of the energy density in the non-integrable regime of this model. Recall that doing so requires

an estimation of the lattice speed of light from the correlation functions of the theory. For the ANNNI model, extracting this estimate requires using a large basis; we used the set of all one-point functions and the two-point functions XX, YY, ZZ, XY, XZ (at all separations) in addition to the JW fermion operators. This is much larger than any basis considered so far.

We use this basis to solve the SDP at a decent system size and with $\gamma = 2$; from the results we extract the approximations of the correlators $\langle X_1 X_{1+n}\rangle$ and $\langle \ddot{X}_1 X_{1+n}\rangle$. The latter is defined by commuting with the Hamiltonian (5.37) and gives a linear combination of 1,2 and 3-point functions. First, we regress an estimate of the scaling dimension from the standard XX correlator, then we compute the ratio in Eq. (5.29). With the large basis we used, we were only able to reach $N = 12$ for this process due to memory constraints, which can be mildly remediated by moving to first-order solvers instead of second-order methods like MOSEK.

Recall that at $\gamma = 2$, the ANNNI model is in a phase with an emergent Ising CFT. The results of regressing the connected equal time correlator give a scaling dimension $\Delta_X \simeq 0.12575$, an excellent result completely consistent with expectations. Regressing the speed of light gives $v \approx 16.73$; we did not estimate this parameter by other means. Finally, we use the same basis to approximate the energy density over a range of system sizes. Combining all these estimates and using the scaling formula (5.27), we obtain an estimate of the central charge $c \simeq 0.4657$, a relatively accurate result! With more computational resources, larger bases and system sizes can be used to further decrease the error. There is no barrier in principle to estimating emergent central charges by this method. Indeed, if one were to find sufficiently well-performing bases, one could attempt to extract the three unique central charges of the phase diagram of the ANNNI model using this approach.

5.5 Discussion: spin chain SDP

We have investigated semidefinite bootstrap approaches to directly determining ground-state correlation functions of quantum spin chains. The benefit of the bootstrap approach is its polynomial scaling in the system size, the lack of a parametric ansatz for the exact state, and the wide ecosystem of numerical algorithms available to use for solution. We have demonstrated procedures that can be used to estimate emergent conformal data and other physical predictions of the collective physics associated to quantum spin chains. For simple models, these procedures allowed us to estimate scaling dimensions and central charges of the emergent CFTs associated to the Ising model and the non-integrable self-dual ANNNI model. Across these models, we see excellent performance in ground energy estimation, qualitative agreement with correlation functions and, with well-chosen problem setups, numerically satisfactory results when regressing conformal data directly from the optima of the semidefinite programs.

Semidefinite relaxations are known to provide hierarchies of approximations to exact optima of exponentially complex optimization problems. Both the physical and mathematical literature have studied in depth the convergence of the relaxed optima to the exact optima of the full theory. However, the perspective taken by these works usually does not address directly the role of the slack variables which, in the present case, have direct physical interpretations as measurements of observables in the putative state of the system. There is still much work to be done, both in the mathematics and in the physical application, to understand more precisely how the optimal values of the optimization variables, not just the objective function, approach their exact values. As our results show, the convergence of these quantities is not bound by the same monotonicity as the convergence of the objective function.

The bootstrap's strength lies in its generality. Essentially any quantum-mechanical

system with a Hilbert space of unitary representations and an algebra of observables may be approximated by a bootstrap approach. There is nothing preventing one from considering this approach for spin systems in higher dimensions and on lattices of arbitrary geometry. All the same methods apply. As a practical application, a better idea of how correlation functions converge with these methods would open up semidefinite methods to problems in quantum chemistry and molecular dynamics, where state-oriented variational methods are dominant.

The difficulty of the bootstrap is in how to correctly specify the problem. The task of determining small yet strongly constraining bases of operators is related to an array of computationally hard problems in the study of spin systems, including the representability problem. Physical intuition may prove a deciding factor in the successful construction of approximations, though algorithmic methods to search for efficient bases may be possible, as was briefly investigated by Lawrence [70]. Though beyond the scope of the present work, it may be possible to use the rank of the moment matrix to characterize the benefit of adding a certain operator to the basis. Since any sub-exponential size operator basis furnishes a strict approximation of the exact result (i.e. a global optimizer), one is guaranteed that the rank of the moment matrix grows consistently as the number of operators included in the basis grows. Operators which most increase the rank of the moment matrix should in theory contribute most to convergence toward the global optimum.

Beyond the choice of operator basis, correctly handling symmetries of the problem statement and automorphisms of the operator algebra could also assist in lowering the computational overhead of the problem. Invariant semidefinite programming—finding a block-diagonal decomposition of the moment matrix into irreducible representations of a symmetry—has been applied by various works e.g. [69], though we are unaware of research which addresses these ideas for optimization over non-commutative variables.

Chapter 6

Conclusion and further directions

In this thesis we have developed, tested, and benchmarked the bootstrap approach to solving numerical quantum systems in one dimension. The work laid out here, part of a modern resurgence in the application of bootstrap techniques to non-conformal quantum systems, is intended to serve as a foundation for the continued application and development of the bootstrap program. We have shown how the bootstrap converges exponentially for bound state problems and how semidefinite programming can be used to determine the spectrum of one-dimensional Hamiltonians. We generalized this approach to domains with boundary, where anomalous contributions allowed boundary information to enter algebraically into the problem. This permitted an extension to determining scattering phases directly through a bound-state bootstrap. Finally, we demonstrated how the methods can be applied to spin systems and in particular to the determination of conformal data through the correlation functions.

Each bootstrap system analyzed here required a slightly different approach. Physical expectations informed our choice of constraints and of the construction of hierarchies. Despite the generality of the bootstrap method, a blind application of the tools we have developed here is limited in its effectiveness. There is therefore a rich variety of work yet

to be done, and domain knowledge on a specific species of quantum systems is sure to assist in successful numerical study by bootstrap methods.

While bootstrap methods may not yet compare in speed to well-established numerical techniques for one-dimensional quantum systems, their generality cannot be understated. Already, the program has demonstrated applications to string theory, matrix quantum mechanics, Feynman loop integrals, lattice gauge theories, many-fermion systems, thermalized systems, and more. If a system has a known algebraic structure and unitary representations on a Hilbert space, then these tools, or some variation thereof, can be applied to constrain and study it. With a broad future of possibilities in mind, we conclude this work by suggesting a number of future directions for expansion or improvement of the results laid out in this thesis.

Schrödinger quantum mechanics. In developing SDP algorithms for determining the spectrum of Hamiltonians with polynomial potentials, the moment recursion represents a way to eliminate moments involving the momentum operator from the recursion relations. As some authors have shown [128], this is not entirely necessary in order to constrain the physics. Mixed position-momentum correlation functions can still function as optimization variables in the SDP. It seems that for problems in higher than one dimension including these mixed correlation functions is required. Understanding optimal ways to construct bases of position/momentum operators, rather than eliminating all momentum factors to obtain closed recursions for the moments, could open up the approach to bound state problems in higher dimensions.

For one dimensional systems with polynomial potentials, the moment recursion essentially defines, at each depth K, a polynomial optimization problem. The SDP approach is then the Lasserre relaxation of this problem. It is known that the problem of rational function optimization also has a formulation as a moment problem and therefore admits a relaxation [87]. By formally connecting polynomial optimization and the SDP approach

to polynomial potentials described here, the method could be subsequently generalized to handle rational potentials by making the analogous with rational function optimization. Since any function may be extremely well-approximated by rational Pade approximants, understanding how to handle rational potentials in the one-dimensional bootstrap would essentially open up the approach to studying any potential.

While our study of domains with boundary addressed completely the conditions associated with half-line problems, the problem on the interval is less well-understood. We expect that given Robin boundary conditions on each side of a closed interval, these conditions enter the recursion simply through two anomaly terms. This would allow direct study of e.g. Sturm-Liouville type systems on a closed interval. Periodic boundary conditions are a bit more subtle; it seems that the anomalies cannot pick up the quasi-momentum phase factor. More work remains to be done to confirm that this aspect of the dispersion is truly inaccessible from the moment or trigonometric moment recursion.

Semidefinite algorithms for energy spectra. We used an eigenvalue extremization method to create a semidefinite programming algorithm to accept or reject a putative energy value an as eigenenergy in an increasingly constrained hierarchy. We experimented with this approach in spin chains, but did not observe the same convergence to a discrete spectrum when used to scan over energies. We suspect this is due to the fact that the constraints $\langle[\hat{H},\hat{\mathcal{O}}]\rangle = 0$, $\langle\hat{H}\hat{\mathcal{O}}\rangle = \langle\hat{H}\rangle\langle\hat{\mathcal{O}}\rangle$ do not obviously close on spin correlators. It would be interesting to understand when the method does work, and what conditions must be met in order for disjoint subsets of allowed energies to arise using the method. If eigenenergies of spin systems could be extracted with this approach, conformal weights could be determined directly from the finite-size scaling of gaps in the spectrum [122]. Even if the constraints do not close, the non-linear constraint $\langle\hat{H}\hat{\mathcal{O}}\rangle = \langle\hat{H}\rangle\langle\hat{\mathcal{O}}\rangle$ could be relaxed as $\langle\hat{H}\hat{\mathcal{O}}\rangle - \langle\hat{H}\rangle\langle\hat{\mathcal{O}}\rangle \geq 0$ (which has a semidefinite formulation) and potentially increase the performance of the spin SDP.

Additionally, the implementation of the algorithm when searching for allowed energies could be easily improved. Thus far, a basic grid search across energy values is done, with the goal of finding where the objective of the problem is positive. This could be instead accomplished by a gradient descent-like approach. One chooses an energy value and solves two SDPs determining an approximate derivative $\partial t^\star/\partial E$. Then, with the Newton method, one looks for the zero crossings above which $t^\star$ is maximized. Once two zero crossings are identified, the interval will shrink rapidly at successive depths and can be studied with a straightforward grid approach at little cost. Regressing the convergence after a few iterations could inform the resolution of the grid generated at each successive depth. For true computational speed, the script SDPA functions should be used instead of reading/writing files and calling command line executables.

Spin system bootstrapping. The study of spin systems with semidefinite methods showed that while the determination of energies was quite effective, the convergence of correlation functions to their true values was less decisive. From a mathematical perspective, understanding the convergence properties of optimization variables not contained in the objective function would greatly inform the construction of bases and the correct identification of physical predictions. In the context of spin systems these variables have direct physical interpretations.

When constructing these problems, all of the data of the geometry of the lattice is essentially contained in the couplings of the Hamiltonian. The construction of the moment matrix relies only on the algebraic relations obeyed by the different operators in the theory. Theories defined on e.g. $2d$ lattices of arbitrary unit cell can be embedded in a $1d$ chain by a suitable mapping of site indices to the integers and a corresponding mapping of the objective function. There is really no obstacle to studying spin systems in arbitrary dimensions by the exact methods used here except for the exponential growth in the number of operators.

In our approach, linear constraints like $\langle[\hat{H}, \hat{\mathcal{O}}]\rangle = 0$ were implemented for spin systems by adding direct constraints on the optimization variables. However, a more mathematical approach can be taken. The algebra of observables $\mathcal{A}$ defines all relations between possible optimization variables. The expectation value on eigenstates defines a map from the algebra to the complex numbers. Given a Hamiltonian $\hat{H}$, commutators $[\hat{H}, \hat{\mathcal{O}}] \in \mathcal{A}$ lie in the kernel of the expectation value. This motivates considering the sequence $\mathcal{A} \to \mathcal{A}/\{[\hat{H}, \hat{\mathcal{O}}] = 0\} \to \mathbb{C}$. From an abstract algebra perspective, the relation $[\hat{H}, \hat{\mathcal{O}}] = 0$ defines an ideal $\mathcal{I}$ in the ring $\mathcal{A}$, and one has $\langle\mathcal{A}\rangle \cong \langle\mathcal{A}/\mathcal{I}\rangle$. Constructing an operator basis which incorporates the commutator constraints is equivalent to finding a linear basis for the quotient ring $\mathcal{A}/\mathcal{I}$. Such bases are called Gröbner bases, they are guaranteed to exist, and algorithms exist for their construction [89]. For a given SDP, the cardinality of the Gröbner basis will be the number of unique optimization variables after constraints are solved. Doing this procedure up front will save computational resources when compiling the SDP.

Finally, it is clear that while SDP representations of correlation functions may not be exactly correct, they will be good approximations. Methods which use semidefinite approaches to obtain good starting guesses, or to constrain variational parameters, could be combined with other techniques to determine ground-state properties and leverage the strengths and weaknesses of each approach.

Other systems and the future of bootstrapping. Much work has already been done studying otherwise inscrutable systems by the bootstrap approach. Lin's work on bootstrapping matrix correlators in the BFSS model shows that these techniques could plausibly be used to study numerically aspects of black hole physics and quantum gravity, at least in regimes where those theories admit an algebraic Hamiltonian description. Kazakov and Zheng have continued their study of the bootstrap for lattice Yang-Mills theory [129], a program of great interest and with a wealth of interesting directions for

research.

Other systems of interest which could be amenable to bootstrapping include random spin systems like the SYK model or the Sherrington-Kirkpatrick spin glass. The former, admitting a conformal description, has been analytically studied by a bootstrap approach [130]. Understanding how the SDP handles random couplings—likely requiring an ensemble of semidefinite programs—would be a worthwhile direction for investigation. Since spin glass models lack translation invariance in general, the use of Hamiltonian constraints will likely prove indispensable for obtaining sharp bounds on energies.

The bootstrap program is young in its applications beyond the world of conformal symmetry. New advances in the theory of non-commutative optimization, large-scale semidefinite programming, and algebraic perspectives on quantum and gravitational systems set the stage for a rich development of these techniques. As physicists wait for fault-tolerant quantum computation to become available for determining the behavior of quantum systems, semidefinite and bootstrap methods present a strong classical approach to close the gap between numerical and analytical methods. Much work remains to be done to bring the methods up to par with traditional numerical approaches, but there exist few limitations to its applicability and relevance as computation becomes an increasingly powerful tool for the study of theoretical physics.

Appendix A

The delta function potential

Consider the Hamiltonian with a delta function potential:

$$\hat{H} = -\frac{d^2}{dx^2} - \frac{1}{a}\delta(x), \tag{A.1}$$

where the parameter a has dimensions of length. We can use the recursion (3.9) for moments of distributions on the real line. When we evaluate the expectation values of the potential, the delta-function will pick up residues of the state ψ.

$$\begin{aligned} m\langle x^{m-1}V(x)\rangle &= -\frac{m}{a}\int_{\mathbb{R}} dx\ x^{m-1}\psi(x)^2\delta(x) \\ &= -\frac{1}{a}\lim_{x\to 0}\ mx^{m-1}\psi(x)^2 \\ \implies \quad m\langle x^{m-1}V(x)\rangle &= -\frac{1}{a}\delta_{m,1}\psi_0^2, \end{aligned}$$

where $\psi_0 \equiv \psi(0)$ and we're now using the Kronecker delta. Similarly,

$$\begin{aligned}
\langle x^m V'(x)\rangle &= -\frac{1}{a}\int_{\mathbb{R}} dx\ x^m \frac{d}{dx}[\delta(x)]\psi^2 \\
&= \frac{1}{a}\int_{\mathbb{R}} dx\ \delta(x)\frac{d}{dx}[x^m\psi^2] \\
&= \frac{1}{a}\int_{\mathbb{R}} dx\ \delta(x)[mx^{m-1}\psi^2 + 2x^m\psi\psi'] \\
\implies \quad \langle x^m V'(x)\rangle &= \frac{1}{a}\delta_{m,1}\psi_0^2,
\end{aligned}$$

where we integrate by parts to make sense of the distributional derivative, and are considering only $m \geq 1$. This results in a recursion relation with a contact term:

$$0 = 2mE\langle x^{m-1}\rangle + \frac{1}{2}m(m-1)(m-2)\langle x^{m-3}\rangle + \frac{1}{a}\delta_{m,1}\psi_0^2, \tag{A.2}$$

which furnishes constraints for $m \geq 1$. The known solution for an inverted delta-function potential is $\psi(x) \sim e^{-\kappa|x|}$. Hence the moments should grow approximately like gamma functions, and the wavefunction derivative will be undefined at the origin. When $m = 1$ the recursion gives

$$E = -\frac{1}{2a}\psi_0^2. \tag{A.3}$$

This is the virial theorem. Continuing, the vanishing of the odd moments is guaranteed by the $m = 1$ case which sets $\langle x\rangle = 0$. The rest of the even moments may be computed by a simple recursion for $n \geq 1$:

$$\langle x^{2n}\rangle = -\frac{n}{2E}(2n-1)\langle x^{2n-2}\rangle. \tag{A.4}$$

Note that positivity of the even moments requires $E < 0$, which by (A.3) requires $a > 0$. The bootstrap already tells us that normalizable states only live in the inverted delta

potential.

We can actually solve this recursion explicitly. First, the normalization constraint fixes $\langle x^2 \rangle = -(2E)^{-1}$. This then uniquely determines all higher moments $\langle x^{2n} \rangle$. The result is

$$\langle x^{2n} \rangle = (-1)^n \frac{(2n)!}{(4E)^n}.$$

We know the wavefunction PDF to be even by symmetry. Consider the Fourier transform of the wavefunction PDF. It may be expressed as a power series in the moments:

$$\mathcal{F}[|\psi(x)|^2](k) = \int_{-\infty}^{\infty} dx\ e^{-ikx} |\psi|^2 = \sum_{m=0}^{\infty} \frac{(-ik)^m}{m!} \langle m \rangle = \sum_{n=0}^{\infty} (-1)^n \frac{k^{2n}}{(2n)!} \langle 2n \rangle,$$

where we have used the vanishing of the odd moments in the last step. Using our expression for the even moments we can evaluate the sum as

$$\mathcal{F}[|\psi(x)|^2](k) = \sum_{n=0}^{\infty} \frac{k^{2n}}{(4E)^n} = \frac{4E}{4E - k^2}.$$

Finally we invert the Fourier transform to obtain an explicit form of the wavefunction (PDF):

$$|\psi(x)|^2 = \sqrt{-E} e^{-2\sqrt{-E}|x|}.$$

This is an example where the moment recursion solves the system explicitly.

Appendix B

Exact results for the transverse-field XY model

Here we reproduce the known solution of the transverse-field XY model, which contains as a special case the transverse-field Ising model. The original solution of the Ising model was given in [131] and expressions for the correlators in the general case are given in [132, 133]. For other studies of the model, including the finite-size scaling, see [134, 123, 135, 136]. The authors did not find a source which includes all these results in the exact form at finite N, which the present appendix aims to do.

The model is a spin chain on N sites. The operator algebra is $su(2)^{\oplus N}$ and is composed of the Pauli matrices I_j, X_j, Y_j, Z_j at each site j. They obey the usual commutation rules at each site and commute off-site. The Hamiltonian is given by

$$\hat{H}_{XY} = -\sum_{j=1}^{N} \left[\frac{(1+\gamma)}{2} X_j X_{j+1} + \frac{(1-\gamma)}{2} Y_j Y_{j+1} + h Z_j \right],$$

and depends on two parameters: the transverse field $h > 0$ and the anisotropy γ, where $0 \leq \gamma \leq 1$. Here, we assume periodic boundary conditions, where $N + 1 \equiv 1$.

The model is solved by performing a Jordan-Wigner transformation and subsequently diagonalizing the quadratic fermion Hamiltonian via a Boguliobov transformation. The result is a free fermion model for any values of h, γ.

The transverse field Ising model is the case $\gamma = 1$. For any value of γ, at the quantum critical point $h = 1$ and in the thermodyanmic limit $N \to \infty$, the model falls in the Ising universality class and is described by the Ising CFT with $c = 1/2$.

Restricting to the case of even N, we first define some auxiliary functions. The dispersion ω_ϕ is given by

$$\omega_\phi = \sqrt{(h - \cos(\phi))^2 + \gamma^2 \sin^2(\phi)}. \tag{B.1}$$

We define the set of ground state modes K as

$$K = \left\{ \frac{(2n-1)\pi}{N}, \quad n = 1, \ldots, N/2 \right\}. \tag{B.2}$$

The ground state is given by the Jordan-Wigner fermion vacuum, and its energy is

$$E_0 = -2 \sum_{k \in K} \omega_k. \tag{B.3}$$

The correlation functions depend on the two-particle Green's function:

$$G_N(R) = -\frac{2}{N} \sum_{k \in K} \cos(kR) \left(\frac{h - \cos(k)}{\omega_k} \right) - \gamma \sin(kR) \frac{\sin(k)}{\omega_k}. \tag{B.4}$$

This function is written in terms of the Jordan-Wigner fermions as

$$G_N(R) = -\delta_{R0} + \langle c_0^\dagger c_R^\dagger \rangle + \langle c_R^\dagger c_0 \rangle + \langle c_0^\dagger c_R \rangle - \langle c_0 c_R \rangle. \tag{B.5}$$

The order parameter of the quantum phase transition at $h = 1$ is the magnetization $\langle Z \rangle$. In the limit $h \to \infty$, the system becomes completely ordered and $\langle Z \rangle \to 1$. In the disordered phase $h \to 0$, the magnetization $\langle Z \rangle \to 0$ in either (degenerate) ground state. The magnetization is given in terms of $G_N(R)$ as

$$\langle Z \rangle = -G_N(0) = \frac{2}{N} \sum_{k \in K} \left(\frac{h - \cos(k)}{\omega_k} \right). \tag{B.6}$$

For the purposes of this paper, we are concerned with the connected two point functions of each Pauli operator X, Y, Z. The simplest of these is given by

$$\langle Z_i Z_{i+R} \rangle^c = -G_N(R) G_N(-R). \tag{B.7}$$

The XX, YY connected correlators are given in terms of determinants (a result of the fermionic description). They are

$$\langle X_i X_{i+R} \rangle^c = \begin{vmatrix} G_1 & G_0 & \cdots & G_{-R+2} \\ G_2 & G_1 & \cdots & G_{-R+3} \\ \vdots & \vdots & \ddots & \vdots \\ G_R & G_{R-1} & \cdots & G_1 \end{vmatrix}, \tag{B.8}$$

and

$$\langle Y_i Y_{i+R} \rangle^c = \begin{vmatrix} G_{-1} & G_{-2} & \cdots & G_{-R} \\ G_0 & G_{-1} & \cdots & G_{-R+1} \\ \vdots & \vdots & \ddots & \vdots \\ G_{R-2} & G_{R-3} & \cdots & G_{-1} \end{vmatrix}, \tag{B.9}$$

with $G_r \equiv G_N(R)$. The thermodynamic limit $N \to \infty$ may be obtained in a natural way

by making the substitution

$$\frac{2}{N}\sum_{k\in K} \longmapsto \frac{1}{\pi}\int_0^{\pi} dk. \tag{B.10}$$

These expressions are used to compute the exact finite-size correlation functions in Chapter 5.

Appendix C

Lattice speed of light computations

In a continuum CFT, the scaling dimension of an operator $\hat{\mathcal{O}}$ is $\Delta = 2h$, and conformal symmetry dictates the form of the following correlation functions

$$\langle \mathcal{O}(0,t)\mathcal{O}(x,0)^\dagger \rangle \propto \frac{1}{(x^2 - v^2t^2)^\Delta}, \tag{C.1}$$

$$\langle \dot{\mathcal{O}}(0,t)\mathcal{O}(x,0)^\dagger \rangle \propto \frac{2\Delta v^2 t}{(x^2 - v^2t^2)^{\Delta+1}}, \tag{C.2}$$

$$\langle \ddot{\mathcal{O}}(0,t=0)\mathcal{O}(x,0)^\dagger \rangle \propto \frac{-2\Delta v^2}{(x^2)^{\Delta+1}}. \tag{C.3}$$

Taking the ratio of the first and last expressions above removes any unphysical normalization and one has the continuum expression

$$\frac{\langle \ddot{\mathcal{O}}(0,0)\mathcal{O}(x,0)^\dagger \rangle}{\langle \mathcal{O}(0,0)\mathcal{O}(x,0)^\dagger \rangle} = \frac{-2\Delta v^2}{x^2} \tag{C.4}$$

To place this expression on the lattice, we use the same substitution as in (5.25): we let $x \mapsto (N/\pi)\sin(\pi x/N)$. This gives us the following lattice expression:

$$\frac{\langle \ddot{\mathcal{O}}(0,0)\mathcal{O}(x,0)^\dagger \rangle}{\langle \mathcal{O}(0,0)\mathcal{O}(x,0)^\dagger \rangle} = \frac{-2\pi^2 v^2 \Delta}{N^2 \sin(\pi x/N)^2}, \tag{C.5}$$

from which we can regress an estimate of the speed of light v on the lattice.

For the Ising model (with Hamiltonian (5.12) and $h = 1$), choosing $\mathcal{O} = X$ one has $-[\hat{H}, [\hat{H}, X]] = \ddot{X}$ and thus $\langle \ddot{X}_1 X_a \rangle = -\langle [\hat{H}, [\hat{H}, X_1]] X_a \rangle$. We can calculate this correlation function as follows:

$$\begin{aligned}
[H, X_1] &= [-Z_1, X_1] \\
&= -2iY_1 = \dot{X}_1 \\
[H, \dot{X}] &= 2i \left([X_1 X_2, Y_1] + [X_1 X_N, Y_1] + [Z_1, Y_1] \right) \\
&= -4 \left(Z_1 X_2 + Z_1 X_N - X_1 \right) \\
&= \ddot{X}_1 \\
\implies \langle \ddot{X}_1 X_a \rangle &= 4 \left(Z_1 X_2 X_a + Z_1 X_N X_a - X_1 X_a \right).
\end{aligned} \tag{C.6}$$

We use this to regress estimates of the lattice speed of light in Chapter 5.

Bibliography

[1] Kenneth G. Wilson. Confinement of quarks. *Physical Review D*, 10(8):2445–2459, October 1974.

[2] John Kogut and Leonard Susskind. Hamiltonian formulation of Wilson's lattice gauge theories. *Phys. Rev. D*, 11:395–408, Jan 1975.

[3] Gaopei Pan and Zi Yang Meng. *The sign problem in quantum Monte Carlo simulations*, page 879–893. Elsevier, 2024.

[4] Stephen D. H. Hsu and David Reeb. On the sign problem in dense qcd. *International Journal of Modern Physics A*, 25(01):53–67, January 2010.

[5] Thomas Hartman, Dalimil Mazac, David Simmons-Duffin, and Alexander Zhiboedov. Snowmass White Paper: The Analytic Conformal Bootstrap. In *Snowmass 2021*, 2 2022.

[6] David Simmons-Duffin. A semidefinite program solver for the conformal bootstrap. *Journal of High Energy Physics*, 2015(6):174, June 2015.

[7] David Simmons-Duffin. TASI lectures on the conformal bootstrap. 2016.

[8] A. M. Polyakov. NonHamiltonian approach to conformal quantum field theory. *Zh. Eksp. Teor. Fiz.*, 66:23–42, 1974.

[9] S. Ferrara, P. Gatto, and A. F. Grilla. *Ergebnisse der exakten Naturwissenschaften*, volume 67 of *Springer Tracts in Modern Physics*, page 1–64. Springer Berlin Heidelberg, Berlin, Heidelberg, 1973.

[10] S. Ferrara, R. Gatto, and A. F. Grillo. Properties of partial-wave amplitudes in conformal invariant field theories. *Il Nuovo Cimento A*, 26(3):226–236, April 1975.

[11] A.A. Belavin, A.M. Polyakov, and A.B. Zamolodchikov. Infinite conformal symmetry in two-dimensional quantum field theory. *Nuclear Physics B*, 241(2):333–380, July 1984.

[12] Riccardo Rattazzi, Vyacheslav S Rychkov, Erik Tonni, and Alessandro Vichi. Bounding scalar operator dimensions in 4D CFT. *Journal of High Energy Physics*, 2008(12):031–031, December 2008.

[13] David Poland, David Simmons-Duffin, and Alessandro Vichi. Carving out the space of 4D CFTs. *Journal of High Energy Physics*, 2012(5):110, May 2012.

[14] Sheer El-Showk, Miguel F. Paulos, David Poland, Slava Rychkov, David Simmons-Duffin, and Alessandro Vichi. Solving the 3D Ising model with the conformal bootstrap. *Physical Review D*, 86(2):025022, July 2012.

[15] Sheer El-Showk, Miguel F. Paulos, David Poland, Slava Rychkov, David Simmons-Duffin, and Alessandro Vichi. Solving the 3D Ising model with the conformal bootstrap ii: c-minimization and precise critical exponents. *Journal of Statistical Physics*, 157(4–5):869–914, December 2014.

[16] Filip Kos, David Poland, and David Simmons-Duffin. Bootstrapping mixed correlators in the 3D Ising model. *Journal of High Energy Physics*, 2014(11):109, November 2014.

[17] Luca Iliesiu, Filip Kos, David Poland, Silviu S. Pufu, David Simmons-Duffin, and Ran Yacoby. Bootstrapping 3d fermions. *Journal of High Energy Physics*, 2016(3):120, March 2016.

[18] Filip Kos, David Poland, David Simmons-Duffin, and Alessandro Vichi. Precision islands in the Ising and $O(N)$ models. *Journal of High Energy Physics*, 2016(8):36, August 2016.

[19] João Penedones, Emilio Trevisani, and Masahito Yamazaki. Recursion relations for conformal blocks. *Journal of High Energy Physics*, 2016(9):70, September 2016.

[20] Luis F. Alday and Alexander Zhiboedov. An algebraic approach to the analytic bootstrap. *Journal of High Energy Physics*, 2017(4):157, April 2017.

[21] David Poland, Slava Rychkov, and Alessandro Vichi. The conformal bootstrap: theory, numerical techniques, and applications. *Reviews of Modern Physics*, 91(1):015002, January 2019.

[22] David Poland and David Simmons-Duffin. Snowmass white paper: The numerical conformal bootstrap. 2022.

[23] Slava Rychkov and Ning Su. New developments in the numerical conformal bootstrap. 2023.

[24] Maho Nakata, Hiroshi Nakatsuji, Masahiro Ehara, Mitsuhiro Fukuda, Kazuhide Nakata, and Katsuki Fujisawa. Variational calculations of fermion second-order reduced density matrices by semidefinite programming algorithm. *The Journal of Chemical Physics*, 114(19):8282–8292, May 2001.

[25] David A. Mazziotti. Realization of quantum chemistry without wave functions through first-order semidefinite programming. *Physical Review Letters*, 93(21):213001, November 2004.

[26] Mituhiro Fukuda, Bastiaan J. Braams, Maho Nakata, Michael L. Overton, Jerome K. Percus, Makoto Yamashita, and Zhengji Zhao. Large-scale semidefinite programs in electronic structure calculation. *Mathematical Programming*, 109(2–3):553–580, January 2007.

[27] *Reduced-Density-Matrix Mechanics: With Application to Many-Electron Atoms and Molecules*, volume 134 of *Advances in Chemical Physics*. Wiley, 1st edition, March 2007.

[28] Maho Nakata, Bastiaan J. Braams, Katsuki Fujisawa, Mituhiro Fukuda, Jerome K. Percus, Makoto Yamashita, and Zhengji Zhao. Variational calculation of second-order reduced density matrices by strong N -representability conditions and an accurate semidefinite programming solver. *The Journal of Chemical Physics*, 128(16):164113, April 2008.

[29] Christine A. Schwerdtfeger and David A. Mazziotti. Convex-set description of quantum phase transitions in the transverse Ising model using reduced-density-matrix theory. *The Journal of Chemical Physics*, 130(22):224102, June 2009.

[30] Brecht Verstichel, Helen Van Aggelen, Dimitri Van Neck, Paul W. Ayers, and Patrick Bultinck. Variational density matrix optimization using semidefinite programming. *Computer Physics Communications*, 182(9):2025–2028, September 2011.

[31] Scott Lawrence. Semidefinite programs at finite fermion density. *Physical Review D*, 107(9):094511, May 2023.

[32] David A. Mazziotti. Structure of fermionic density matrices: Complete N -representability conditions. *Physical Review Letters*, 108(26):263002, June 2012.

[33] Daniel Gibney, Jan-Niklas Boyn, and David A. Mazziotti. Toward a resolution of the static correlation problem in density functional theory from semidefinite programming. *The Journal of Physical Chemistry Letters*, 12(1):385–391, January 2021.

[34] David A. Mazziotti. Quantum many-body theory from a solution of the N -representability problem. *Physical Review Letters*, 130(15):153001, April 2023.

[35] Nathan Argaman and Guy Makov. Density functional theory: An introduction. *American Journal of Physics*, 68(1):69–79, January 2000.

[36] Neil Shenvi and Weitao Yang. An algebraic operator approach to electronic structure. *The Journal of Chemical Physics*, 135(24):244111, December 2011.

[37] Thomas Barthel and Robert Hübener. Solving condensed-matter ground-state problems by semidefinite relaxations. *Physical Review Letters*, 108(20):200404, May 2012.

[38] Arbel Haim, Richard Kueng, and Gil Refael. Variational-correlations approach to quantum many-body problems. (arXiv:2001.06510), January 2020. arXiv:2001.06510 [cond-mat, physics:quant-ph].

[39] Ilya Kull, Norbert Schuch, Ben Dive, and Miguel Navascués. Lower bounding ground-state energies of local Hamiltonians through the renormalization group. (arXiv:2212.03014), December 2022. arXiv:2212.03014 [cond-mat, physics:quant-ph].

[40] Lin Lin and Michael Lindsey. Variational embedding for quantum many-body problems. *Communications on Pure and Applied Mathematics*, 75(9):2033–2068, September 2022.

[41] Takeshi Morita. Universal bounds on quantum mechanics through energy conservation and the bootstrap method. 2022.

[42] Ojas Parekh and Kevin Thompson. An optimal product-state approximation for 2-local quantum Hamiltonians with positive terms. (arXiv:2206.08342), June 2022. arXiv:2206.08342 [quant-ph].

[43] Minjae Cho and Xin Sun. Bootstrap, Markov chain Monte Carlo, and LP/SDP hierarchy for the lattice ising model. *Journal of High Energy Physics*, 2023(11):47, November 2023.

[44] Stefano Pironio, Miguel Navascues, and Antonio Acin. Convergent relaxations of polynomial optimization problems with non-commuting variables. *SIAM Journal on Optimization*, 20(5):2157–2180, January 2010. arXiv:0903.4368 [quant-ph].

[45] Tong Chen, Jean-Bernard Lasserre, Victor Magron, and Edouard Pauwels. A sublevel moment-SOS hierarchy for polynomial optimization. *Computational Optimization and Applications*, 81(1):31–66, January 2022.

[46] Mateus Araújo, Igor Klep, Andrew J. P. Garner, Tamás Vértesi, and Miguel Navascues. First-order optimality conditions for non-commutative optimization problems. 2023.

[47] Jun Takahashi, Chaithanya Rayudu, Cunlu Zhou, Robbie King, Kevin Thompson, and Ojas Parekh. An SU(2)-symmetric semidefinite programming hierarchy for quantum max cut. 2023.

[48] Hamza Fawzi, Omar Fawzi, and Samuel O. Scalet. Entropy constraints for ground energy optimization. (arXiv:2305.06855), May 2023. arXiv:2305.06855 [math-ph, physics:quant-ph].

[49] Hamza Fawzi, Omar Fawzi, and Samuel O. Scalet. Certified algorithms for equilibrium states of local quantum Hamiltonians. (arXiv:2311.18706), November 2023. arXiv:2311.18706 [cond-mat, physics:math-ph, physics:quant-ph].

[50] Armin Tavakoli, Alejandro Pozas-Kerstjens, Peter Brown, and Mateus Araújo. Semidefinite programming relaxations for quantum correlations. (arXiv:2307.02551), August 2023. arXiv:2307.02551 [quant-ph].

[51] Jie Wang, Jacopo Surace, Irénée Frérot, Benoît Legat, Marc-Olivier Renou, Victor Magron, and Antonio Acín. Certifying ground-state properties of quantum many-body systems. 2023.

[52] Hanna Westerheim, Jingxuan Chen, Zoë Holmes, Ivy Luo, Theshani Nuradha, Dhrumil Patel, Soorya Rethinasamy, Kathie Wang, and Mark M. Wilde. Dual-VQE: A quantum algorithm to lower bound the ground-state energy. (arXiv:2312.03083), December 2023. arXiv:2312.03083 [quant-ph].

[53] Yuehaw Khoo and Michael Lindsey. Scalable semidefinite programming approach to variational embedding for quantum many-body problems. *Journal of Computational Physics*, 510:113041, August 2024.

[54] Henry W. Lin. Bootstraps to strings: solving random matrix models with positivity. *Journal of High Energy Physics*, 2020(6):90, June 2020.

[55] Xizhi Han, Sean A. Hartnoll, and Jorrit Kruthoff. Bootstrapping matrix quantum mechanics. *Physical Review Letters*, 125(4):041601, July 2020.

[56] Yu Aikawa, Takeshi Morita, and Kota Yoshimura. Application of bootstrap to a θ term. *Physical Review D*, 105(8):085017, April 2022.

[57] Jyotirmoy Bhattacharya, Diptarka Das, Sayan Kumar Das, Ankit Kumar Jha, and Moulindu Kundu. Numerical bootstrap in quantum mechanics. *Physics Letters B*, 823:136785, December 2021.

[58] Hamed Hessam, Masoud Khalkhali, and Nathan Pagliaroli. Bootstrapping Dirac ensembles. *Journal of Physics A: Mathematical and Theoretical*, 55(33):335204, August 2022.

[59] Yu Aikawa, Takeshi Morita, and Kota Yoshimura. Bootstrap method in harmonic oscillator. *Physics Letters B*, 833:137305, October 2022.

[60] Matthew J. Blacker, Arpan Bhattacharyya, and Aritra Banerjee. Bootstrapping the Kronig-Penney model. *Physical Review D*, 106(11):116008, December 2022.

[61] Robert De Mello Koch, Antal Jevicki, Xianlong Liu, Kagiso Mathaba, and João P. Rodrigues. Large N optimization for multi-matrix systems. *Journal of High Energy Physics*, 2022(1):168, January 2022.

[62] Yu Nakayama. Bootstrapping microcanonical ensemble in classical system. *Modern Physics Letters A*, 37(09):2250054, March 2022.

[63] Sakil Khan, Yuv Agarwal, Devjyoti Tripathy, and Sachin Jain. Bootstrapping PT symmetric quantum mechanics. *Physics Letters B*, 834:137445, November 2022.

[64] Serguei Tchoumakov and Serge Florens. Bootstrapping Bloch bands. *Journal of Physics A: Mathematical and Theoretical*, 55(1):015203, January 2022.

[65] Bao-Ning Du, Min-Xin Huang, and Pei-Xuan Zeng. Bootstrapping Calabi–Yau quantum mechanics. *Communications in Theoretical Physics*, 74(9):095801, September 2022.

[66] Rajesh Gopakumar, Eric Perlmutter, Silviu S. Pufu, and Xi Yin. Snowmass white paper: Bootstrapping string theory. 2022.

[67] Henry W. Lin. Bootstrap bounds on D0-brane quantum mechanics. *Journal of High Energy Physics*, 2023(6):38, June 2023.

[68] Xihe Hu. Different bootstrap matrices in many QM systems. 2022.

[69] Vladimir Kazakov and Zechuan Zheng. Bootstrap for lattice yang-mills theory. *Physical Review D*, 107(5):L051501, March 2023.

[70] Scott Lawrence. Bootstrapping lattice vacua. 2021.

[71] Colin Oscar Nancarrow and Yuan Xin. Bootstrapping the gap in quantum spin systems. *Journal of High Energy Physics*, 2023(8):52, August 2023.

[72] David Berenstein and George Hulsey. Bootstrapping simple QM systems. (arXiv:2108.08757), September 2021. arXiv:2108.08757 [hep-lat, physics:hep-th, physics:quant-ph].

[73] David Berenstein and George Hulsey. Bootstrapping more QM systems. *Journal of Physics A: Mathematical and Theoretical*, 55(27):275304, July 2022. © IOP Publishing. Reproduced with permission. All rights reserved.

[74] David Berenstein and George Hulsey. Anomalous bootstrap on the half-line. *Physical Review D*, 106(4):045029, August 2022. Copyright 2022 by the American Physical Society.

[75] David Berenstein and George Hulsey. Semidefinite programming algorithm for the quantum mechanical bootstrap. *Physical Review E*, 107(5):L053301, May 2023. Copyright 2023 by the American Physical Society.

[76] David Berenstein and George Hulsey. One-dimensional reflection in the quantum mechanical bootstrap. *Phys. Rev. D*, 109:025013, Jan 2024. Copyright 2024 by the American Physical Society.

[77] Wei Fan and Huipen Zhang. A non-perturbative formula unifying double-wells and anharmonic oscillators under the numerical bootstrap approach. (arXiv:2309.09269), 2023. arXiv:2309.09269 [hep-th, physics:quant-ph].

[78] Wei Fan and Huipeng Zhang. Non-perturbative instanton effects in the quartic and the sextic double-well potential by the numerical bootstrap approach. 2023.

[79] Yongwei Guo and Wenliang Li. Solving anharmonic oscillator with null states: Hamiltonian bootstrap and Dyson-Schwinger equations. *Physical Review D*, 108(12):125002, December 2023.

[80] Wenliang Li. The ϕ^n trajectory bootstrap. 2024.

[81] Zhijin Li and Shutong Zhou. Bootstrapping the abelian lattice gauge theories. 2024.

[82] Kagiso Mathaba, Mbavhalelo Mulokwe, and João P. Rodrigues. Large N master field optimization: the quantum mechanics of two Yang-Mills coupled matrices. *Journal of High Energy Physics*, 2024(2):54, February 2024.

[83] Mao Zeng. Feynman integrals from positivity constraints. *Journal of High Energy Physics*, 2023(9):42, September 2023.

[84] M. B. Hastings. Field theory and the sum-of-squares for quantum systems. 2023.

[85] Zechuan Zheng. Bootstrap method in theoretical physics. 2024.

[86] Stephen P. Boyd and Lieven Vandenberghe. *Convex optimization*. Cambridge University Press, Cambridge, UK; New York, 2004.

[87] Jean Bernard Lasserre. *Moments, positive polynomials and their applications*. Imperial College Press, London, 2016.

[88] Emil Artin. Über die zerlegung definiter funktionen in quadrate. *Abhandlungen aus dem Mathematischen Seminar der Universität Hamburg*, 5(1):100–115, December 1927.

[89] Monique Laurent. *Sums of Squares, Moment Matrices and Optimization Over Polynomials*, volume 149 of *The IMA Volumes in Mathematics and its Applications*, page 157–270. Springer New York, New York, NY, 2009.

[90] Raul E. Curto and Lawrence A. Fialkow. Recursiveness, positivity, and truncated moment problems. *Houston Journal of Mathematics*, 17:603–635, 1991.

[91] Raul E. Curto and Lawrence A. Fialkow. Truncated k-moment problems in several variables. *Journal of Operator Theory*, 54(1):189–226, 2005.

[92] Yi-Kai Liu, Matthias Christandl, and F. Verstraete. Quantum computational complexity of the N -representability problem: QMA complete. *Physical Review Letters*, 98(11):110503, March 2007.

[93] Julia Kempe, Alexei Kitaev, and Oded Regev. *The Complexity of the Local Hamiltonian Problem*, volume 3328 of *Lecture Notes in Computer Science*, page 372–383. Springer Berlin Heidelberg, Berlin, Heidelberg, 2004.

[94] Andris Ambainis. On physical problems that are slightly more difficult than QMA. 2013.

[95] J. William Helton and Scott A. McCullough. A positivstellensatz for non-commutative polynomials. *Transactions of the American Mathematical Society*, 356(9):3721–3737, 2004.

[96] Konrad Schmüdgen. *Archimedean Quadratic Modules and Positivstellensätze*, volume 285 of *Graduate Texts in Mathematics*, page 225–249. Springer International Publishing, Cham, 2020.

[97] H. J. W. Müller-Kirsten. *Introduction to quantum mechanics: Schrödinger equation and path integral*. World Scientific, New Jersey, second edition edition, 2012.

[98] Hagen Kleinert. *Path integrals in quantum mechanics, statistics, polymer physics, and financial markets*. World Scientific, New Jersey, 5th ed., repr edition, 2010.

[99] Vladimir Kazakov and Zechuan Zheng. Analytic and numerical bootstrap for one-matrix model and "unsolvable" two-matrix model. *Journal of High Energy Physics*, 2022(6):30, June 2022.

[100] Makoto Yamashita, Katsuki Fujisawa, Mituhiro Fukuda, Kazuhiro Kobayashi, Kazuhide Nakta, and Maho Nakata. Latest developments in the SDPA family for solving large-scale sdps. In Miguel F. Anjos and Jean B. Lasserre, editors, *Handbook on Semidefinite, Cone and Polynomial Optimization: Theory, Algorithms, Software and Applications*, chapter 24, pages 687–714. Springer, NY, USA, 2011.

[101] N. I. Akhiezer. *The classical moment problem and some related questions in analysis*. Mathematics. Dover Publications, Inc, Garden City, New York, dover edition edition, 2020.

[102] *NIST Digital Library of Mathematical Functions*. http://dlmf.nist.gov/, Release 1.1.4 of 2022-01-15. F. W. J. Olver, A. B. Olde Daalhuis, D. W. Lozier, B. I. Schneider, R. F. Boisvert, C. W. Clark, B. R. Miller, B. V. Saunders, H. S. Cohl, and M. A. McClain, eds.

[103] Michael Reed and Barry Simon. *Methods of modern mathematical physics*. Academic press, San Diego New York Berkeley [etc.], 1975.

[104] Michael Reed and Barry Simon. *Methods of modern mathematical physics*. Academic Press, New York, rev. and enl. ed edition, 1980.

[105] J. G. Esteve. Origin of the anomalies: The modified heisenberg equation. *Physical Review D*, 66(12):125013, December 2002.

[106] Tajron Jurić. Observables in quantum mechanics and the importance of self-adjointness. *Universe*, 8(2):129, February 2022.

[107] M. H. Al-Hashimi and U.-J. Wiese. Canonical quantization on the half-line and in an interval based upon an alternative concept for the momentum in a space with boundaries. *Physical Review Research*, 3(3):033079, July 2021.

[108] Jun John Sakurai and Jim Napolitano. *Modern quantum mechanics*. Cambridge University Press, Cambridge, 3rd ed edition, 2021.

[109] C Carathéodory. Über den variabilitätsbereich der fourierschen konstanten von positiven harmonischen funktionen. *Rend. Circ. Mat.*, 32:193–217, 1911.

[110] Derek J. Daniel. Exact solutions of Mathieu's equation. *Progress of Theoretical and Experimental Physics*, 2020(4):043A01, April 2020.

[111] M. Lüscher. Volume dependence of the energy spectrum in massive quantum field theories: Ii. scattering states. *Communications in Mathematical Physics*, 105(2):153–188, June 1986.

[112] Lev Davidovich Landau and Evgenii Mikhailovich Lifshitz. *Quantum mechanics: non -relativistic theory*, volume 3. Elsevier, 2013.

[113] Yu Nakayama. Liouville field theory: A decade after the revolution. *International Journal of Modern Physics A*, 19(17n18):2771–2930, July 2004.

[114] Nathan Seiberg. Notes on quantum liouville theory and quantum gravity. *Progress of Theoretical Physics Supplement*, 102:319–349, 1990.

[115] Yijian Zou, Ashley Milsted, and Guifre Vidal. Conformal data and renormalization group flow in critical quantum spin chains using periodic uniform matrix product states. *Physical Review Letters*, 121(23), December 2018.

[116] Yijian Zou and Guifre Vidal. Emergence of conformal symmetry in quantum spin chains: Antiperiodic boundary conditions and supersymmetry. *Physical Review B*, 101(4), January 2020.

[117] Ashley Milsted and Guifre Vidal. Extraction of conformal data in critical quantum spin chains using the koo-saleur formula. *Physical Review B*, 96(24):245105, December 2017.

[118] David A. Mazziotti. Realization of quantum chemistry without wave functions through first-order semidefinite programming. *Phys. Rev. Lett.*, 93:213001, Nov 2004.

[119] Jarrod R. McClean et al. OpenFermion: the electronic structure package for quantum computers. *Quantum Sci. Technol.*, 5(3):034014, 2020.

[120] Akshay Agrawal, Robin Verschueren, Steven Diamond, and Stephen Boyd. A rewriting system for convex optimization problems. *Journal of Control and Decision*, 5(1):42–60, 2018.

[121] MOSEK ApS. *MOSEK Optimization Suite 10.1.28*, 2019.

[122] John L. Cardy. Operator content of two-dimensional conformally invariant theories. *Nuclear Physics B*, 270:186–204, January 1986.

[123] Malte Henkel. Finite-size scaling and universality in the spectrum of the quantum Ising chain. i. periodic and antiperiodic boundary condition. *Journal of Physics A: Mathematical and General*, 20(4):995, 1987.

[124] Glen Bigan Mbeng, Angelo Russomanno, and Giuseppe E. Santoro. The quantum Ising chain for beginners. September 2020.

[125] W Selke. The ANNNI model — theoretical analysis and experimental application. *Physics Reports*, 170(4):213–264, November 1988.

[126] A. Milsted, L. Seabra, I. C. Fulga, C. W. J. Beenakker, and E. Cobanera. Statistical translation invariance protects a topological insulator from interactions. *Phys. Rev. B*, 92:085139, Aug 2015.

[127] Armin Rahmani, Xiaoyu Zhu, Marcel Franz, and Ian Affleck. Phase diagram of the interacting Majorana chain model. *Phys. Rev. B*, 92:235123, Dec 2015.

[128] Yu Zhang. Microscopic ensemble bootstrap in phase space. *Communications in Theoretical Physics*, 76(6):065102, June 2024.

[129] Vladimir Kazakov and Zechuan Zheng. Bootstrap for Finite N Lattice Yang-Mills Theory. April 2024.

[130] Thomas G. Mertens, Gustavo J. Turiaci, and Herman L. Verlinde. Solving the schwarzian via the conformal bootstrap. *Journal of High Energy Physics*, 2017(8):136, August 2017.

[131] Pierre Pfeuty. The one-dimensional Ising model with a transverse field. *Annals of Physics*, 57(1):79–90, March 1970.

[132] Eytan Barouch, Barry M. McCoy, and Max Dresden. Statistical mechanics of the XY model I. *Physical Review A*, 2(3):1075–1092, September 1970.

[133] Eytan Barouch and Barry M. McCoy. Statistical mechanics of the XY model. II: Spin-correlation functions. *Physical Review A*, 3(2):786–804, February 1971.

[134] Elliott Lieb, Theodore Schultz, and Daniel Mattis. Two soluble models of an antiferromagnetic chain. *Annals of Physics*, 16(3):407–466, December 1961.

[135] Tobias J. Osborne and Michael A. Nielsen. Entanglement in a simple quantum phase transition. *Physical Review A*, 66(3):032110, September 2002.

[136] Tohru Koma and Nobuyuki Mizukoshi. Finite-size scaling for correlations of quantum spin chains at criticality. *Journal of statistical physics*, 83:661–726, 1996.